UNIVERSITY OF OKLAHOMA

GRADUATE COLLEGE

IRON TRANSPORT AND REMOVAL DYNAMICS IN THE OXIDATIVE UNITS OF A PASSIVE TREATMENT SYSTEM

A DISSERTATION

SUBMITTED TO THE GRADUATE FACULTY

in partial fulfillment of the requirements for the

Degree of

DOCTOR OF PHILOSOPHY

By

LEAH OXENFORD
Norman, Oklahoma
2016

IRON TRANSPORT AND REMOVAL DYNAMICS IN THE OXIDATIVE UNITS

OF A PASSIVE TREATMENT SYSTEM

A DISSERTATION APPROVED FOR THE
SCHOOL OF CIVIL ENGINEERING AND ENVIRONMENTAL SCIENCE

BY

_____
Dr. Robert Nairn, Chair

_____
Dr. Elizabeth Butler

_____
Dr. Andrew Madden

_____
Dr. David Sabatini

_____
Dr. Keith Strevett

For first generation college graduates

Acknowledgements

There are many people that have been essential to my growth as both a scientist and as a person through the various forms that one's education can take. I would like to thank each of them for their specific role in as my mentors, colleagues, confidants, and friends.

A special thanks goes to my adviser, Dr. Robert Nairn, for his role in my development as a scientist, an educator, and as an engaged member of my community. His passion and integrity serve as inspiration as to how commitment and dedication can yield lasting change in the world of environmental remediation as well as education. His mentorship challenged me every step of the way in this process, and gave me the freedom to learn from my own mistakes. Thank you for taking a chance on me.

This research would not have been possible without the commitment of so many students from the Center for the Restoration of Ecosystems and Watersheds (CREW). Through countless hours on the road, in the field, in the classroom, and in the laboratory, we have worked diligently to support each other in making a difference within the field of environmental science. We are a part of something greater than ourselves: *J. LaBar, B. Holzbauer-Schweitzer, B. Page, N. Shepherd, E. Thornton, N. Berg-Mattson, E. Fielding, A. Marsh, D. Nguyen, A. Sikora, K. Steele, Z. Tang, J. Arango, M. Rice, B. Furneaux, J. Brumley, S. Yepez, A. Smith, J. McAllister, W. Andrews, A. Brewer, B. Santamaria, C. Neely, A. Garrido, W. Strosnider, D. Lutes, and S. Guzman.*

Likewise, my colleagues at the University of Science and Arts of Oklahoma (USAO) have supported me with interesting scheduling solutions, encouragement, meals, and a base of operations in Norman, OK for field or laboratory work requiring my full and undivided attention. *Jeannette Loutsch, Rachel Jones, Jason Shaw, Mike Mather, James Addams, and JC Sanders.*

And finally, my mentors / role models that have shaped me into the scientist I am today, and are responsible for the scientist that I will become through my service to others: *Mike Sadar (Hach Co.), Dr. David Pringle (UNC-Greeley), Dr. Najati Kaval (OSU), Tim Messer (Verus), Margaret Dunn (ASMR), and Dr. Robert Nairn (OU).*

Table of Contents

List of Tables

List of Figures

Abstract

Mine drainage is threat to water systems in legacy mining districts as elevated concentrations of dissolved iron, sulfate, and trace metals have an unmitigated impact on water quality. Changes in pH due to acidity loading as well as the mobilization of trace metals poses an unacceptable risk to environmental and human health. A variety of active remediation strategies exist, but differ in their initial capital investment, operational requirements, and maintenance making them less attractive options for remote or abandoned locations due to cost. Passive treatment systems (PTS) have become an increasingly more popular technology for the treatment of acid mine drainage (AMD) with the goal of improving water quality through (1) acid neutralization, (2) metals removal and retention and (3) alkalinity generation. Passive treatment systems are composed of a series of treatment cells, in which each unit is designed to meet one or more of the afore mentioned goals through the control of physical, chemical, and biological aspects of the treatment cells. The preliminary oxidation cells of a passive treatment system focus on the removal and retention of iron specifically due to its roll in physical (solids accumulation and retention to maintain hydraulic conductivity through the system), chemical (latent acidity produced via oxidation and hydrolysis; trace metals sorption to $FeOOH_{(s)}$), and biological (use of emergent hydrophytes to facilitate solids sedimentation) system functions.

The premise of this dissertation is that passive treatment system performance is dependent on the dynamic removal, fate, and transport of iron oxides over time. The following chapters each contribute to a detailed assessment of the design and performance of the oxidative unit of a full scale passive treatment system under expected (design driven) operational conditions and under periods of disturbance due to frequent storm activity. The performance of the oxidative

unit, and the performance of the system overall for the first seven years of operation are addressed through intracellular transport, removal, and accumulation profiling.

Chapter One, “Full Scale Passive Treatment of Net-Alkaline Ferruginous Acid Mine Drainage at the Tar Creek Superfund Site” describes the need for site specific passive treatment, and the critical decisions involved in treatment system design. This chapter represents data as a collaborative work of monitoring by the Center for the Restoration of Ecosystems and Watersheds over a period of nearly 10 years (2004-2015) leading up to the installation and application of full scale treatment technologies in fall of 2008, and their performance evaluation over the next seven years of operation to assess effectiveness in achieving the goal of water quality improvement. The Mayer Ranch Passive Treatment system meets water quality improvement expectations as seep concentrations of iron (192 mg/L), zinc (9.78 mg/L), nickel (0.933 mg/L), cadmium (15.1 µg/L), lead (60 µg/L) and arsenic (66 µg/L) are attenuated prior to discharge into a tributary of Tar Creek [99% (Fe), 95%(Zn), 83% (Ni), 93%(Cd), with Pb and As being removed to levels below detection limits]. The system also generates alkalinity in multiple steps (Cells 3N/S; 5N/S) to mitigate what has been lost due to metals latent acidity yielding a net alkalinity of nearly 200 mg/L as $CaCO_3$ equivalence. The MRPTS has successfully removed iron within the oxidative unit specifically (iron oxidation pond+ two surface flow wetland cells) over the lifetime of the system, yet the variability in the efficiency of the preliminary oxidation cell (Cell 1) demands additional investigation.

Chapter Two, “Spatial Profiling of Seasonally Influenced Iron Removal in an Oxidation Treatment Cell”, provides a detailed evaluation of seasonal iron removal within Cell 1 thorough a series of samples collected between the influent and effluent flows typically used for cell performance evaluation. This detailed survey of iron removal corresponds well with the solids accumulation profiling detailed within Chapter 5, “Characterization of the Spatial Iron Accumulation in the

Preliminary Oxidative Cells of a Passive Treatment System", as the accumulation of precipitated iron oxides follows spatial orientation consistent with average removal dynamics. Periods of colder temperatures (winter: ~6^{o}C) decrease the rate of iron removal within Cell 1 with the majority of material transported into Cells 2N/2S being in the dissolved state (Fe^{2+}). The overall function of removal for the oxidative unit is not compromised during the winter months of operation as the surface flow wetlands provide additional hydraulic residence time for the removal of iron prior to discharge on to the vertical flow bioreactors (VFBR). Although iron removal has not been impacted by the accumulation of iron oxides thus far, the hydraulic retention time of Cell 1 has been reduced from a design time of 7.7 days to 5.5 days based on the results of a rhodamine dye tracer study. Cells 2N/2S were assessed to have shorter retention times (2.5 days) versus design (3.5 days) in 2009, yet demonstrate extended retention times approach 9 days due to successive rain events and flow restriction due to the vertical flow bioreactors (VFBRs) indicating that short term storm events play a role in iron transport and removal dynamics.

Chapters Three and Four focus on the role of acute storm disturbance on iron transport between the cells of the oxidative unit, exported from the oxidative unit to the VFBRs, and exported out the system into the receiving stream. Storm frequency, intensity, yield, and duration were evaluated from archived data from the Oklahoma Mesonet to determine a storm classification criteria based on intensity (Low: 0.25-0.99 cm/hr; Moderate: 1.00-1.99 cm/hr; High: 2.00-2.99 cm/hr; Extreme: >3.00 cm/hr). Iron transport out of cells 1, 2N, 2S, and 6 was determined for a select group of individual storms between 2009-2013 and mass transport of iron was determined on a storm by storm basis. The amount of iron transported during a 30-hour sampling window following the storm event did not correlate to rainfall intensity, and thus the mechanism of transport is not believed to be due to resuspension of accumulated materials.

Rather, disruption of sedimentation of iron oxide flocs is suspected due to the frequency between rain events. Low intensity rainfall events dominate the precipitation profile for the MRPTS, and significance in transport is not only observed for individual rain events, but also for seasonal and annual transport within the oxidative unit. Iron transport out of the passive treatment system due to storm events was minimal as iron removal and storage occurs multiple cells before the final polishing wetland (spatially isolated from oxidative unit transport).

Chapter 1: Full-Scale Passive Treatment of Net-Alkaline Ferruginous Acid Mine Drainage at the Tar Creek Superfund Site

This chapter has been formatted for submission to *Mine Water and the Environment*

Abstract

A legacy of mining at the Tar Creek Superfund Site has led to many remediation challenges including surface tailings, subsidence collapses, and acid mine drainage (AMD) seeps. Although the EPA has acted in remediation efforts, surface waters remain impacted and in need of treatment. Passive treatment is a viable option for the removal of dissolved metals, neutralization of acidity, and generation of alkalinity through a series of treatment cells designed based on local hydrology and water quality. The AMD seeps at Mayer Ranch supply nearly 20% of the AMD load to Tar Creek, and has a flow rate that varies seasonally. Water quality was evaluated for total and dissolved metals, sulfate, *in situ* parameters including pH, conductivity, dissolved oxygen, temperature, oxidation reduction potential, total dissolved solids, salinity, turbidity, and alkalinity for four years prior to system installation and startup. The design of the Mayer Ranch Passive Treatment System was based on mass loading from the net-alkaline seeps, area adjusted removal rates, and sizing to handle hydraulic retention of treatment volumes. The system has successfully operated for 8 years at the time of this publication meeting its goals of metals removal and alkalinity generation. The discharge of treated water has had a positive impact on the quality of the receiving stream, with biological indicators supporting ecosystem recovery. The success of the MRPTS encourages the detailed profiling of treatment processes to better understand performance efficiencies.

Introduction

The legacy of the Tar Creek Superfund Site originates from successive subsurface lead zinc mining operations in northeastern Oklahoma; Ottawa County during the early 1890s through the 1970's (US EPA, 2016a), as part of the larger Tri-State Lead-Zinc Mining District of Oklahoma, Kansas, and Missouri (TSMD). Although large-scale production maximized yields in the 1920s with 130,410 tons of lead and 749,254 tons of zinc being produced annually from the TSMD, small scale mining operations within the Picher Field continued to extract materials up until the cessation of mining activities in the 1970s (US EPA, 2016a). After the mine workings were abandoned, they were allowed to fill with groundwater, and the increased surface area of materials coupled with the presence of oxygen and water, initiated a series of chemical reactions resulting in the production of acid mine drainage (AMD). Concern over the potential risk associated with AMD to surface waters began in the early 1980s with individual landowners noting the emergence of AMD seeps on their properties and with detection of water contamination within the aquifer supplying water to the towns of Picher, Cardin, Quapaw, Commerce, and others (Sheibach et al, 1982). With the passing of the Comprehensive Environmental Response, Compensation and Liability Act (CERCLA) (1980, amended 1986), financial resources collected from taxation of the chemical and petroleum industries were pooled into a "Superfund" designated to pay for remediation efforts at legacy sites if the waste generators were no longer available to be held as responsible parties for reclamation efforts or cost (US EPA, 2016). CERCLA operates under the Polluter Pays Principle in which the principle responsible parties (PRPs) for Tar Creek were sued for damages, yet the financial settlements were insufficient to cover the full cost of remediation activities.

The Tar Creek Superfund site covers approximately 40 square miles and was listed on the National Priorities List (NPL) in 1983 with the Oklahoma Department of Environmental Quality (DEQ), and the Quapaw Tribe cited as cleanup oversite agencies under the control of the United States Environmental Protection Agency (EPA) (OKDEQ, 2016). The Hazard Ranking System (HRS) score applied by the EPA to classify the risk associated with the diversity and severity of exposures through the assessment of physical and chemical properties and their abiotic exposure pathways (US EPA, 2016b). Tar Creek remained ranked at 58.15 through 2003 due to the complexity and scope of contamination surveyed during preliminary assessment and site inspection (US EPA, 2016b). The EPA has designated five Operable Units (OU) so far for action at the Tar Creek Superfund Site, as listed in Table 1.1.

Table 1.1: Summary EPA Operable Units at the Tar Creek Superfund Site (OKDEQ, 2015; Christensen, 1995)

Unit	Issue	Status
OU 1	Surface water contamination in Tar Creek and tributaries from discharge and the threat of contamination of the Roubidoux Aquifer beneath the site from mine water and abandoned wells	No significant improvement in surface water quality, partial effectiveness for damming/ diking and there were insufficient data to evaluate well plugging
OU 2	High concentration of lead found in children and connected to surface contamination in yards, playgrounds, and other soils.	Soil removal and clean fill dirt replacement on a yard-by-yard basis for over 2000 properties.
OU 3	Storage and retention of chemical laboratory stocks at the Eagle Picher Industries	Laboratory chemicals were removed from the site and disposed of in accordance with current safety protocols.
OU 4	Chat Piles, Other Mine and Mill Wastes, Smelter Wastes, Surface contamination and subsidence	Cleanup has been completed on some distal area projects. Voluntary buyout of citizens within the Relocation Assistance Zone has been completed.
OU 5	Sediments and surface water contamination (ongoing)	Model sediment, water quality concentrations, and flow for the Spring River for sediment cleanup methodology selection.

Acid Mine Drainage

Acid mine drainage (AMD) is an environmental problem of unique complexity in its sources, composition, and impacts (Sheppard 1993; Younger et al. 2002; Soucek et al. 2003; Johnson and Hallberg 2005; Zipper et al. 2005). AMD is produced through natural weathering processes in which exposed sulfide minerals react with oxygen and water to liberate dissolved metals and acidity (Dubbin et al. 2005). This phenomenon is enhanced when the exposed surface area of sulfide minerals is dramatically increased through mining disturbance (Watzlaf et al. 2004). The weathering process is catalyzed by biotic and abiotic factors including bacteria like *Ferroplasma acidarmanus or Acidithiobacillus ferrooxidans* and the presence of dissolved iron and acidity (Nemati et al. 1998; Gleisner, et al. 2006). Regardless of whether or not this process occurs underground, or on the surface at exposed tailings or waste rock piles, the end result is the production of AMD.

Although AMD is commonly referred to as "acid mine drainage" its overall properties may be net acidic or net alkaline based on composition of the water. AMD is characterized as having elevated loadings of metals such as iron, lead, zinc, and cadmium, which also contribute to the acidity of impacted waters, over reference site conditions, (Cravotta 2008a; Cravotta 2008b). The concentration of principle dissolved metals species, pH, and alkalinity are used to calculate net acidity based on equation 1.1 (Hedin 2004). Waters are classified as net-acidic if acidity calculations exceed available alkalinity (a positive value), and are classified as net alkaline if the available alkalinity exceeds the acidic potential (a negative value) of the AMD (Kirby and Cravotta 2005).

$$\text{net acidity} = 50\left[1000(10^{-\text{pH}}) + \frac{2(\text{Fe}^{2+})}{56} + \frac{3(\text{Fe}^{3+})}{56} + \frac{2(\text{Mn})}{55} + \frac{3(\text{Al})}{27}\right] - \text{Alkalinity} \quad (1.1)$$

AMD can directly impact ecosystems by exceeding the buffering capacity of surface water sources via acidification if it is net acidic and will require the addition of alkalinity as a component of treatment. Net alkaline waters will lose a fractional amount of their alkalinity to acidity via equilibration with surface conditions, yet some alkalinity remains to buffer pH circumneutral despite the hydrogen ions produced from metals hydrolysis (Kirby and Cravotta 2005). Accumulated iron oxides and associated metals have indirect impacts on ecological health such as smothering benthic invertebrates and increasing turbidity leading to the attenuation of light for photosynthesis (Blowes et al. 2007; Jennings et al. 2008).

Treating AMD demands an interdisciplinary approach involving partnerships between scientific, governmental, and academic disciplines along with local agencies and communities to fully understand project goals and scope. The source, matrix, loadings, reaction kinetics, and seasonal influences on AMD must be considered in conjunction with available land dimensions to develop a treatment system design best suited for each location (Kirby and Cravotta 2005; Gazea et al. 1996). The geology of a region defines the properties and composition of the AMD; therefore, a one-solution-fits-all approach to treating AMD is not realistic as the quality and quantity vary based on location (Skousen 1997).

Active and passive treatment options exist for AMD, and are selected based on site specific requirements that include both water quality and quantity as part of the design criteria (Glazer et al 2000; Army Corps 2003). Both active and passive treatment are based on the same principles of physical and chemical control of conditions during the treatment process, yet differ in application. Active systems are effective in treating AMD yet typically have higher operational and maintenance expenses when compared to passive treatment (Damarisotta 2003). Growing concern for the AMD problem has led to increased research into treatment and remediation processes suited for long-term, sustainable treatment at remote or

abandoned sites (Younger et al. 2002). Passive treatment systems hold particular promise for decreasing AMD impacts via source remediation (Gazea et al. 1996; Sapsford and Williams, 2009) when properly selected and sized for each location (Hedin and Nairn, 1992). Lessons learned from the study of passive treatment successes and failures are critical contributions to the body of literature that the scientific and engineering reclamation communities rely upon to make informed decisions in design refinement and process management (Skousen and Ziemkiewicz 2005).

Passive Treatment Technology

Passive treatment systems typically consist of a series of treatment cells that are selected, sized, and placed in series based on the contaminant mass loading to achieve maximum treatment effectiveness. Each cell is sized conservatively to accommodate variability precipitation and seasonal fluctuations in AMD flow rate (Tarutis et al., 1999; Sapsford and Williams, 2009). The hydrology of passive treatment systems is controlled utilizing elevation head changes to move water from cell to cell without pumps, grid electricity, or fossil fuels. The absence of active chemical dosing or pumped flow regimes in passive treatment systems makes them increasingly attractive options for derelict or remote sites where active/conventional treatment is not practical due to financial restrictions and resource availability (Cravotta, 2008a; Cravotta, 2008b). Federal regulations emphasize the limit of 1.0 mg/L (30-day average) and 2.0 mg/L (daily maximum) for total iron in surface water discharges for ore mining (40 CFR 125.30) with increasingly lower thresholds for other trace metals from hard rock sites via the Clean Water Act.

Net-acidic waters require an alkalinity generation treatment step prior to iron removal, while net-alkaline waters have enough alkalinity present to buffer the latent acidity released via

oxidation and hydrolysis processes. Each unit of a passive treatment system is designed for a specific type of water quality improvement, wherein the oxidative units consist of aerobic sedimentation basins, surface flow wetlands, or hybrid designs of pond-marsh-pond bathymetry (Watzlaf et al. 2004). These cells are typically positioned first in the treatment series when the influent AMD is net-alkaline with a pH > 6, and iron is a principle component of the AMD matrix (Younger et al. 2002). If the water is net acidic, then an anoxic limestone drain (ALD) is used to generate alkalinity prior to iron oxidation and hydrolysis cells. The targeted removal of iron from net-alkaline AMD decreases the concentration of secondary dissolved species like zinc, lead, and arsenic through adsorption (Swedlund et al. 2009; Lenoble et al. 2002), while the retention of precipitated iron solids within the designed storage volume of the oxidative cells prevents flow attenuation from accumulation on the surface of vertical flow bioreactors (VFBR). The installation of a preliminary sedimentation basin paired with a secondary aerobic surface flow wetland is a proposed solution to mitigate iron solids transfer onto the compost layer of a VFBR (Jarvis and Younger, 2001; Stark and Williams, 1995). Any dissolved iron (II) species transported into the VFBRs will be removed as iron sulfides, yet this is not the most efficient approach for iron removal. Reduction to an iron sulfide is favored over other metals species such as Ni, Cd, Zn, Pb, and Cu due to their relative reduction potentials and may impact the removal efficiencies of other metals (Watzlaf et al. 2004). Therefore, the efficiency of metals removal for the passive treatment system overall is dependent on the removal and retention of iron species early within the system to minimize physical and chemical impacts on down-stream treatment processes (Demchak et al. 2001).

Although passive treatment systems continue to show promise in increasingly challenging situations, they still have not been fully accepted as competitive treatment options due to performance efficiency being impacted by spatial and seasonal variability (Johnson and

Hallberg, 2005; Watzlaf et al. 2004; Hedin 2008, Zipper and Skousen 2010). There are many questions that remain regarding the performance of passive treatment systems over short-term seasonal periods and for long-term operation leading to issues associated with estimated design life of each process unit. Performance prediction methodologies based on design parameters have been well defined in the literature through a "black box" approach to AMD source monitoring, as well as through the use of modeling (Mitsch and Wise, 1997; Sapsford and Watson, 2011; Stark and Williams, 1995; Flanagan et al. 1994). However, there is a lack of information regarding the use of spatial and temporal profiling within a treatment cell to assess performance mechanisms from an empirical perspective. Since the efficiency of iron removal within the primary oxidative treatment unit is essential for optimized system-level performance (Hall 2005), a detailed survey of oxidative unit function is a valuable contribution for long-term performance estimates and maintenance decisions regarding solids accumulation and volume displacement. Some detailed descriptions of mechanistic processes exist, but they are typically limited to bench- or pilot-scale operations due to time and cost constraints (Champagne et al. 2005). Therefore, the spatial and temporal profiling of the oxidative unit of a full-scale passive treatment system will compliment this growing body of knowledge and better support design decisions for future full-scale development projects.

Mayer Ranch Passive Treatment System

The Mayer Ranch Passive Treatment System (MRPTS) is located within the Tri-State Mining District near Commerce, OK in association with the Tar Creek Superfund Site (36°55'18.58"N, 94°52'22.64"W). This collaborative research demonstration project between academic, state, federal, private, municipal, and tribal interests has direct application to primary research and ongoing development projects. The mission of the MRPTS is water quality improvement of

artesian flowing net-alkaline ferruginous lead-zinc mine waters by decreasing metals concentrations through precipitation and sequestration as hydroxide, oxide, sulfide, or carbonate minerals to the criteria continuous concentrations recommended by USEPA's National Recommended Water Quality Criteria (EPA 1986).

This site was selected for the intensive performance analysis of the oxidative unit as it was designed to be a long-term ecological engineering research site, represents the implementation of a full-sized passive treatment system, and presents the challenges associated with long term operation and maintenance. The MRPTS was designed based on the current approach for treating net-alkaline ferruginous lead-zinc mine waters with the passive strategy (Younger et al 2002; Cravotta 2007) The challenges of balancing optimized system function with land availability led to design modifications including a uniquely shaped oxidative unit with a layout that accommodates a compromise between system form and function with large scale equipment accessibility.

The MRPTS is sized in accordance with the relationships between analyte mass loading, and the kinetics of contaminant removal based on surface water chemistry. The available area of 3.6 ha is framed by private landowners in addition to a natural gas pipeline corridor, with approximately <1.5 ha reserved for the system itself (Nairn et al. 2009). Table 1.2 summarizes a four-year survey of water quality and quantity measurements from Mayer Ranch AMD seeps (2004-2008) to determine treatment system design features including: (1) treatment cell type, (2) cell order and placement within the treatment system, (3) treatment cell size (surface area), (4) bathymetry of cell design, and (5) hydraulic retention time (HRT) for each cell and the full system (Nairn et al. 2010). Figure 1.1 is an aerial photo of the treatment system layout after startup in November 2008, while Table 1.3 summarizes cell size and function for each treatment process unit. The location of the system in its particular region / climate also makes

it an ideal research site for determining how storm-induced and seasonal removal dynamics impacts passive treatment success indicators such as effluent water quality.

The AMD emerges at Mayer Ranch from two exploratory bore holes (Seeps A and B) and a collapsed shaft (Seep D). All three seeps are within close proximity to each other and are likely supplied by the same source based on the consistency between influent seep water quality data; thus, only flow adjusted average seep data are represented. Reducing conditions prior to surface discharge maintain the dissolved metals species in solution until surface conditions favor oxidative processes supporting the precipitation of iron oxyhydroxides. Prior to the construction of the Mayer Ranch Passive Treatment System, a cattail marsh served to mitigate impacts of AMD on the stream tributary as it promoted conditions for the oxidation and hydrolysis of iron to form iron oxyhydroxides (35% natural attenuation of loaded total iron – see Table 1.2). Trace metals like As, Zn, Pb, Ni, and Cd have been observed to sorb to iron oxide precipitates, resulting in a fraction of these constituents being removed from solution as the iron settles out of the water column. The water quality of the receiving tributary indicates that it was impacted by AMD before the confluence of flow from Mayer Ranch, yet the addition of Mayer Ranch water further reinforced the impact with elevated metals concentrations, turbidity, and a decrease in pH and dissolved oxygen.

The Mayer Ranch Passive Treatment System was constructed in 2008 to remediate the AMD from the seeps before it reaches the tributary steam, thus reducing the metals loading and impact on the downstream ecosystems.

Table 1.2: Water Quality Parameters That Influenced the Design of the Mayer Ranch Passive Treatment System: mean concentration ± standard deviation impacting the tributary

Total Metals	units	Mean of AMD Seeps	Mayer Ranch Weir	Tributary Upstream from Future PTS	Tributary Downstream from Future PTS
Iron	mg/L	192 ± 10	124 ± 67	11.1 ± 19.0	92.2 ± 68.2
Zinc	mg/L	9.78 ± 1.01	8.57 ± 4.80	8.09 ± 6.27	8.85 ± 4.70
Nickel	mg/L	0.933 ± 0.055	0.703 ± 0.235	0.271 ± 0.219	0.565 ± 0.264
Cadmium	µg/L	15.1 ± 5.1	16.0 ± 14.2	27.4 ± 42.6	20.3 ± 25.6
Lead	µg/L	60.0 ± 14.0	46.0 ± 16.4	23.9 ± 15.9	39.4 ± 14.9
Arsenic	µg/L	66.1 ± 15.2	39.1 ± 12.0	BDL	40.3 ± 10.9

Dissolved Metals	units	Mean of AMD Seeps	Mayer Ranch Weir	Tributary Upstream from Future PTS	Tributary Downstream from Future PTS
Iron	mg/L	197 ± 9	65.8 ± 69.7	18.2 ± 24.0	43.6 ± 36.9
Zinc	mg/L	9.10 ± 0.61	4.97 ± 2.79	8.08 ± 02.95	7.01 ± 2.69
Nickel	mg/L	0.963 ± 0.070	0.515 ± 0.274	0.298 ± 174	0.439 ± 0.227
Cadmium	µg/L	19.3 ± 13.0	9.33 ± 6.86	21.5 ± 9.6	13.8 ± 4.1
Lead	µg/L	75.8 ± 10.6	45.0 ± 16.4	34.3*	36.1 ± 6.5
Arsenic	µg/L	63.9 ± 6.6	BDL	BDL	BDL

Field Parameters	units	Mean of AMD Seeps	Mayer Ranch Weir	Tributary Upstream from Future PTS	Tributary Downstream from Future PTS
Cond	uS/cm	2949 ± 238	2509 ± 238	1581 ± 789	2365 ± 735
TDS	g/L	2.23 ± 0.18	1.9 5± 0.49	1.17 ± 0.53	1.78 ± 0.55
Salinity	ppt	1.88 ± 0.03	1.03 ± 0.58	1.08 ± 0.48	1.08 ± 0.48
DO_{Sat}	%	11.9 ± 16.0	26.4 ± 19.0	77.3 ± 32.8	47.9 ± 24.2
DO	mg/L	1.13 ± 1.52	2.60 ± 1.90	7.67 ± 1.90	4.84 ± 2.70
pH	--	5.94 ± 0.06	6.12 ± 0.18	6.70 ± 0.36	6.18 ± 0.22
Flow	L/min	126 ± 130	1310 ± 2005	868 ± 1217	1937 ± 2090
Turbidity	NTU	6.66 ± 6.17	6.72 ± 6.22	17.7 ± 6.6	26.7 ± 9.6
Sulfate	mg/L	2218 ± 427	1621 ± 755	1621 ± 765	1416 ± 752
Alkalinity	mg/L $CaCO_3$ eq.	405 ± 15	298 ± 112	122 ± 47	250 ± 103

*single value above the detection limit for the dataset

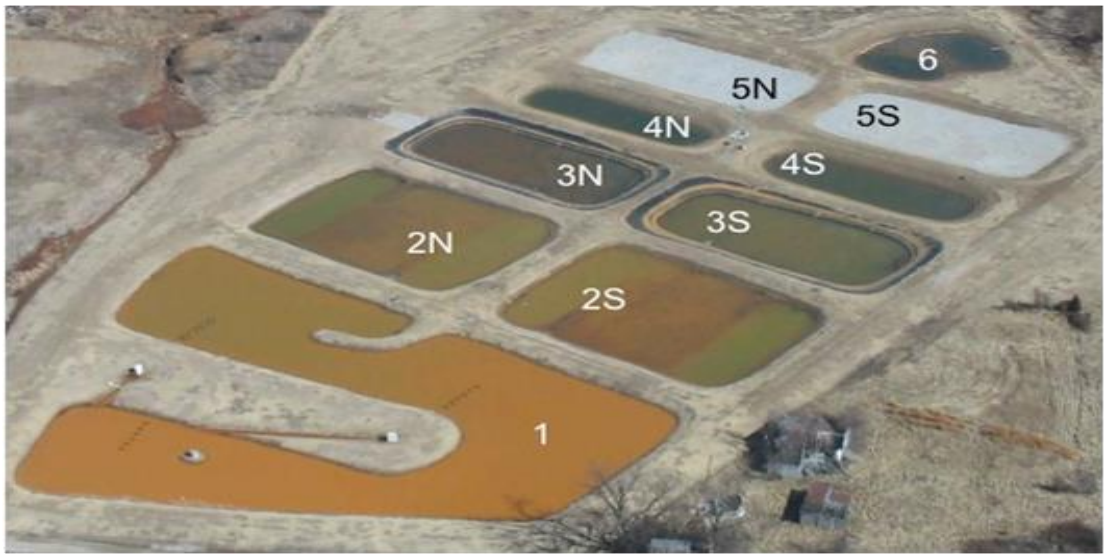

Figure 1.1: Mayer Ranch Passive Treatment System (MRPTS) Cell Configuration with alpha numeric cell designations indicated: C1 (oxidation/sedimentation), C2N/S (surface flow wetlands), C3N/S (vertical flow bioreactors), C4N/S (re-aeration ponds), C5N/S (horizontal flow limestone beds), and C6 (polishing wetland for consolidated flow prior to effluent discharge to an unnamed tributary of Tar Creek). Photo from February 2009.

Table 1.3: Mayer Ranch Passive Treatment System Summary of Cell Form and Function (Design) with hydraulic retention times per unit in parallel trains (for half of the influent flow)

Cell(s)	Cell Description	Targeted Parameter	Surface Area (m^2)	Design Retention Time
1	Preliminary Iron Oxidation and Sedimentation Basin	Fe, trace metals sorption	4084	7.7 days
2(N/S)	Surface Flow Wetlands (pond-marsh-pond design for additional iron oxidation and sedimentation)	Fe, solids retention, trace metals sorption	1685	3.4 days
3(N/S)	Vertical Flow Bio Reactors for metal sulfide formation under reducing conditions. Alkalinity Generation.	Zn, Pb, Ni, Cd	1027	3.1 days
4(N/S)	Re-Aeration solar versus wind aeration strategies	Oxygen Demand, Odor, H_2S	833	3.5 days
5(N/S)	Horizontal flow limestone beds facilitating additional zinc removal via Smithsonite precipitation ($ZnCO_3$).	Zn, Mn and hardness	1147	1.2 days
6	Polishing cell (pond-marsh-pond design) for flow consolidation and reaeration prior to discharge.	Residual solids	1096	0.8 days
		Complete System Retention Time		20 days

Construction of the MRPTS began in July of 2008, with rain-induced construction delays pushing system start-up to late November 2008. Flow control and consolidation structures were added to the three AMD seeps (A, B, and D) ensuring that system loading could be quantified. The preliminary oxidation cell (Cell 1) was designed based on the surface area-adjusted removal rate of 20 $g/m^2/day$ with 1.6 meters of vertical storage depth for accumulation and storage of iron oxides over time. The system is a cells-in-series / parallel design with gravity flow via a net elevation head change of 1.52 meters from system influent to effluent driving the hydrology. The cells alternate between oxidative and reductive processes and flows are recombined in a polishing cell (cell 6) prior to discharge into an unnamed tributary of Tar Creek (Figure 1.1). A storm water diversion structure diverts runoff from the surrounding area around the system ensuring that the source of the hydraulic load is only from the influent mine water seeps, and direct precipitation that falls on the surface area of the system.

MRPTS Performance Assessment

Sample Collection and Analysis Methodologies

The performance of the MRPTS was monitored over time by research team members with the University of Oklahoma Center for Restoration of Ecosystems and Watersheds (CREW) with respect to design expectations. Data presented are the results of these cooperative efforts. Water quality measurements (*in situ*) and grab samples were collected in 250-mL HDPE bottles monthly (2008 to 2010) and quarterly (2011 through 2015) for total metals, dissolved metals, and anions. Dissolved metals samples were prepared on site using 0.45-µm filters to remove particulates. The total and the dissolved metals samples were digested

following EPA Method 3015A and analyzed for Al, As, Ca, Cd, Co, Cr, Cu, Fe, K, Mg, Mn, Na, Ni, Pb, and Zn concentrations via inductively coupled plasma-optical emission spectroscopy (ICP-OES) following EPA Method 6010A. Turbidity was measured via triplicate grab samples with a Hach 2100P turbidimeter. Total alkalinity was measured via three replicate digital titrations with 1.6-N sulfuric acid and bromocresol green-methyl red indicator in the field (Hach Method 8203/APHA 2320). *In situ* water quality physical parameters (temperature (^{o}C), pH (su), conductivity (µS/cm), specific conductance (mS/cm), salinity (ppt), total dissolved solids (g/L), dissolved oxygen (mg/L and %), and oxidation-reduction potential (mV) were measured with a field-calibrated YSI 600 Series Sonde/650 MDS interface at the outflow of each treatment unit and for the three system influent seeps.

CREW operates under an EPA-approved Quality Management Plan and related Quality Assurance Project Plans. CREW quality assurance-quality control (QA/QC) protocols dictate instrument calibration, and field verification. Inclusion of duplicate, blank, and standard spike samples for all analyses are included in a suite of Standard Operating Procedures (SOPs). Chain of Custody (COC) forms identify, track, and document sample handling and analysis outputs throughout the laboratory testing process. Field equipment is serviced and calibrated before deployment to determine any performance issues, and then recalibrated on site to ensure accuracy by correcting for environmental influences. Total and dissolved metals samples are preserved with 2 mL of concentrated trace metal-grade nitric acid upon collection. Field duplicate and blank samples are collected for every 10 samples, and calibration checks to document drift are performed at the end of the sample collection period. Samples are transported on ice (4^{o} C) back to CREW laboratories for processing. Sample processing is monitored for random and systematic error with duplicate, blank, and standard spikes to assess matrix effects for positive / negative measurement bias. Samples analyzed in

the laboratory are also accompanied by a set of laboratory duplicate, blank, and standard spikes for every 10 samples collected to assess precision and accuracy of methodologies and instrumentation. Laboratory equipment is calibrated before each analysis, with verification standards and blanks placed into the sample analysis queue for every 10 samples. Yttrium (3 ppm) is used as an internal standard for all ICP-OES analyses as a correction for non-spectral interferences. Waste loadings from sample processing and analysis are documented alongside collection vessels that are managed by OU Environmental Health and Safety protocols and personnel.

MRPTS Performance

Table 1.4 is a summary of mean values ± standard deviation (σ) for each treatment cell type in the system with parallel cells averaged together for reporting purposes. The MRPTS has functioned in accordance with its objectives of metals removal and alkalinity generation over the first seven years of operation. The metals loaded into the passive treatment system are in the dissolved state, and are removed through the cooperative effort of oxidation/reduction reactions favored by individual cell design. Iron oxidation, hydrolysis, sedimentation, and accumulation within Cell 1 removes 73% of the total iron on average. The addition of Cell 2N/2S in series with Cell 1 removes approximately 95% of the iron load as iron oxyhydroxides (Figure 1.2). The average removal rate of iron within Cell 1 (19.0 ± 3.4 g Fe / m^2/day for 2009-2013) is consistent with the design rate of 20 g/m^2/day. The greatest variability in iron removal was observed in Cell 1 as indicated by the large standard deviation error bars in figure 1.2 and warrants a more detailed assessment for the optimization of the iron removal mechanism.

Table 1.4: Seven Year Average Performance Evaluation Summary for the Mayer Ranch Passive Treatment System (Average ± Standard Deviation) from 2009-2015 for select Total and Dissolved Metals concentrations as well as field measured parameters.

Total Metals	units	Influent	C1Out	2N/S	3N/S	4N/S	5N/S	C6Out
Iron	mg/L	169 ± 16	45.9 ± 38.1	7.94 ± 11.6	1.76 ± 2.43	1.17 ± 1.57	0.743 ± 1.12	0.510 ± 0.433
Zinc	mg/L	7.78 ± 0.74	6.20 ± 0.85	4.86 ± 1.76	1.02 ± 1.20	0.805 ± 1.18	0.530 ± 0.981	0.458 ± 0.879
Nickel	mg/L	0.895 ± 0.080	0.812 ± 0.080	0.733 ± 0.156	0.203 ± 0.222	0.174 ± 0.202	0.160 ± 0.210	0.160 ± 0.202
Cadmium	µg/L	17.8 ± 6.3	5.40 ± 5.06	2.19 ± 1.97	1.22 ± 0.42	1.07 ± 0.44	0.908 ± 0.249	1.05 ± 0.214
Lead	µg/L	73.7 ± 10.2	38.9 ± 15.0	27.8 ± 2.9	BDL	BDL	BDL	BDL
Arsenic	µg/L	59.5 ± 7.07	BDL	BDL	BDL	BDL	BDL	BDL

Dissolved Metals	units	Influent	C1Out	2N/S	3N/S	4N/S	5N/S	C6Out
Iron	mg/L	169 ± 9	29.1 ± 24.1	6.23 ± 13.8	1.47 ± 2.86	0.532 ± 0.959	0.250 ± 0.251	0.130 ± 0.144
Zinc	mg/L	7.88 ± 0.63	5.79 ± 0.87	4.63 ± 1.46	0.338 ± 0.724	0.473 ± 1.10	0.477 ± 1.11	0.438 ± 1.02
Nickel	mg/L	0.908 ± 0.051	0.796 ± 0.069	0.740 ± 0.103	0.188 ± 0.222	0.179 ± 0.223	0.165 ± 0.220	0.165 ± 0.213
Cadmium	µg/L	18.0 ± 7.6	4.09 ± 2.14	1.98 ± 1.40	1.08 ± 0.28	0.908 ± 0.353	0.928 ± 0.035	BDL
Lead	µg/L	75.6 ± 10.6	34.1 ± 6.9	27.8 ± 4.4	BDL	BDL	BDL	BDL
Arsenic	µg/L	61.7 ± 8.6	BDL	BDL	BDL	BDL	BDL	BDL

Parameters	units	Influent	C1Out	2N/S	3N/S	4N/S	5N/S	C6Out
Cond	uS/cm	2938 ± 198	2597 ± 646	2677 ± 747	2627 ± 750	2619 ± 739	2515 ± 782	2550 ± 747
TDS	g/L	2.21 ± 0.13	2.12 ± 0.11	2.08 ± 0.17	2.11 ± 0.18	2.08 ± 0.20	2.03 ± 0.32	2.05 ± 0.21
Salinity	ppt	1.79 ± 0.11	1.71 ± 0.10	1.67 ± 0.15	1.69 ± 0.15	1.67 ± 0.17	1.63 ± 0.26	1.64 ± 0.18
DO_{Sat}	%	17.6 ± 22.2	37.1 ± 30.9	90.5 ± 35.5	12.0 ± 14.9	37.0 ± 28.5	13.6 ± 17.3	35.7 ± 21.2
DO	mg/L	1.62 ± 1.85	3.79 ± 3.19	8.54 ± 3.17	1.29 ± 1.60	4.01 ± 3.33	1.50 ± 1.99	3.77 ± 2.52
pH	--	6.00 ± 0.14	6.05 ± 0.23	6.46 ± 0.36	6.80 ± 0.16	7.00 ± 0.20	6.95 ± 0.14	7.05 ± 0.19
Turbidity	NTU	7.59 ± 11.4	155 ± 116	44.7 ± 27.3	11.7 ± 10.6	39.9 ± 37.4	6.99 ± 6.55	26.4 ± 36.9
Sulfate	mg/L	2294 ± 565	2288 ± 265	2325 ± 454	2291 ± 704	2260 ± 628	2281± 643	2252 ± 611
Alkalinity	mg/L $CaCO_3$	385 ± 44	182 ± 43	151 ± 27	231 ± 76	215 ± 65	205 ± 53	200 ± 51

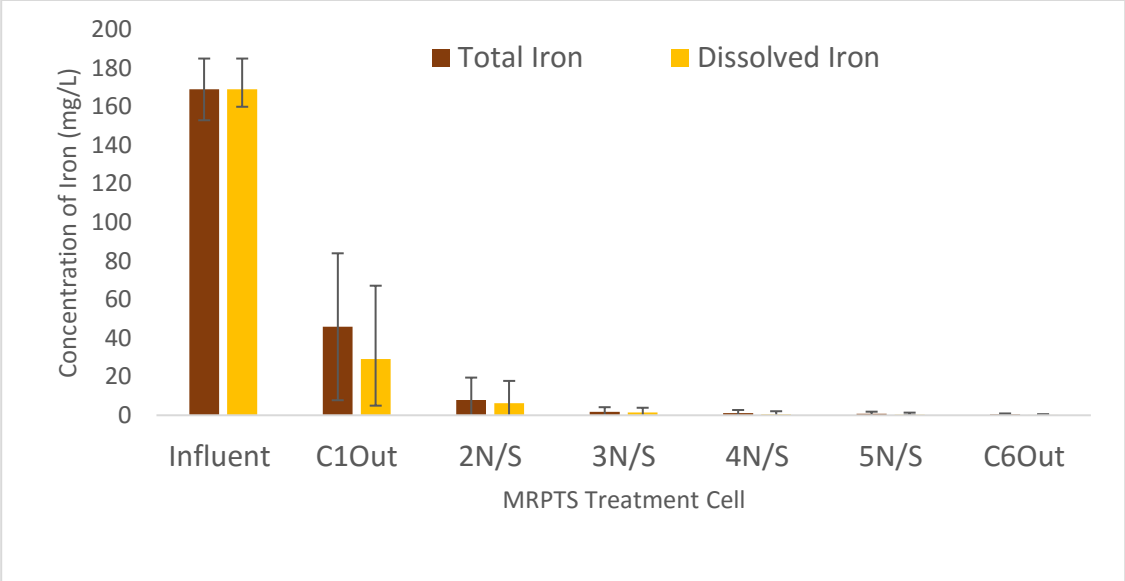

Figure 1.2: Total and Dissolved iron removal in the MRPTS with respect to treatment cell. Error bars indicate the standard deviation of the dataset.

Most trace metals are removed in the vertical flow bioreactors (VFBRs) per design of Cell 3N/S. Bacterial communities within the compost layer and the continuously flooded substrate maintain reducing conditions that favor the precipitation of trace metals as metal sulfides and sorption onto organic surfaces. Zinc loading into the passive treatment system is attenuated by 20% within Cell 1, and by 37% by Cell 2N/S effluent through iron sorption within the oxidative unit (Cell 1 + Cell 2N/S). Cadmium concentrations diminished by 70% within Cell 1, and by 88% by the effluent flow out of C2N/S. Lead concentrations decreased by 54% of the initial concentration within Cell 1 and 62% within the oxidative units (Cell 1 + C2N/S). Arsenic concentrations dropped below detection limits within Cell 1, indicating effective sorption to iron solids before reaching C2N/S. Alkalinity is consumed within the oxidative unit as iron oxidation and hydrolysis liberate latent acidity, yet additional alkalinity is generated within Cell 3N/S and maintained throughout the rest of the system (Cells 4N/S, 5N/S, and 6).

The impact of the passive treatment system on the water quality of the tributary stream is documented in Table 1.5. The removal of iron from the water column (oxidation, hydrolysis, and sedimentation) and retention (accumulation of sequestered precipitates) of metals within the passive treatment system yielded improved water quality in the tributary downstream from the passive treatment system for iron, zinc, nickel, cadmium, lead, and arsenic. The removal and storage of metals species from the Mayer Ranch seeps improves water quality through prevention of point source impacts, as well as through dilution of metals concentrations being transported within the tributary from upstream AMD loading. Although a primary function of the passive treatment system is removal and retention, it does export sulfate and hardness as total dissolved solids. Nairn et al. (2010) reported over the first-year performance of the passive treatment system including sulfate, hardness, and alkalinity export in addition to metals removal with performances consistent to the seven-year average. Labar et al. (2010) reported on tributary water quality improvement after one year of operation. Fish diversity and abundance surveys area currently underway to determine ecosystem-level effects of site-specific AMD remediation of surface water resources previously impacted by the Mayer Ranch seeps, with sunfish, darters, and largemouth bass being observed in the channel for the first time since the initial mine water discharge in 1979 (Franssen 2009; Bergey and White 2010; Sheppard et al 2014). Lessons learned from system performance, maintenance, and operations influence the design of future passive treatment systems within the same watershed.

Table 1.5: Mean (±standard deviation) Water Quality Impact of the Mayer Ranch Passive Treatment System on the Unnamed Tributary 2009-2015. (Continued on next page)

Total Metals	units	Tributary Upstream from PTS	MRPTS Effluent (C6Out)	Tributary Downstream from PTS
Iron	mg/L	46.3 ± 27.9	0.510 ± 0.433	18.5 ± 15.5
Zinc	mg/L	6.45 ± 2.37	0.458 ± 0.879	3.64 ± 02.01
Nickel	mg/L	0.385 ± 0.176	0.160 ± 0.202	0.247 ± 0.141
Cadmium	µg/L	13.7 ± 9.1	1.05 ± 0.214	6.32 ± 3.76
Lead	µg/L	38.1 ± 15.0	BDL	26.5 ± 3.52
Arsenic	µg/L	BDL	BDL	BDL

Dissolved Metals	units	Tributary Upstream from PTS	MRPTS Effluent (C6Out)	Tributary Downstream from PTS
Iron	mg/L	38.2 ± 24.6	0.130 ± 0.144	13.8 ± 11.4
Zinc	mg/L	5.90 ± 2.21	0.438 ± 1.02	3.20 ± 1.55
Nickel	mg/L	0.376 ± 0.163	0.165 ± 0.213	0.232 ± 0.115
Cadmium	µg/L	10.2 ± 5.3	BDL	4.60 ± 2.46
Lead	µg/L	37.8 ± 8.9	BDL	28.4 ± 2.2
Arsenic	µg/L	BDL	BDL	BDL

Field Parameters	units	Tributary Upstream from PTS	MRPTS Effluent (C6Out)	Tributary Downstream from PTS
Cond	µS/cm	2039 ± 791	2550 ± 747	2152 ± 787
TDS	g/L	1.63 ± 0.47	2.05 ± 0.21	1.77 ± 0.37
Salinity	ppt	1.30 ± 0.39	1.64 ± 0.18	1.41 ± 0.37
DO_{sat}	%	50.1 ± 29.5	35.7 ± 21.2	50.4 ± 29.1
DO	mg/L	5.00 ± 3.08	3.77 ± 2.52	5.29 ± 3.27
pH	--	6.32 ± 1.145	7.05 ± 0.19	6.55 ± 0.25
Flow	L/min	1126± 1954	430 ± 77	818 ± 988
Turbidity	NTU	44.6 ± 29.4	26.4 ± 36.9	42.3 ± 35.2
Sulfate	mg/L	1644 ± 518	2252 ± 611	1778 ± 474
Alkalinity	mg/L $CaCO_3$	182 ± 51	200 ± 51	167 ± 54

Conclusions

Mine drainage is an environmental problem that demands an interdisciplinary approach to fully understand the source, matrix, reactions and processes responsible for its fate and transport within a watershed. Passive treatment systems are integrated environmental biogeochemical reactors designed to optimize conditions favoring the precipitation and retention of metals, acidity neutralization, and alkalinity generation. Biotic and abiotic processes such as oxidation, hydrolysis, precipitation, sedimentation, phytoremediation,

limestone dissolution, and bacterial sulfate reduction each contribute to overall system performance and are influenced by design-phase choices. The MRPTS is an example of full-scale design and implementation of passive treatment technology based on the current monitoring, sizing, and engineering practices. The MRPTS has met its performance objectives of metals removal and alkalinity generation over the first seven years of operation resulting in quantitative improvements in surface water quality. Environmental indicators including fish species diversity and abundance further illustrate the qualitative aspects of long-term impact attenuation through maintained system operation. The MRPTS demonstrates the successful application of passive treatment to AMD impacted waters previously unaddressed under CERCLA Operable Unit 1 within the Tar Creek Superfund Site. Investigation and documentation of system design, construction, operation, and maintenance influences on performance will serve as a guide for the success of future systems.

Influent / effluent monitoring of passive treatment systems gives an overall assessment of function, yet lacks the resolution needed for system optimization based on individual treatment processes. Comparing iron mass loadings into a cell with the mass export of iron out the cell to calculate removal efficiencies provides insight into the function of individual treatment cells. Yet, one must look beyond the "black box" approach to systems monitoring to evaluate how spatial and temporal aspects of removal within a treatment cell relate to removal efficiency and ultimately design. In the next few chapters, progressive iron removal, accumulation and storm induced transport will be discussed

Literature Cited

Bergey E, and J. White. 2010. Mine Effluent Effects on the Macroinvertebrates and Habitat in a Small Stream in the Tar Creek Watershed (Ottawa County, Oklahoma). Proc. Okla. Acad. Sci. 90: pp 11-26

Blowes DW, Ptacek CJ, Jambor JL, Weisener CG, Paktunc D, Gould WD, Johnson DB. 2013. The Geochemistry of Acid Mine Drainage. *Treatise Geochemistry*, Second Ed. 11:131–190.

Champagne P, Van Geel P, Parker W. 2005. A bench-scale assessment of a combined passive system to reduce concentrations of metals and sulphate in acid mine drainage. Mine Water Environ. 24:124–133.

Christenson, S.C., Parkhurst, D.L., and Fairchild, R.W., 1994, Geohydrology and water quality of the Roubidoux aquifer, northeastern Oklahoma: Oklahoma Geological Survey Circular 96, 70 p

Cravotta CA. 2008. Dissolved metals and associated constituents in abandoned coal-mine discharges, Pennsylvania, USA. Part 2: Geochemical controls on constituent concentrations. Appl. Geochemistry 23:203–226.

Demchak J, Morrow T, Skousen J. 2001. Treatment of acid mine drainage by four vertical flow wetlands in Pennsylvania. Geochemistry Explor. Environ. Anal. 1:71–80.

Flanagan NE, Mitsch WJ, Beach K. 1994. Predicting metal retention in a constructed mine drainage wetland. Ecol. Eng. 3:135–159.

Franssen, C.M.2009. The Effects of Heavy Metal Mine Drainage on Population Size Structure, Reproduction, and Condition of Western Mosquitofish, *Gambusia affinis.* Arch Environ Contam Toxicol 57: 145.

Gazea B, Adam K, Kontopoulos A. 1996. A review of passive systems for the treatment of acid mine drainage. Miner. Eng. 9:23–42.

Gleisner M, Herbert RB, Frogner Kockum PC. 2006. Pyrite oxidation by *Acidithiobacillus ferrooxidans* at various concentrations of dissolved oxygen. Chem. Geol. 225:16–29.

Hall GH, Puhlmann T. 2005. Spatial distribution of iron oxidation in the aerobic cells of the Wheal Jane Pilot Passive Treatment Plant. Sci. Total Environ. 338:73–80.

Hedin RS. 2008. Iron removal by a passive system treating alkaline coal mine drainage. Mine Water Environ. 27:200–209.

Hedin RS, Nairn RW. 1992. Designing and Sizing Passive Mine Drainage Treatment Systems. U.S. Bureau of Mines, Pittsburgh Research Center

Jarvis AP, Younger PL. 2001. Passive treatment of ferruginous mine waters using high surface area media. Water Res. 35:3643–3648.

Jennings SR, Blicker S, Neuman P, Dennis R. 2008. Acid mine drainage and effects on fish health and ecology: a review. , 2008. Reclam. Res. Gr. 1:1–26.

Johnson DB, Hallberg KB. 2005. Acid mine drainage remediation options: A review. Sci. Total Environ. 338:3–14.

Kirby CS, Cravotta CA. 2005. Net alkalinity and net acidity 2: Practical considerations. Appl. Geochemistry 20:1941–1964.

Labar JA, Nairn RW, Strevett KA, Strosnider WH, Morris D, Neely CA, Garrido AE, Kauk K. 2010. Stream water quality improvements after installation of a passive treatment system. Jt. Min.

Reclam. Conf. 2010 - 27th Meet. ASMR, 12th Pennsylvania Abandon. Mine Reclam. Conf. 4th Appalach. Reg. Refor. Initiat. Mined L. Refor. Conf. 1:525–535.

Lenoble V, Bouras O, Deluchat V, Serpaud B, Bollinger J-C. 2002. Arsenic adsorption onto pillared clays and iron oxides. J. Colloid Interface Sci. 255:52–58.

Mitsch, W., Wise, K.M. 1998. Water quality, fate of metals, and predictive model validation of a constructed wetland treating acid mine drainage. Water Res. 32, 1888–1900.

Nairn, R.W, T. Beisel, R. Thomas, J. LaBar, K. Strevett, D. Fuller, W. Strosnider, W. Andrews, J. Bays, and R. Knox. (2009). Challenges in Design and Construction of a Large Multi-Cell Passive Treatment System for Ferruginous Lead-Zinc Mine Waters. Proceedings America Society of Mining and Reclamation, pp 871-892

R. W. Nairn, J. A. LaBar, K. A. Strevett, W. H. Strosnider, D. Morris, A. E. Garrido, C. A. Neely, K. Kauk. 2010. Initial Evaluation of a Large Multi-Cell Passive Treatment System for Net-Alkaline Ferruginous Lead-Zinc Mine Waters . Proceedings America Society of Mining and Reclamation, pp 635-649

Nemati M, Harrison STL, Hansford GS, Webb C. 1998. Biological oxidation of ferrous sulphate by *Thiobacillus ferrooxidans*: A review on the kinetic aspects. Biochem. Eng. J. 1:171–190.

Datin, D.2015. Oklahoma Department of Environmental Quality: Tar Creek Superfund Site. <http://www.deq.state.ok.us/lpdnew/SF/Superfund Summaries/TarCreek.html> Accessed 2016 Sep 11.

Sapsford DJ, Williams KP. 2009. Sizing criteria for a low footprint passive mine water treatment system. Water Res. 43:423–432.

Scheibach RB, Williams RE, Genes BR, Jarman R. 1983. Controlling acid mine drainage from the Picher Mining District, Oklahoma. Ground Water 21:225-250

Sheppard MI. 1993. Heavy Metals in the Environment.Journal of Environment Quality. Vol. 22. p. 213.

Shepherd, N. Matthews, W. Nairn, RW. Barkstedt, J. Franssen, N.2014. Fishes of a Contaminated Stream After Operation of a Passive Treatment System. Proceedings America Society of Mining and Reclamation

Skousen J. 1997. Overview of passive systems for treating acid mine drainage. Green Lands 27:34–43.

Skousen J, Ziemkiewicz P. 2005. Performance of 116 passive treatment systems for acid mine drainage. Proceedings, Am. Soc. Min. Reclamation, Breckenridge, CO:1100–1133.

Stark LR, Williams FM. 1995. Assessing the performance indices and design parameters of treatment wetlands for H^+, Fe, and Mn retention. Ecol. Eng. 5:433–444.

Swedlund PJ, Webster JG, Miskelly GM. 2009. Goethite adsorption of Cu(II), Pb(II), Cd(II), and Zn(II) in the presence of sulfate: Properties of the ternary complex. Geochim. Cosmochim. Acta 73:1548–1562.

Tarutis WJ, Stark LR, Williams FM. 1999. Sizing and performance estimation of coal mine drainage wetlands. Ecol. Eng. 12:353–372.

US Environmental Protection Agency. 2016a. Superfund: CERCLA Overview. [accessed 2016 Sep 11]. <https://www.epa.gov/superfund/superfund-cercla-overview>

US Environmental Protection Agency. 2016b. USEPA: Site Information for Tar Creek (Ottawa Co). [accessed 2016 Sep 11. <https://cumulis.epa.gov/supercpad/>

Watzlaf GR, Schroeder KT, Kleinmann RLP, Kairies CL, Nairn RW, Street WB. 2004. The Passive Treatment of Coal Mine Drainage. :1–72. DOE/NETL-2004/1202

Younger PL.2002. Mine Water: Hydrology, Pollution, Remediation. Vol 5. Alloway, Brian; Trevors J, editor. Springer-Science+Business Media, BV.pp 27-49

Zipper CE, Skousen JG. 2010. Influent water quality affects performance of passive treatment systems for acid mine drainage. Mine Water Environ. 29:135–143.

Chapter 2: Spatial Profiling of Seasonally Influenced Iron Removal Rates in an Oxidative Treatment Cell

Introduction

For net-alkaline discharges, oxidative treatment via a oxidation pond/ sedimentation basin / aerobic surface flow wetland is the recommended approach to remove and store large quantities of precipitated iron oxyhydroxides (Hedin et al 1994; Watzlaf et al. 2004; Kadlec and Wallace 2009). Iron oxidation, hydrolysis, precipitation, and sedimentation are the key processes promoted within passive treatment oxidation cells and are critical in defining the rate of removal and quantity of precipitate retained over time (Nordstrom 2011; Blowes et al. 2013). Iron oxidation converts dissolved iron (II) to iron (III) in the presence of dissolved oxygen (Equation 2.1). Under alkaline condition, the newly formed iron (III) readily undergoes hydrolysis with water to form a precipitate (Equation .2.2). Flocculation and sedimentation of the iron oxyhydroxide occurs and the solids are retained within the system (Younger 2002).

$$4Fe^{2+} + O_2 + 4H^+ \rightarrow 4Fe^{3+} + 2H_2O \quad \text{(Equation 2.1)}$$

$$Fe^{3+} + 3H_2O \rightarrow Fe(OH)_{3(s)} + 3H^+ \quad \text{(Equation 2.2)}$$

The removal of dissolved iron from solution via precipitation follows first-order kinetics with respect to iron concentration and is dependent on both heterogeneous and homogeneous mechanisms (Stumm and Sulzberger 1992; Younger 2000; Barnes et al. 2009). Passive treatment oxidative cells feature high water surface areas, extended hydraulic retention times, and storage volume for retained solids. Aeration structures are often included in the design to maintain oxidative conditions; as oxidation is the rate-determining step for iron removal (Singer and Stumm, 1970; Eggleston et al. 1996; Dempsey et al. 2001). For physical removal, the rate of sedimentation is dependent on floc size and density and can be described

using a modified version of Stokes Law to account for non-spherical particles (Chakraborti and Kaur 2014).

Performance assessment is a reactive strategy to investigate treatment system operation and maintenance practices on a case by case basis. This strategy is used to refine system designs for future projects, but can also be used to retrofit existing designs for select performance deficiencies. One practice to assess metals removal efficiency of a treatment system, unit, or cell is to measure the difference between influent and effluent metals concentrations and mass loadings (Equation 2.3) (Wieder 1989). However, this is not currently used as an effective metric for performance assessment. Rather, surface area adjusted removal efficiency (Equation 2.4) accounts for analyte loadings rather than concentrations (Hedin and Nairn 1992), and the first order removal (k_1 in m/day) has been derived by Tarutis et al. 1999(Equation 2.5).

$$\text{Treatment Efficiency (\%)} = (C_{in}-C_{out})/C_{in} \times 100 \qquad \text{(Equation 2.3)}$$

$$\text{Area-adjusted Removal (g m}^{-2}\text{ day}^{-1}\text{)} = (C_{in}-C_{out})Q/A \qquad \text{(Equation 2.4)}$$

$$\text{First-order removal (m day}^{-1}\text{)} = Q/A \ln (C_{in}-C_{out}) \qquad \text{(Equation 2.5)}$$

These performance indicators are limited in that they may not represent spatial and temporal variability within a treatment cell (Wieder 1993). A survey of removal efficiency and area-adjusted removal rates with respect to position within a treatment cell will yield an enhanced mechanistic understanding of cell function within design (cell shape) and environmental (seasonal) constraints. The spatial distribution of total and dissolved metal concentrations with respect to the variables driving oxidation and hydrolysis rates (dissolved oxygen, pH, and temperature) will reveal the location of the dominant processes supporting optimal iron removal efficiency. This approach will provide essential insight into how the design of the

treatment cell may be refined to optimize processes favoring iron removal and retention in the existing design, as well as insight into the design of future passive treatment systems in the region. The iron removal performance evaluation of the preliminary oxidation cell of a full-scale passive treatment system will describe the progressive iron removal within the cell rather than just assess performance based on influent/effluent monitoring. Progressive iron removal is documented through the collection of intracellular total and dissolved metals samples and *in situ* physicochemical measurements to assess $[Fe^{2+}]/[Fe^{3+}]$ ratios within the water column. Removal is achieved as precipitated iron (III) oxyhydroxides settle within the water column for long term storage before reaching the effluent of the treatment cell. The determination of how dissolved/particulate ratios and total iron mass loading change with position and season in the preliminary treatment cell will provide insight into how the design of the treatment cell relates to its intended function of removal and retention of solids.

Methods

Site Description

The Mayer Ranch Passive Treatment System at the Tar Creek Superfund Site near Commerce, OK was constructed in 2008, and was fully operational by January of 2009. The system was designed with a U-shaped oxidation pond (Cell 1) as the primary treatment step for three AMD discharges with a combined average flow of 400±63 L/min (n= 28; 2009-2013). Cell 1 has a surface area of 4048 m^2 and was designed based on a 20 $g/m^{-2}/day^{-1}$ removal rate and a hydraulic retention time of 7.7 days. Previous work at this site had determined that Cell 1 has an average iron removal rate 20 $g/m^{-2}/day^{-1}$ over the first year of operation (Nairn et al. 2009) and an average of 19.0 $g/m^{-2}/day^{-1}$ for the first five years of operation (2009-2013) based on influent/effluent grab sampling.

Sampling locations were selected based on physical features of the design, like points of flow restriction and curvature resulting in a change of flow direction. Figure 2.1 features an aerial photograph of Cell 1 with sample locations indicated. Progressive iron removal and storage patterns with increased distance from the AMD source of influent flow (horizontal component) as well as water quality changes with increased water depth (vertical component) were evaluated based on these locations.

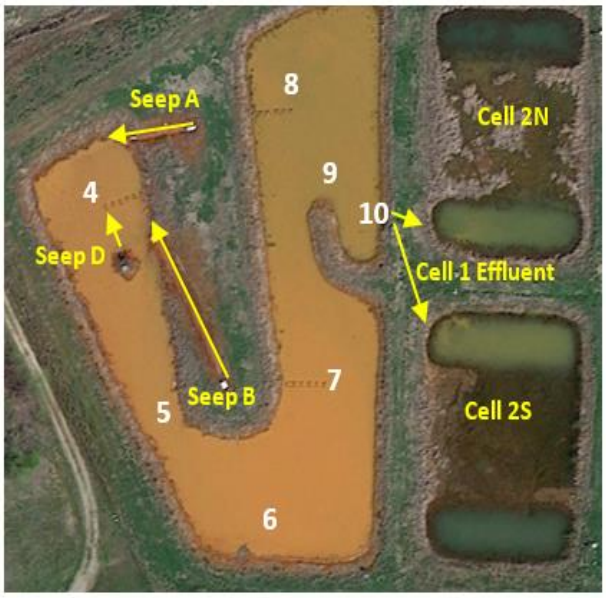

#	Location	Sample Type
1	Seep A	
2	Seep B	Grab from Source
3	Seep D	
4	Catwalk 1	Stabilized, vertical profile: Surface, 0.5,1.0,1.5m depths
5	Bottleneck	Grab with Pole (0.5m depth)
6	U-Bend	Grab with Pole (0.5m depth)
7	Catwalk 2	Stabilized, vertical profile: Surface, 0.5,1.0,1.5m depths
8	Catwalk 3	Stabilized, vertical profile: Surface, 0.5,1.0,1.5m depths
9	C1 Effluent	Grab with Pole (0.5m depth)
10	C1 Agridrain	Grab/Pole from Agridrain/Perforated Pipe

Figure 2.1: Cell 1 progressive iron profile sample locations with corresponding sample types collected at each location. Influent and effluent flows noted with yellow arrows.

Sampling

Cell 1 was divided into three sections based on visual inspection from aerial photographs. These divisions were for sampling protocol only and did not represent any real type of boundary or separation within the cell itself. Section 1 consists of the area in which all three mine water discharges enter the system (Seeps A, B, and D), and are assumed to be readily mixed prior to flowing through a narrow portion of the treatment cell (bottleneck) into Section 2. Section 2 is characterized by the large U-bend on the farthest south side of the system. Section 3 is designated as the final section of Cell 1 that includes the effluent discharge to the

parallel treatment trains. Each section includes a catwalk sampling structure (visible in Figure 2.1) that allows one to collect samples without extraneous disturbance to the water column or sediment deposits. The estimated distance of each sample location from where the influent seeps flow into the passive treatment cell are summarized in Table 2.1.

Table 2.1: Distance from Influent AMD Discharges to progressive profile locations and the corresponding HRT as derived from the design time of 7.7 days for Cell 1

Sample locations →	4	5	6	7	8	9	10
Distance from AMD Source (Linear Meters)	21.9*	60.9	88.9	118	170	186	202
Timing based on Design HRT (Days)	0.83	2.32	3.39	4.50	6.48	7.09	7.70

*average linear distance from seeps A, B, D averaged to location 4

Measurements and samples were collected at each location over a three-year period (July 2009-April 2012) to evaluate iron removal profiles with respect to season (i.e., temperature) as water levels permitted. Catwalks facilitated sample collection for the evaluation of the vertical component of the profile with increasing depths (surface, 0.5, 1.0, and 1.5 meters) from the edge of each catwalk structure. Vertical water column samples were collected using a discrete horizontal sampler common in limnological studies to capture samples with increasing depth in the water column. Samples were collected starting from the surface, working towards increasingly deeper samples in order to prevent any unnecessary disturbance to the water column. *In-situ* measurements included pH, temperature (^{o}C), specific conductance (mS/cm), dissolved oxygen (%Sat), and oxidation-reduction potential (mV).

Sample Analysis

Total metals, dissolved metals, and anion grab samples were collected at each location. The dissolved metal samples were filtered using a hand-pump apparatus through 0.45-μm filter

cartridges for each sample. Turbidity (NTU) was determined on-site using a Hach 2100P Portable Turbidimeter and the average of three replicate measurements was recorded. Total alkalinity (mg/L as $CaCO_3$ eq.) was determined in the field immediately following sample collection via use of a Hach digital titrator with 1.6-N H_2SO_4 titrant and bromocresol green / methyl red indicator (APHA 1992). All samples were acidified with concentrated trace-metal grade nitric acid and then kept on ice for transport back to the Center for Restoration of Ecosystems and Watersheds (CREW) laboratory for analysis. Anion samples were promptly filtered and run in serial dilution on the MetrOhm 761 Compact Ion Chromatograph (EPA 300) to determine total sulfate concentration (mg/L). The metal samples underwent aqueous digestion using the CEM MARS in accordance with the standard operating procedure (EPA Method 3051). The digested samples were analyzed with a Varian-Vista PRO Inductively Coupled Plasma Optical Emission Spectrometer (ICP-OES) following EPA Method 6010 for total and dissolved metals concentrations. Appropriate QAQC procedures were observed during sample preparation as well as sample analysis to verify instrument calibration and evaluate field and laboratory practices via standard operating procedures and laboratory specific protocols.

Seasonal profile samples were collected quarterly (January = winter; April = spring; July = summer, and October = fall). Seasonal profiles were averaged (n = 3) for performance evaluation. Suspended iron floc samples were collected *in situ* with increasing depth (without nitric acid preservation) at each catwalk sampling location (sites 4, 7, 8). The floc samples were used to physically assess the average size, shape, and distribution of settling solids via laser in situ scattering and transmissometry (LISST), and were accompanied by grab sample turbidity measurements.

Results and Discussion

Influent / Effluent Performance Evaluation

The influent/effluent total metals water quality data for Cell 1 (2009-2013) are summarized in Table 2.2, while Table 2.3 summarizes *in situ* average water quality parameters.

Table 2.2: Total Metals Removal by the MRPTS Preliminary Oxidation Cell (Cell 1) 2009-2013

Influent Average (n=3)	**Iron (mg/L)**	**Zinc (mg/L)**	**Nickel (mg/L)**	**Cadmium (µg/L)**	**Lead (µg/L)**	**Arsenic (µg/L)**
Average	174	7.99	0.917	18.3	74.8	61.5
Standard Deviation	8	0.49	0.058	6.36	10.1	4.27
%RSD	4.6	6.20	6.30	34.9	13.6	7.0
Minimum	161	6.94	0.792	8.00	57.5	53.9
Maximum	190	9.06	1.04	31.0	96.5	72.2
Range	29	2.12	0.25	23.0	39.0	18.3
n	28	28	28	28	28	28
Cell 1 Effluent	**Iron (mg/L)**	**Zinc (mg/L)**	**Nickel (mg/L)**	**Cadmium (µg/L)**	**Lead (µg/L)**	**Arsenic (µg/L)**
Average	34.7	6.25	0.827	4.10	33.3	BDL
Standard Deviation	23.0	0.83	0.711	2.47	8.85	BDL
%RSD	66.1	13.3	8.59	60.4	26.6	BDL
Minimum	4.8	4.63	0.641	0.878	23.7	BDL
Maximum	93.7	7.49	0.947	8.93	56.2	BDL
Range	88.9	2.86	0.306	8.05	32.5	BDL
n	31	31	31	27	19	27
Performance Summary	**Iron (mg/L)**	**Zinc (mg/L)**	**Nickel (mg/L)**	**Cadmium (µg/L)**	**Lead (µg/L)**	**Arsenic (µg/L)**
Change in Concentration	139	1.75	0.09	14.15	41.44	61.54
Removal Efficiency (%)	80.0%	21.9%	9.8%	77.6%	55.4%	100.0%

The decreases in lead, cadmium, and zinc concentrations are likely due to sorption onto the iron solids that are retained in the system, and not a result of direct precipitation of either of these metals in the form of a hydroxide due to solubility constraints at this pH (Cornell and Schwertmann 2004; Cravotta 2008). Arsenic is completed removed to below practical quantification limits within the preliminary oxidation cell likely through sorption (Lenoble et al. 2002; Casiot et al. 2005). The initial alkalinity of the mine drainage is elevated due to the

dissolution of dolomitic limestone in the site host rock increasing the concentration of HCO_3^- in the influent AMD. The dramatic decrease in alkalinity observed in the Cell 1 effluent sample results from the neutralization of the latent acidity that is released as iron is oxidized and hydrolyzed (equations 2.1 and 2.2). Sulfate concentrations did not demonstrate significant change within Cell 1, which is expected based on the oxidizing function of this component of the treatment system. The performance of Cell 1 for the removal efficiency and storage of iron oxides (80% or 19.8 g Fe /m^2/day) with some partial secondary removal of trace metals is consistent with the expected performance based on observations from the long-term monitoring of passive treatment systems (Manceau et al. 1992; Ziemkiewicz et al. 2003; Matthies et al. 2010). Removal rates have demonstrated seasonality but there are conflicting reports as to the whether the source of that variance is due to load limiting via fluctuations in flow rate (Manyin et al. 1997; Matthies et al. 2010) or from the impact of temperature on reaction kinetics and dissolved gas species solubility (Hedin et al. 2013).

The influent seeps supply the MRPTS with an average load of 100 kg/day of total iron predominantly in the dissolved Fe^{2+} oxidation state (97% of loaded iron is dissolved Fe^{2+}). Over the five-year monitoring period (2009-2013), there was only a 5% relative standard deviation (%RSD) in the concentration of iron measured in the seep discharge indicating that loading is governed by variance in flow to the system rather than acute changes in the mine pool chemistry. The statistical comparison of annual and seasonal average flow rates to the five-year average (400±68 L/min) is summarized in Table 2.4

Table 2.4: Statistical Analysis (Two Tailed t-Test) of Oxidative Unit Flow Rate with Respect to the Average Flow Rate (2009-2013)

	Avg (L/min)	Stdev (L/min)	%RSD	n	t	t Critical two-tail	Stat. Sig. with Respect to the 5 Year Mean
(2009-2013)	399	68	17.1	28	--	--	--
2009	410	45	11.0	12	-0.593	2.040	Not Significant
2010	463	29	6.3	7	-3.761	2.064	Significant
2011	344	29	8.4	3	2.646	2.571	Significant
2012	370	89	23.9	3	0.561	4.303	Not Significant
2013	293	52	17.6	3	3.276	3.182	Significant
Spring	461	34	7.3	7	-3.377	2.086	Significant
Summer	391	45	11.6	7	0.391	2.145	Not Significant
Fall	346	66	19.2	6	1.767	2.365	Not Significant
Winter	393	76	19.4	8	0.214	2.228	Not Significant

*Spring – March, April, May; Summer = June, July, August; Fall = Sept, Oct, Nov; Winter = Dec, Jan, Feb

The annual average influent flow rate for the MRPTS was significantly higher during 2010 than the five-year average, while the flow rates for 2011 and 2013 were significantly lower than the five-year average flow. Seasonal impact on flow only appears to have a significant difference with respect to the five-year average for spring (March, April, May) in which higher flow than average is typically observed. The %RSD for the average iron concentrations measured in the effluent flow of Cell 1 over the same five-year period of performance evaluation demonstrated less consistency (66%RSD for total iron; 83%RSD for the dissolved fraction) than the influent concentrations. This indicates that removal efficiency may demonstrate seasonal effects as observed in AMD-impacted streams and other passive treatment system installations (August et al. 2002; Butler et al. 2008, Hedin 2008).

Progressive Iron Removal Profile

The average progressive iron removal profile for Cell 1 of the MRPTS (Figure 2.2) indicates the change in total and dissolved iron concentrations relative to position within the treatment cell.

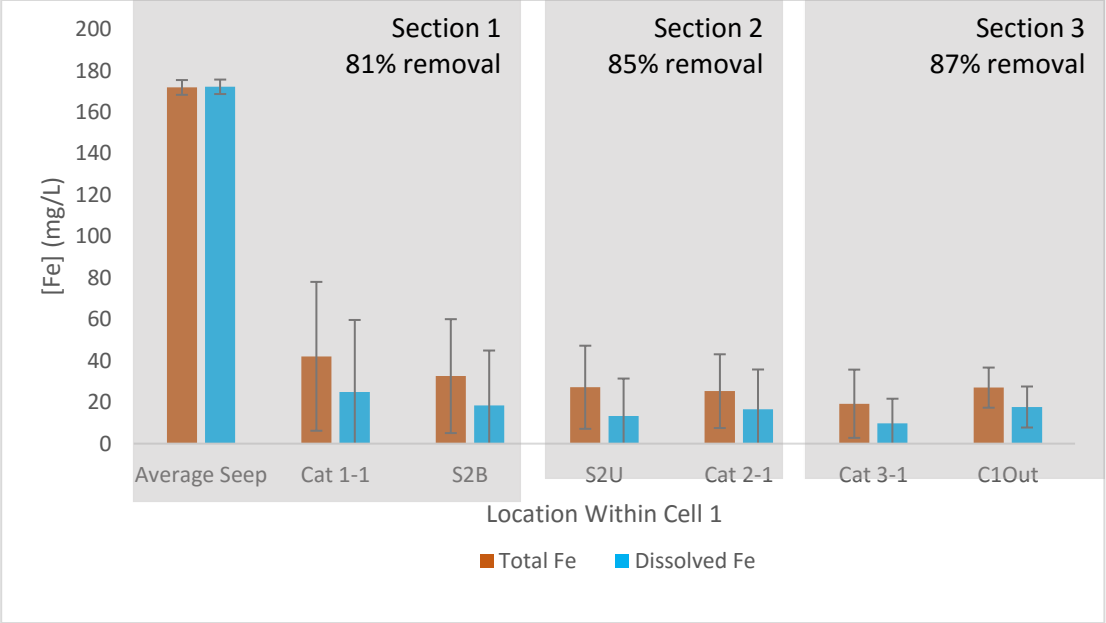

Figure 2.2: Average progressive iron removal profile for Cell 1 of the Mayer Ranch Passive Treatment System based on sample location for 2009-2012 (n = 12 profiles) with ± standard deviation error bars. Percentages are removal efficiencies that summarize the relative removal of iron as water progresses through the cell.

The majority (87% of iron removal within Cell 1, and 81% of removal based on influent loading) is removed from the water column in the first operationally-defined section. Total and dissolved average iron concentrations were plotted versus the approximated HRT for each location in Figure 2.3.

.

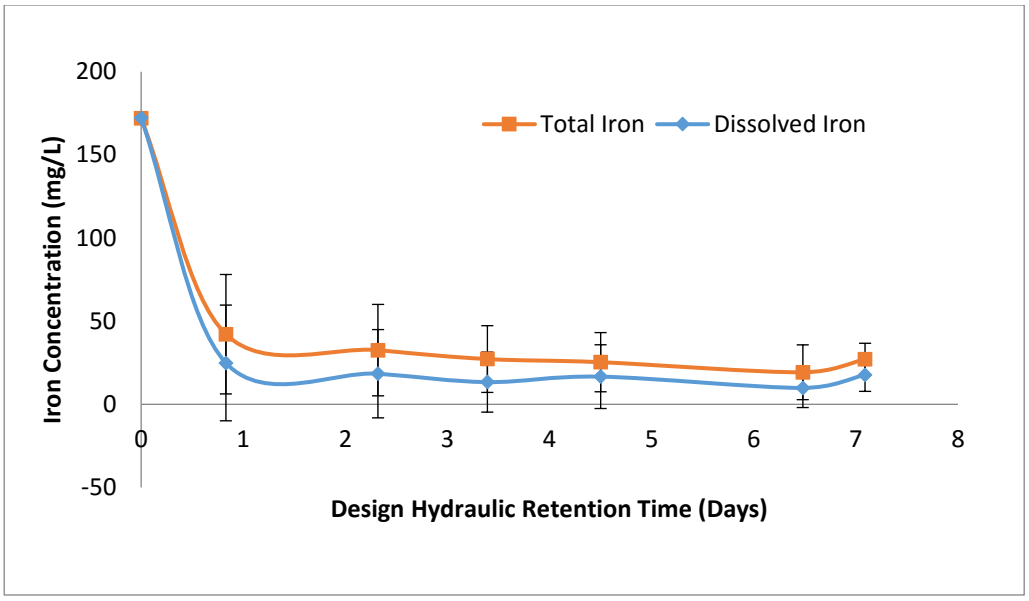

Figure 2.3: Progressive profile of average iron concentrations based on design hydraulic retention time for the unit process (Cell 1 = 7.7 days) scaled to sample collection position (distance from AMD source (meters).

The decrease in both total and dissolved iron concentrations indicates that conditions favored reaction kinetics for the oxidation of $Fe^{2+}_{(aq)}$ to $Fe^{3+}{}_{(aq)}$, hydrolysis of $Fe^{3+}_{(aq)}$ to $FeOOH_{(s)}$, and the sedimentation of $FeOOH_{(s)}$ to all occur within the first day of retention. The average transport fraction of dissolved: particulate iron ($[Fe^{2+}]/[Fe^{3+}]$) equals 1.37 as the larger proportion of iron being transported through sections 2 and 3 of the cell remains dissolved as $Fe^{2+}_{(aq)}$ rather than being transported as a suspended solid. This suggests that iron removal efficiency for Cell 1 is dependent on the rate of oxidation. Rates of oxidation for $Fe^{2+}_{(aq)}$ have been extensively quantified using ideal solutions as well as grab samples of AMD in the laboratory (Liang and Morgan 1990; Retnhardf 2001; Schwertmann 2007). Additionally, field batch reactor experiments have revisited the topic to address concerns regarding the role of CO_2 via pH dependence that is non-ideal in its composition and relative concentrations of ions (Nairn et al 2002; Kirby et al. 2009; Geroni and Sapsford 2011).

Plotting *in situ* parameters measured at each location within Cell 1 versus locational hydraulic retention time yielded no linear relationship (R^2<0.60) for temperature and pH. Yet, the change in total dissolved solids (TDS), conductivity (μS/cm), and salinity throughout the cell were linear up until 4.5 days retention time. After 4.5 days, the slope of the trend line approached zero via no appreciable change in conductivity and its derived measurements over the next three days of theoretical residence within cell 1. Dissolved oxygen (DOsat%) increased with increasing HRT (3.2 %/day; R^2= 0.8373) via surface-area based diffusion from the atmosphere. This corresponded to the oxidation reduction potential (ORP) also increasing with increasing residence time (8.2 mV/day; R^2 = 0.7817). Alkalinity declined with increasing hydraulic retention time as it is consumed by the latent acidity generated via iron oxidation and hydrolysis (-4.0 mg/L $CaCO_3$ eq./day; R^2 = 0.7922). Turbidity also decreased with increasing hydraulic retention time through sedimentation of precipitated iron oxides as the primary source of turbidity for the treatment cell (-16.8 NTU/day; R^2 = 0.8238).

Plotting the concentration of iron versus the approximate hydraulic retention time derived from sample position for sections 2 and 3 specifically yields a linear relationship for the removal of total and dissolved iron from the water column (Figure 2.4). Sections 2 and 3 of the preliminary oxidation cell contributed to overall iron removal efficiency with a removal rate of nearly 4 mg/L total iron per day of which nearly 2.4 mg/L/day is from ferrous iron removal. Other variables that can influence the rate of removal of iron from the water column beyond temperature, pH, and dissolved oxygen content is the saturation index of iron (Cravotta 2008).

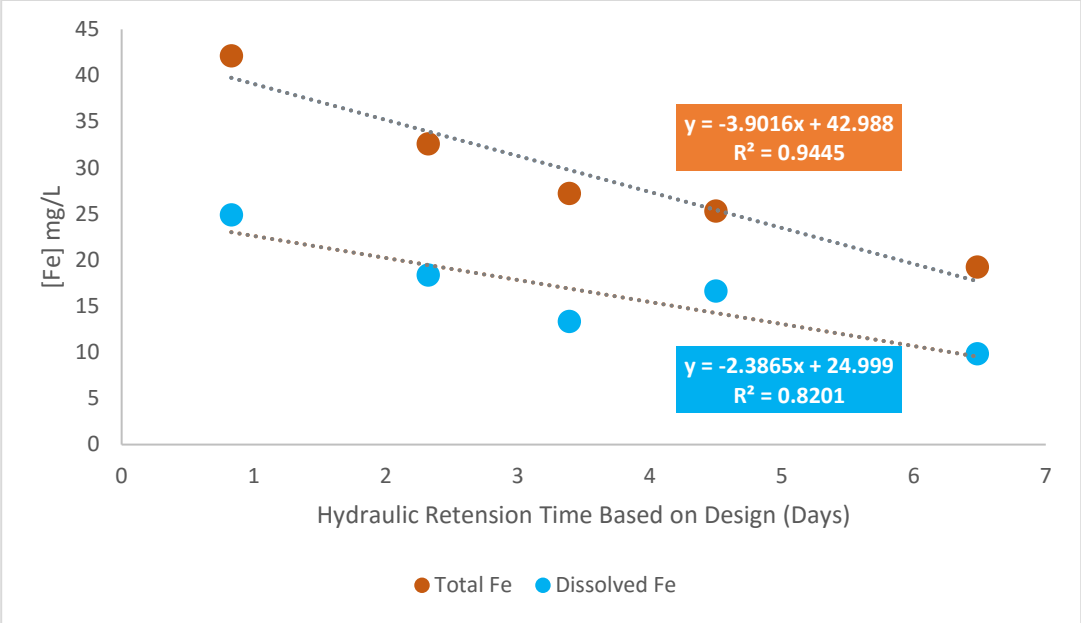

Figure 2.4: Iron removal rates for residual total and dissolved iron species within sections 2 and 3 of Cell 1 of the MRTPS preliminary iron oxidation cell.

Average iron removal water column profiles in Figures 2.5-2.7 indicate that iron concentrations increase with increasing depth of the oxidation pond within all three sections. This is consistent with the idea that as iron precipitates from solution, it coagulates into larger particles and settles to the bottom of the oxidation pond. The lowest total iron concentrations were observed near the surface of the water, whereas samples collected at 1.5 meters may have disturbed the surface of the settled iron oxyhydroxides resulting in the excessively high concentrations of total iron via resuspension. This is important to note, as it demonstrates that the iron oxyhydroxide solids are accumulating in all three sections of Cell 1, rather than just in Sections 1 as the water quality data indicate.

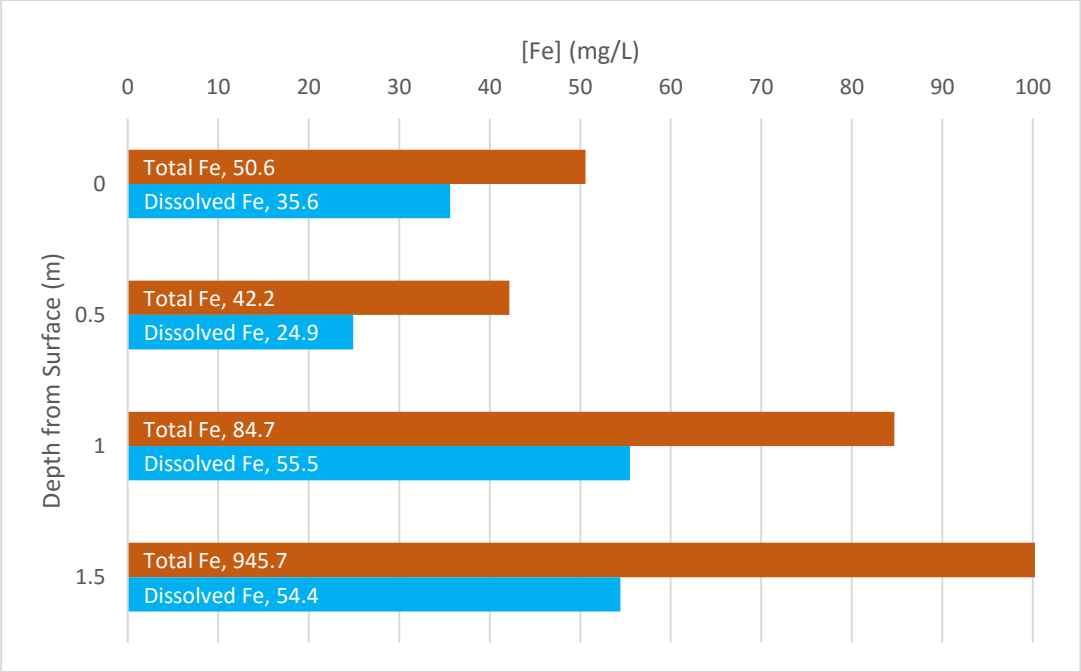

Figure 2.5: Average progressive iron removal profile with increasing depth from the surface of Section 1 of Cell 1 MRPTS (Cat1 sampling location; <1.0 days of retention time)

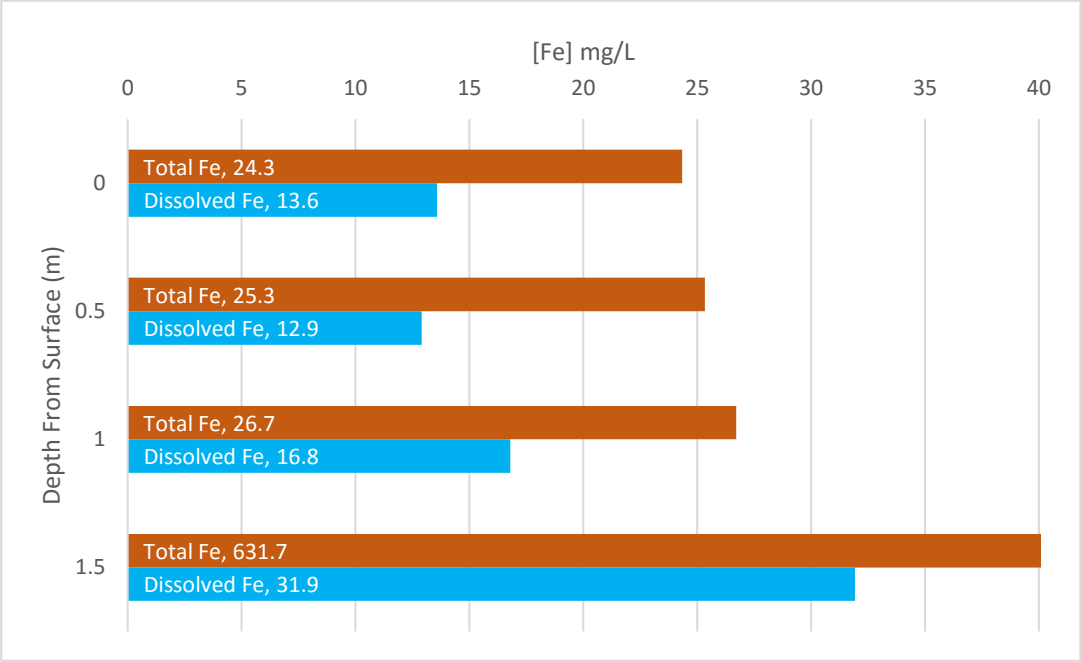

Figure 2.6: Average progressive iron removal profile with increasing depth from the surface of Section 2 of Cell 1 MRPTS (Cat2 sampling location; 4.5 days of retention time)

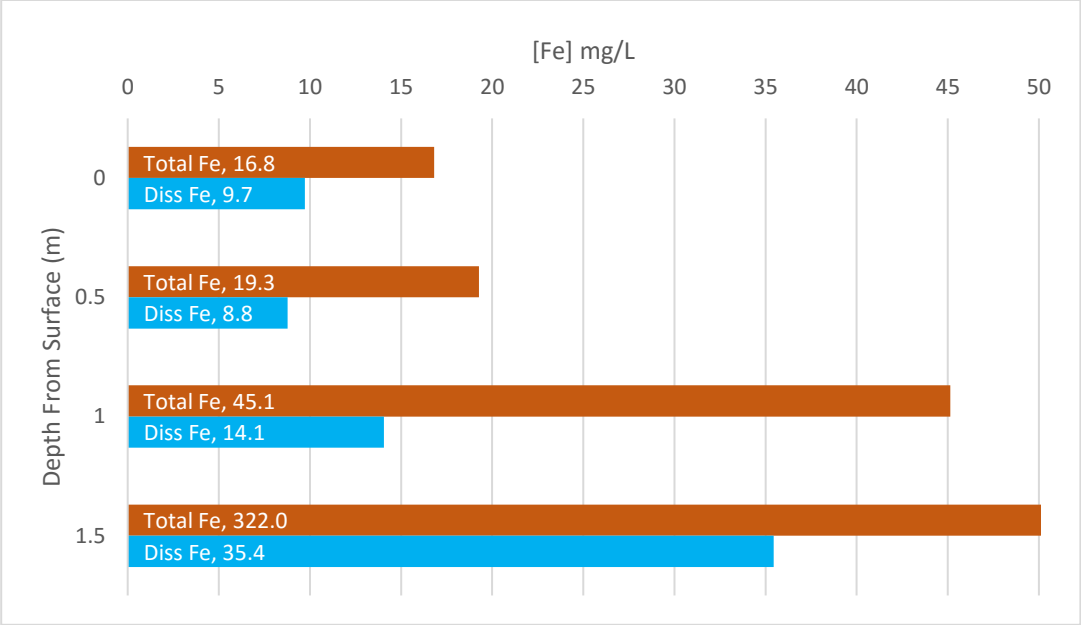

Figure 2.7: Average progressive iron removal profile with increasing depth from the surface of Section 3 of Cell 1 MRPTS (Cat3 sampling location; 6.5 days of retention time)

Average iron removal water column profiles in Figures 2.4-2.7 indicate that iron concentrations increase with increasing depth of the oxidation pond within all three sections of the oxidation cell design. This is consistent with the idea that as iron precipitates out of solution, it coagulates into larger particles and settles to the bottom of the oxidation pond. The lowest total iron concentrations were observed near the surface of the water whereas samples collected at 1.5 meters disturbed the surface of the settled iron oxyhydroxides resulting in the excessively high concentrations of total iron via resuspension. This is important to note, as it demonstrates that the iron oxyhydroxide solids are accumulating in all three sections of Cell 1, rather than just in Sections 1 as the water quality data indicates.

Seasonal Iron Removal Profiles:

The progressive iron removal profiles collected seasonally (quarterly) were averaged over the three-year sample collection period and plotted in Figures 2.8-2.11.

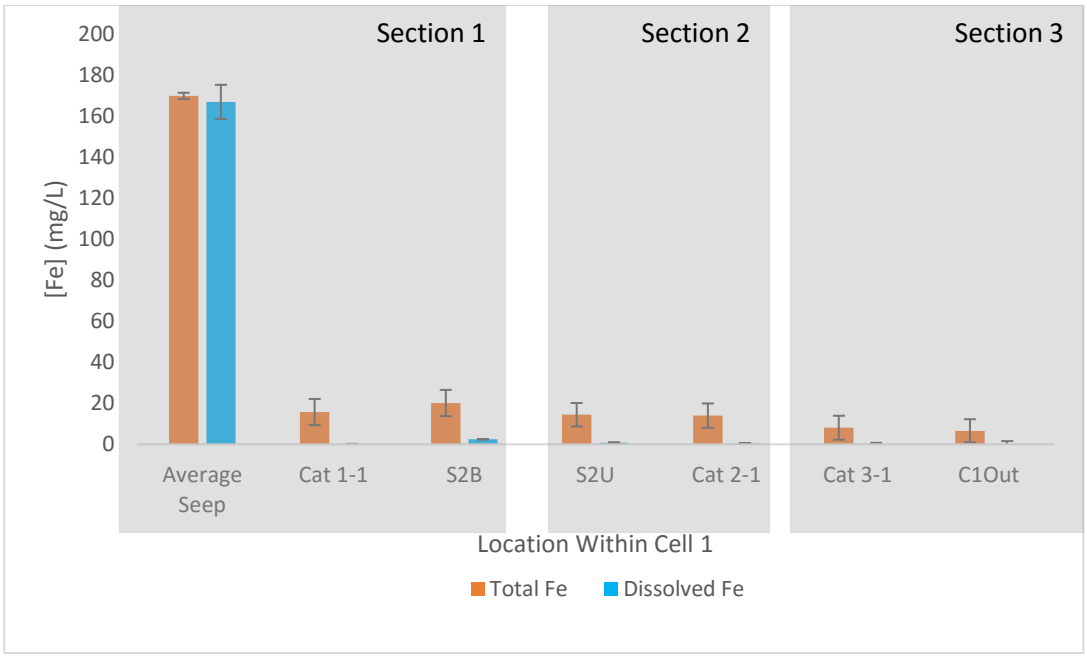

Figure 2.8: Average Spring Iron Removal Profile (April 2010-2012; n=3) with ± standard deviation error bars for each measurement average.

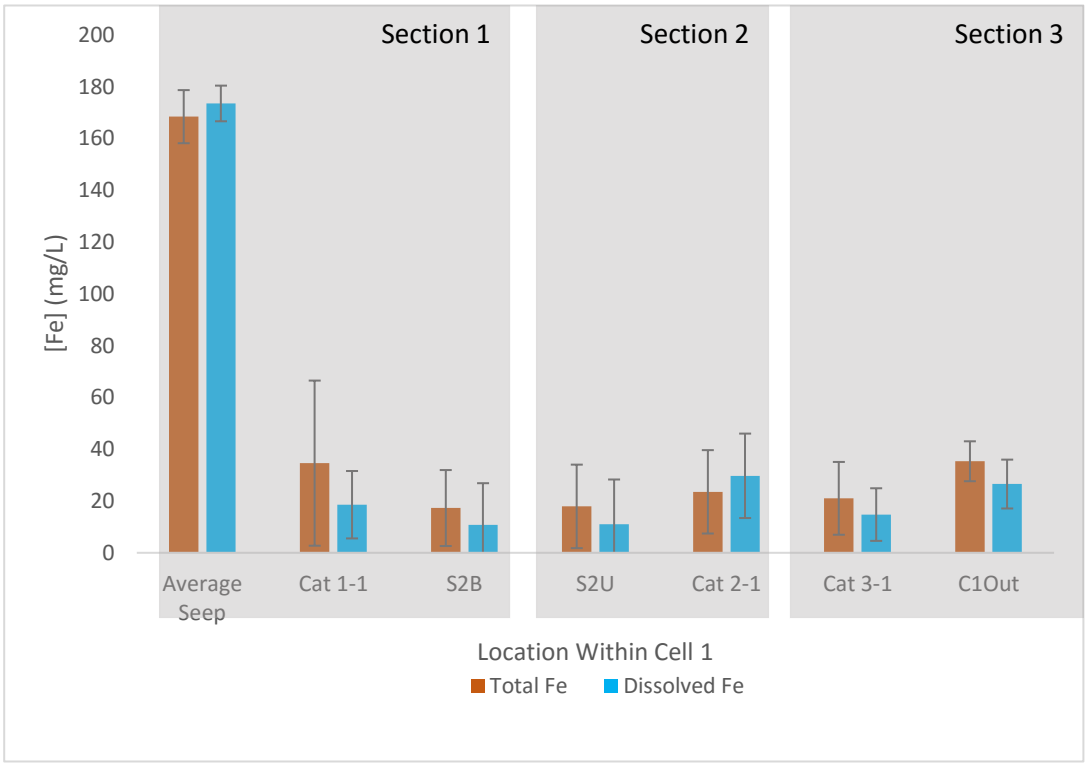

Figure 2.9: Average Summer Iron Removal Profile (July 2009-2011; n=3) with ± standard deviation error bars for each measurement average.

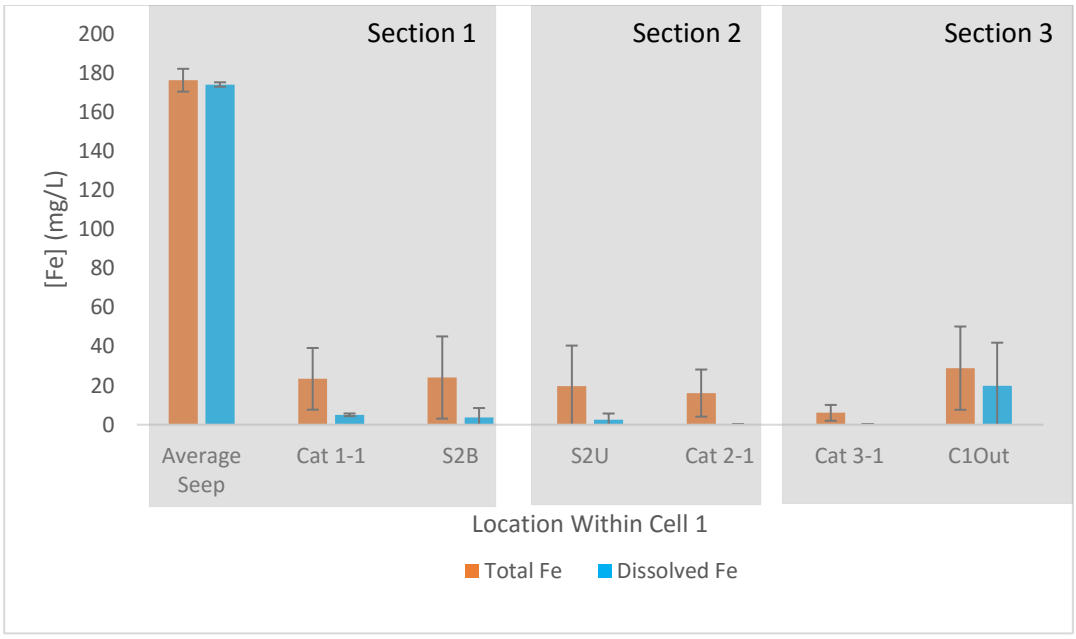

Figure 2.10: Average Fall Iron Removal Profile (October 2009-2011; n=3) with ± standard deviation error bars for each measurement average.

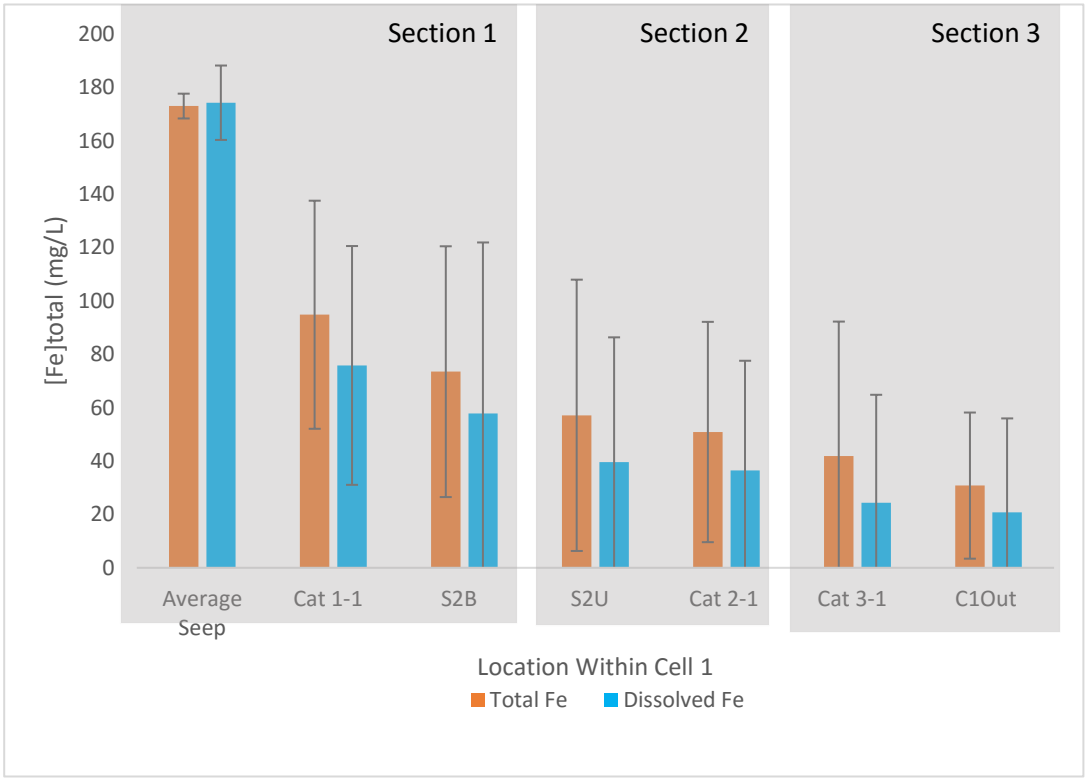

Figure 2.11: Average Winter Iron Removal Profile (January 2010-2012; n=3) with ± standard deviation error bars for each measurement average.

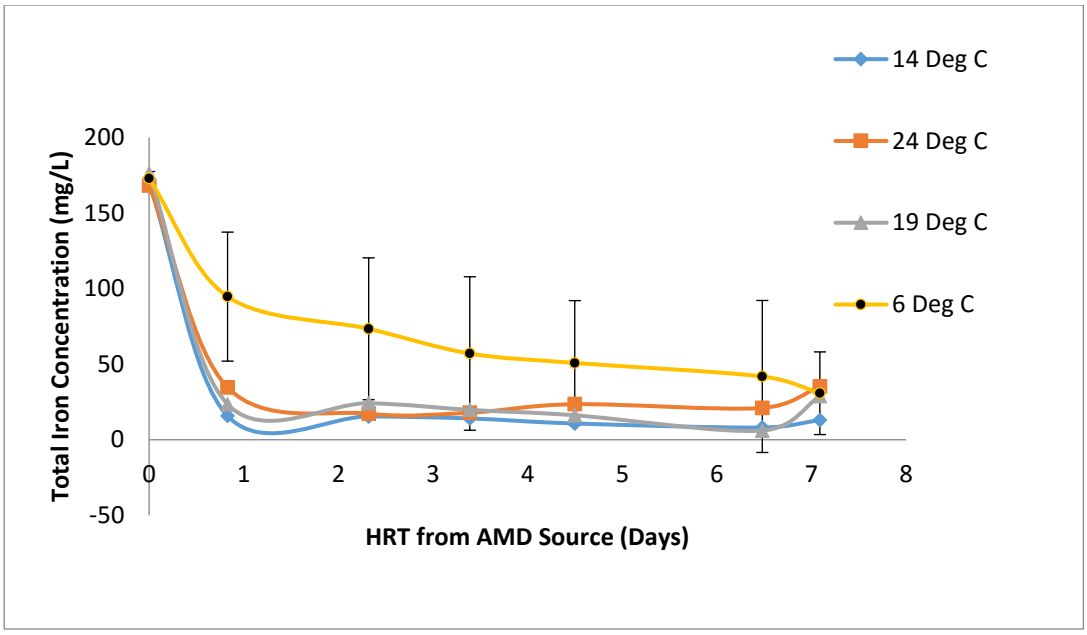

Figure 2.12: Comparison of total iron concentration (mg/L) for seasonal average progressive iron removal profiles. Note the consistency in performance for spring, summer, and fall profiles, yet high variability was observed for winter measurements.

Comparison of the seasonal average progressive iron removal profile (n = 3 years) reveals that spring (88%), summer (81%), and fall (90%) follow a consistent pattern in the decrease of total iron concentration within Section 1 of the treatment cell design. All three profiles mirror each other in form describing cell function, and have less variability on a year to year basis in their individual values (standard deviations between 10-30 mg/L) than the winter data set (standard deviations approaching 65 mg/L). Figure 2.12 compares the total iron based on position-derived hydraulic retention time for the average of each season. Comparison of the removal profiles by season reveals a difference in profile morphology between winter and the rest of the sampled seasons. However, despite these differences, the influent water chemistry remains consistent for all of the seasons, and the removal profiles converge to similar total iron concentrations at the cell effluent discharge. This suggests that variables influencing the removal of iron within Cell 1 are delayed, resulting in the distribution of iron removal over all three sections of the cell 1 design. However, Figure 2.13 does not support the idea of

temperature-dependence as the sole driving factor correlated to decreases in total iron concentrations. There is no apparent relationship between the effluent water temperature of Cell 1 and the decrease in the concentration of total iron. Temperatures between 6-23^{o}C all yielded decreases in total iron concentrations between 145-165 mg/L with two outliers as exceptions.

January 2010 had a water temperature approaching six degrees Celcius and correspondingly low total iron removal, yet comparison with the iron removal and temperature of the other profiles collected makes this point an outlier of the dataset. Similarly, October 2010 had an effluent water temperature of nearly 18 degrees Celcius and had the highest total iron removal of the dataset despite other profiles collected in the summer at higher temperatures being included. Calculation of the average dissolved to particulate ratio for the three-year iron removal profile average yields a composite score indicating the dominant form of iron within the water column (Figure 2.14). Values greater than 1.00 favor conditions supporting Fe^{2+} in the dissolved state versus values less than 1.00 favoring particulate iron as a suspended solid. Winter (D:P ratio = 2.65) indicates that conditions favor iron in the dissolved state (rate of oxidation impaired).

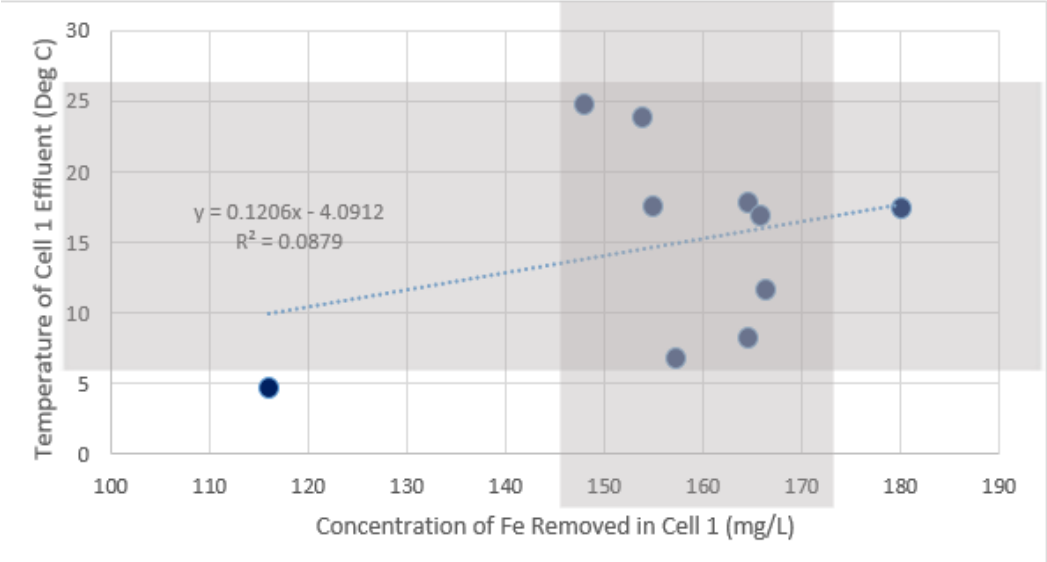

Figure 2.13: Correlation between C1Out water temperature and the total iron concentration change due to iron removal within Cell 1 measured as the difference between the average seep influent concentration and C1Out concentration. The intersection of grey zones indicates the range of temperature values and their associated with the central tendency of the change in iron concentration for the dataset.

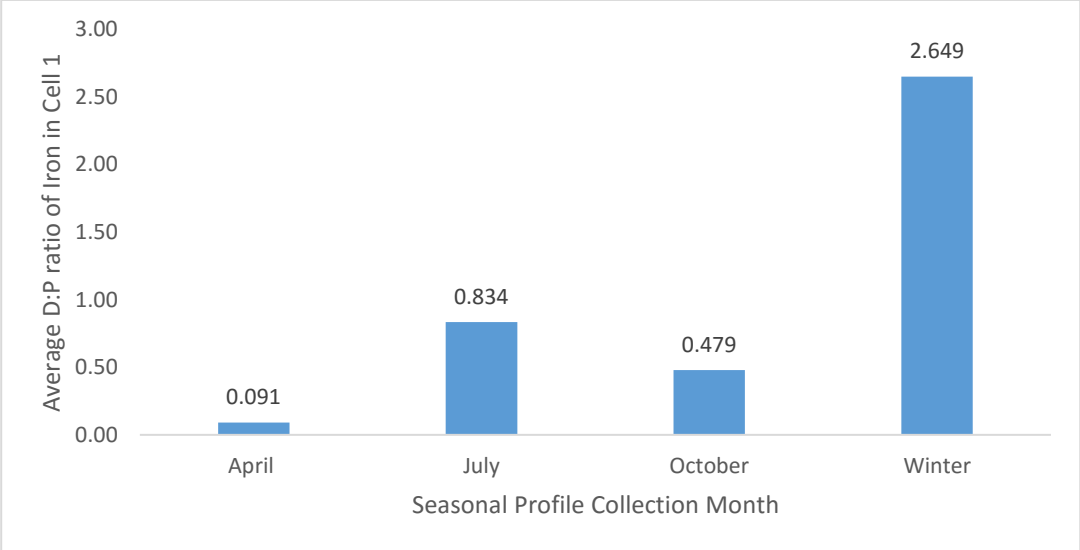

Figure 2.14: Comparison of the average Dissolved: Particulate iron ratios based on seasonal iron removal profiles. Influent concentrations were not included in the reported average ratio as the majority of the iron entering the cell is in the dissolved state, and it skews the dataset systematically.

Figures 2.15-2.17 detail the average vertical winter removal profiles of total and dissolved iron for sections 1,2, and 3 of the Cell 1 design. Each of these figures supports the result that it is

oxidation of Fe^{2+} and not particulate settling rates that are governing seasonal total iron removal.

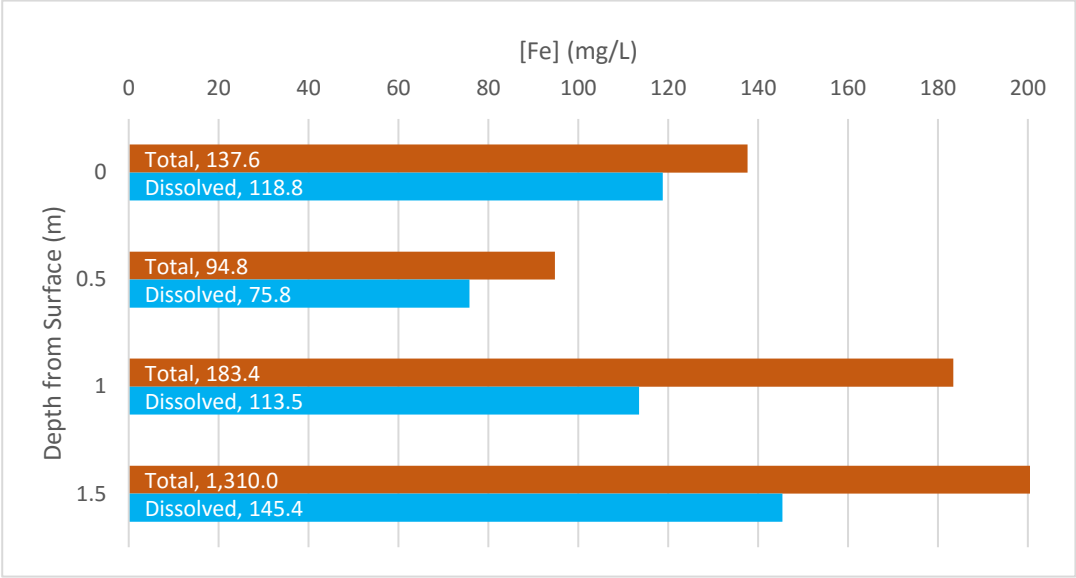

Figure 2.15: Average progressive iron removal profile with increasing depth from the surface of Section 1 of Cell 1 MRPTS (Cat1 sampling location; <1.0 days of retention time)

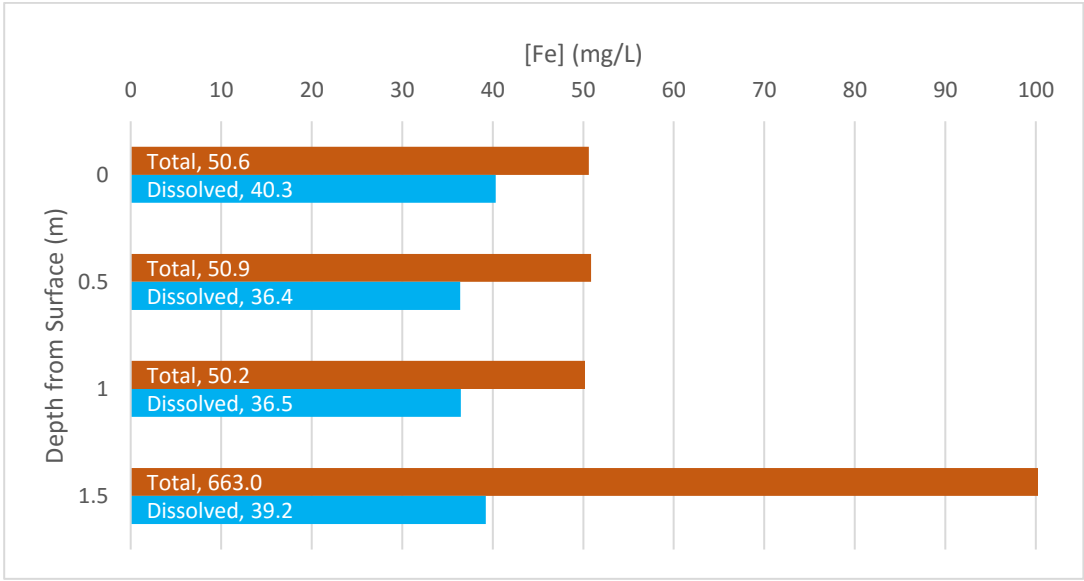

Figure 2.16: Average progressive iron removal profile with increasing depth from the surface of Section 2 of Cell 1 MRPTS (Cat2 sampling location; 4.5 days of retention time)

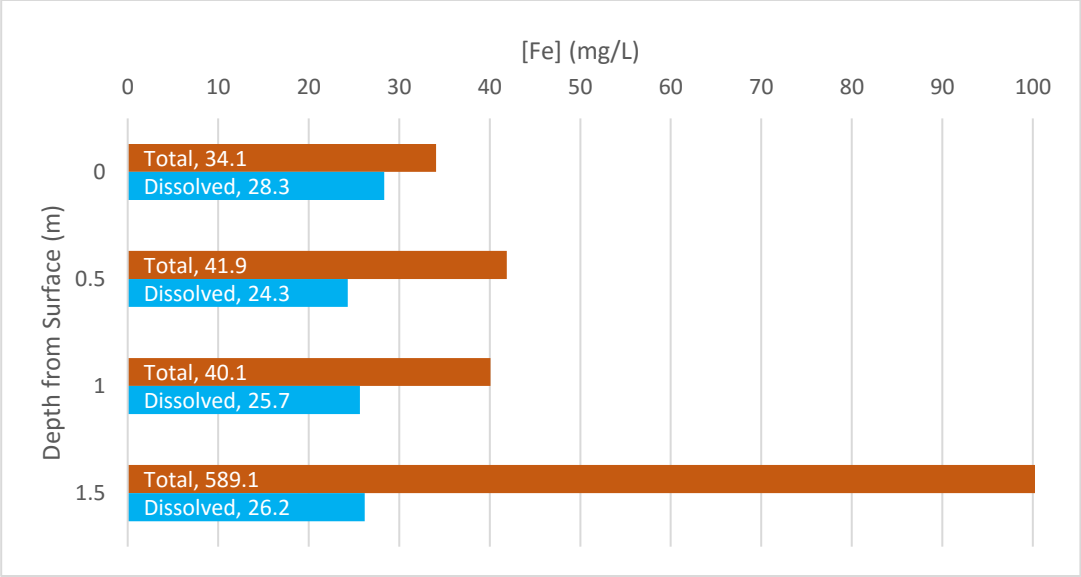

Figure 2.17: Average progressive iron removal profile with increasing depth from the surface of Section 23 of Cell 1 MRPTS (Cat3 sampling location; 6.5 days of retention time)

Conclusions

Iron oxidation, hydrolysis, and settling are key processes promoted in passive treatment system oxidation cells to decrease dissolved iron concentrations in influent mine drainage. Although monitoring the influent and effluent water quality of a treatment cell is sufficient to determine overall performance, it is insufficient to determine the step-wise iron removal profile. Sampling at key points throughout the U-shaped Cell 1 design at MRPTS determined that the majority of the iron removal achieved in the oxidation pond occurred in the first section of the pond (S1), rather than along a uniform gradient throughout all three sections (S1, S2, S3). Total iron concentrations increased with increasing depth of the oxidation cell as precipitated iron oxides underwent sedimentation.

Seasonal impacts on removal efficiency were observed for winter iron removal profiles with iron being found in the dissolved Fe^{2+} form much later in the treatment cell than previously observed for the Spring, Summer, and Fall samples. There was not an explicit relationship

observed between temperature and change of iron concentration. Degassing of dissolved carbon dioxide is suspected to play a critical role synergistically with dissolved oxygen content of the water as well as pH to favor oxidation and hydrolysis reactions. The loss of large quantities of iron from solution in section 1 of cell one may have implications on long-term precipitate deposition and storage within the system. Additional work is required to determine if uneven deposition of the retained iron solids will affect the performance of the system (e.g., retention time, short circuiting, and sediment mineralization) over the life of the system.

Literature Cited

August EE, McKnight DM, Hrncir DC, Garhart KS. 2002. Seasonal variability of metals transport through a wetland impacted by mine drainage in the Rocky Mountains. Environ. Sci. Technol. 36:3779–3786.

Barnes A, Sapsford DJ, Dey M, Williams KP. 2009. Heterogeneous Fe(II) oxidation and zeta potential. J. Geochemical Explor. 100:192–198.

Blowes DW, Ptacek CJ, Jambor JL, Weisener CG, Paktunc D, Gould WD, Johnson DB. 2013. The Geochemistry of Acid Mine Drainage. Treatise Geochemistry Second Ed. 11:131–190.

Butler BA, Ranville JF, Ross PE. 2008. Observed and modeled seasonal trends in dissolved and particulate Cu, Fe, Mn, and Zn in a mining-impacted stream. Water Res. 42:3135–3145.

Casiot C, Lebrun S, Morin G, Bruneel O, Personné JC, Elbaz-Poulichet F. 2005. Sorption and redox processes controlling arsenic fate and transport in a stream impacted by acid mine drainage. Sci. Total Environ. 347:122–130.

Chakraborti and Kaur. 2014. Noninvasive Measurement of Particle-Settling Velocity and Comparison with Stokes' Law. J. Environ. Eng. 140.

Cornell RM, Schwertmann U. 2004. Environmental Significance. Iron Oxides:541–551.

Cravotta CA. 2008. Dissolved metals and associated constituents in abandoned coal-mine discharges, Pennsylvania, USA. Part 2: Geochemical controls on constituent concentrations. Appl. Geochemistry 23:203–226.

Dempsey BA, Roscoe HC, Ames R, Hedin R, Jeon B-H. 2001. Ferrous oxidation chemistry in passive abiotic systems for the treatment of mine drainage. Geochemistry Explor. Environ. Anal. 1:81–88.

Eggleston CM, Ehrhardt J-J, Stumm W. 1996. Surface structural controls on pyrite oxidation kinetics: An XPS-UPS, STM, and modeling study. Am. Mineral. 81:1036–1056.

Geroni JN, Sapsford DJ. 2011. Kinetics of iron (II) oxidation determined in the field. Appl.

Geochemistry 26:1452–1457.

Hedin R, Weaver T, Wolfe N, Watzlaf G. 2013. Effective Passive Treatment of Coal Mine Drainage 1. :1–13. Presented at the 35th Annual National Association of Abandoned Mine Land Programs Conference.

Hedin RS (2008) Iron removal by a passive system treating alkaline coal mine drainage. Mine Water Environ 27:200-209.

Hedin RS, Nairn RW. 1992. Designing and Sizing Passive Mine Drainage Treatment Systems. U.S. Bureau of Mines, Pittsburgh Research Center

Kadlec RH, Wallace SD. 2009. Treatment Wetlands, Second Edition.

Kirby CS, Dennis a., Kahler a. 2009. Aeration to degas CO2, increase pH, and increase iron oxidation rates for efficient treatment of net alkaline mine drainage. Appl. Geochemistry 24:1175–1184.

Lenoble V, Bouras O, Deluchat V, Serpaud B, Bollinger J-C. 2002. Arsenic adsorption onto pillared clays and iron oxides. J. Colloid Interface Sci. 255:52–58.

Liang L, Morgan JJ. 1990. Chemical aspects of iron oxide coagulation in water: Laboratory studies and implications for natural systems. Aquat. Sci. 52:32–55.

Manceau A, Charlet L, Boisset MC, Didier B, Spadini L. 1992. Sorption and speciation of heavy metals on hydrous Fe and Mn oxides. From microscopic to macroscopic. Appl. Clay Sci. 7:201–223.

Manyin T, Williams FM, Stark LR. 1997. Effects of iron concentration and flow rate on treatment of coal mine drainage in wetland mesocosms: An experimental approach to sizing of constructed wetlands. Ecol. Eng. 9:171–185.

Matthies R, Aplin AC, Jarvis AP. 2010. Performance of a passive treatment system for net-acidic coal mine drainage over five years of operation. Sci. Total Environ. 408:4877–85.

Nairn, RW. OSullivan, AD. Coffey, J. 2002. Iron oxidation in CO2 rich net alkaline mine waters. Poster Presented at the Amercian Society of Mining and Reclaimation, 1133-1136.

Nordstrom DK. 2011. Hydrogeochemical processes governing the origin, transport and fate of major and trace elements from mine wastes and mineralized rock to surface waters. Appl. Geochemistry 26:1777–1791.

Schwertmann, U., Cambier, P. and iMurad, E. (1985) Properties of goethites of varying crystallinity. Clays Clay Min. 33: 369-378.

Stumm W, Sulzberger B. 1992. The cycling of iron in natural environments: Considerations based on laboratory studies of heterogeneous redox processes. Geochim. Cosmochim. Acta 56:3233–3257.

Tarutis WJ, Stark LR, Williams FM. 1999. Sizing and performance estimation of coal mine drainage wetlands. Ecol. Eng. 12:353–372.

US Environmental Protection Agency. 2016. USEPA: Site Information for Tar Creek (Ottawa Co). [accessed 2016 Sep 11]. <https://cumulis.epa.gov/supercpad>

Watzlaf GR, Schroeder KT, Kleinmann RLP, Kairies CL, Nairn RW, Street WB. 2004. The Passive Treatment of Coal Mine Drainage. :1–72. DOE/NETL-2004/1202

Wieder, RK. 1993. Diel Changes in Iron(III)/Iron(II) in Effluent from Constructed Acid Drainage

Treatment Wetlands. J. Environ. Qual. 23.

Younger P. Banwart, S. Hedin R. 2002. Mine Water: Hydrology, Pollution, Remediation. Volume 5. Springer Science+Business Media Dordrecht. P 150-167

Younger PL. 2000. Nature and practical implications of heterogeneities in the geochemistry of zinc-rich, alkaline mine waters in an underground F-Pb mine in the UK. Appl. Geochemistry 15:1383–1397.

Ziemkiewicz P., J.G S, Simmons J. 2003. Long-term Performance of Passive Acid Mine Drainage Treatment Systems. J. Mine Water Environ. 22:118.129.

Chapter 3: Storm Event-Driven Metal Transport Dynamics Between Oxidative Treatment Cells

This chapter has been formatted in compliance with the journal of *Ecological Engineering* for submission.

Abstract

Iron oxidation, hydrolysis and settling are key processes promoted in passive treatment systems (PTS) to remove iron from influent acid mine drainage (AMD). Intense storm events have been qualitatively observed to transport iron and thus storms may impact routine sample collection and monitoring of oxidation cells within PTS. The purpose of this study was to investigate iron transport between the preliminary oxidative treatment cell and the surface flow wetland cells, iron export out of the oxidative unit, and iron loading via the PTS effluent discharge into a tributary of Tar Creek. Ottawa County, OK. Automatic samplers were installed at the effluent of the preliminary oxidation cell, secondary aerobic wetlands, and treatment system to collect total metals samples when rainfall intensity exceeded 0.25 cm/hour for 35 hours. Laboratory determination of total metals produced a series of transport profiles for individual storm events and the total amount of iron transport was approximated with respect to a rainfall intensity classification system (low: 0.25-0.99 cm/hr; moderate: 1.00-1.99 cm/hr; high: 2.00-2.99 cm/hr; extreme: >3.00 cm/hr). The mass of iron transported during individual storm events was significant when compared to baseline values for storms of all intensity classifications. The mass loading of storm-induced iron into the receiving stream was minimal as the majority of iron was removed in Cells 1 and 2N/2S rather than relying on Cell 6 for removal. The amount of iron transported did not correlate to rainfall intensity, so low intensity storms controlled storm-induced iron transport as they are more frequent than moderate, high, and extreme events. The independence of storm induced transport with

respect to rainfall intensity suggests a transport mechanism based on settling disruption rather than solids resuspension.

Introduction

Passive treatment systems are designed to remediate acid mine drainage (AMD) using physical, chemical, and biological processes selected for optimized metals removal and alkalinity generation (Hedin et al. 1994). Intensive study of influent water quality and quantity guide the selection and order of engineered treatment cells that alternate between the promotion of aerobic and anaerobic processes (Skousen and Sexstone 2000). Oxidative treatment cells emphasize conditions that favor the removal of iron specifically, as iron is converted from the dissolved state (typically Fe^{2+} at circumneutral pH) to the solid state ($FeOOH_{(s)}$ particulates) via oxidation and hydrolysis reactions (Hedin et al. 1994; Equations 3.1, 3.2 and 3.3).

$$4Fe^{2+} + O_2 + 4H^+ \rightarrow 4Fe^{3+} + 2H_2O \quad \text{(Equation 3.1)}$$

$$Fe^{3+} + 2H_2O \rightarrow FeOOH(s) + 3H^+ \quad \text{(Equation 3.2)}$$

$$FeOOH\ (\text{suspended solid}) \rightarrow FeOOH\ (\text{settled solid}) \quad \text{(Equation 3.3)}$$

The hydraulic flow rate though the passive treatment system governs the amount of time that water will remain in each treatment cell (hydraulic retention time or HRT) and is important to sedimentation basin sizing during the design phase of a project, as well as efficiency assessments during system operation (Chakraborti and Kaur 2014).

Solids retention in oxidative treatment cells is dependent on the rate of sedimentation for precipitates in addition to environmentally-influenced rates of iron oxidation, hydrolysis, and sedimentation (Equations 3.1-3.3). Stokes' Law is applied to suspended solids fate and

transport where laminar flow conditions are met (Reynold's number <0.1, viscous forces dominant) with an emphasis on smooth, continuous flow for transport (Brown and Lawler 2003). Settling velocity of iron floc precipitates (V_s, Equation 3.4) are dependent on particle diameter (d), density of the particle (ρ_p), acceleration due to gravity (g), viscosity of the medium (μ) and density of the aqueous medium (ρ_w) described by Stokes' Law (Perkins et al. 2007). Setting rates can also be empirically measured *in situ* or from grab samples (Chakraborti and Kaur 2014); Van der Lee 2000).

$$V_s = \frac{g}{18}\left(\frac{\rho_s - \rho_w}{\mu}\right) d^2 \qquad \text{(Equation 3.4)}$$

Oxidation ponds are designed to promote sedimentation of suspended iron flocs prior to reaching the point of discharge into the next treatment cell. Storage volume for accumulated solids is included into the design of the cell to ensure that the deposition and subsequent volume displacement by solids will not impair performance over time (Hedin and Nairn 1992; Kruse et al. 2009). The iron that is not removed and sequestered by the oxidative cell is transported to the next unit in the treatment series where it can have negative impacts on function. Transport occurs for both dissolved (Fe^{2+}) and particulate iron ($FeOOH_{(s)}$) with the ratio of dissolved to particulate iron being critical to removal efficiency in performance assessment (Sapsford and Watson 2011)

Total iron transported as effluent of an oxidation pond may be monitored through a regularly scheduled sampling regimen to determine area-adjusted removal rates for performance evaluation (Younger 2002). However, quarterly and/or monthly sampling lacks the resolution to capture short-term transport events induced by storm activity as they occur. Furthermore, routine sampling is often delayed or avoided following periods of rain as to not bias the dataset with values associated with an acute disturbance event that does not represent typical

performance conditions. Yet for passive treatment systems installed in regions with frequent and severe thunderstorms, it is unclear how much of a contribution these storm events may make to the total amount of transported materials from each cell over time (Eger and Wagner 1997). It is also uncertain how much time is required to return to a baseline performance level following an event, which is important to monitoring and performance evaluation in water treatment systems.

Although tornados (Enhanced Fugita scale) and hurricanes (Saffir-Simpson scale) are formally classified based on wind speed, precipitation and impacts; thunderstorm classifications are not unified by a single approach (NOAA 2013; FAA 2013). The diversity in storm formation conditions and characteristics make a definitive classification system difficult to develop and implement uniformly between regions (Visser 2001). However, guidelines for thunderstorm classifications focus principally on rainfall intensity, duration, storm yield, and storm frequency (Gaál et al. 2014). Wind and hail metrics are also included in select publications, while rainfall intensity is used in both direct measurement (Abshaev et al. 2010) and radar-based approaches (Chen et al. 2009) to define storm classification. A storm classification system needed to define the impact of storm disturbance events on transport of iron within the oxidative unit and from the system effluent was developed as part of this study.

Intense rainfall has been observed to increase the turbidity of oxidation cells through the re-suspension of retained materials via edge effects and in shallow surface-flow systems (Sandén et al. 1997; Nordstrom 2011). The acute mobilization of iron in surface-flow wetlands in a pulse of solid-phase material through re-suspension of accumulated solids has been observed in wastewater treatment wetland applications (Vymazal 2011). Yet, the process has not been fully described for AMD treatment applications using engineered wetlands for passive treatment systems, nor deep water cells like iron oxidation cells. The amount of iron

transported (kg/storm; kg/year) by storm disturbance events, specifically, has not been described quantitatively with respect to storm rainfall intensity, duration, frequency, and precipitation yield.

Transport of dissolved and particulate iron negatively impacts the performance of downstream treatment cells as solids accumulation submerges emergent macrophytes (Jennings et al. 2008), increases water column turbidity to occlude light penetration for algal communities (Pratt et al. 2014), and restricts flow dynamics (Watzlaf et al. 2004). Iron transport out of the system impacts the water quality of the receiving stream and is subject to permitting and regulation. To reduce these negative impacts, design features such as pond-marsh-pond surface-flow wetlands or secondary oxidation ponds / channels are installed as a buffer between preliminary oxidation and vertical flow cells (Cohen and Brown 2007). Facilitating a second stage of removal for residual dissolved and particulate iron is essential for prevention of vertical flow hydraulic conductivity impairment from solids accumulation (Wiseman and Edwards 2004)

The purpose of this study was to quantify the fractional amount of total iron transport associated with storm events of increasing rainfall intensity and to determine if storm disturbance significantly contributed to iron mass transport between treatment units or the system effluent.

Methods

Location

The Mayer Ranch Passive Treatment System (MRPTS) is located at the Tar Creek Superfund Site near Commerce, OK, within the Tri-State Mining District of northeastern Oklahoma,

southeastern Kansas and Southwestern Missouri. It is a full-scale installation treating a continuous flow of circumneutral pH mine drainage with an average iron loading of approximately 36,500 kg/year (2009-2013, n =28, σ= 2080 kg/yr). The system design features a preliminary oxidation pond (Cell 1) with a design hydraulic retention time (HRT) of 7.7 days and a surface area (SA) of 4083 m^2 based on a design removal rate of 20 g Fe / m^2/day. Flow from the oxidation pond is split between two parallel surface flow wetlands designated Cell 2North and Cell 2South (HRT = 3.4 days; SA = 1685m^2) with a pond-marsh-pond design to facilitate additional iron removal and solids retention. The system continues with parallel vertical flow bioreactors (Cell 3North and Cell 3South), reaeration cells (Cell 4North and Cell 4South), and horizontal flow limestone beds (Cell 5North and Cell 5South) before the flow is consolidated into a polishing wetland (Cell 6) with effluent discharge to an unnamed tributary of Tar Creek. The total iron loading leaving the system averaged 107 kg/year (2009-2013, n = 28, σ= 26 kg/yr) with the difference in influent and effluent loading being total iron retained within the system. The design hydraulic retention time (HRT) of Cell 6 is 0.8 days (SA = 1096 m^2) while the HRT for MRPTS is approximately 20 days. The cell configuration of the MRPTS is featured in Figure 3.1.

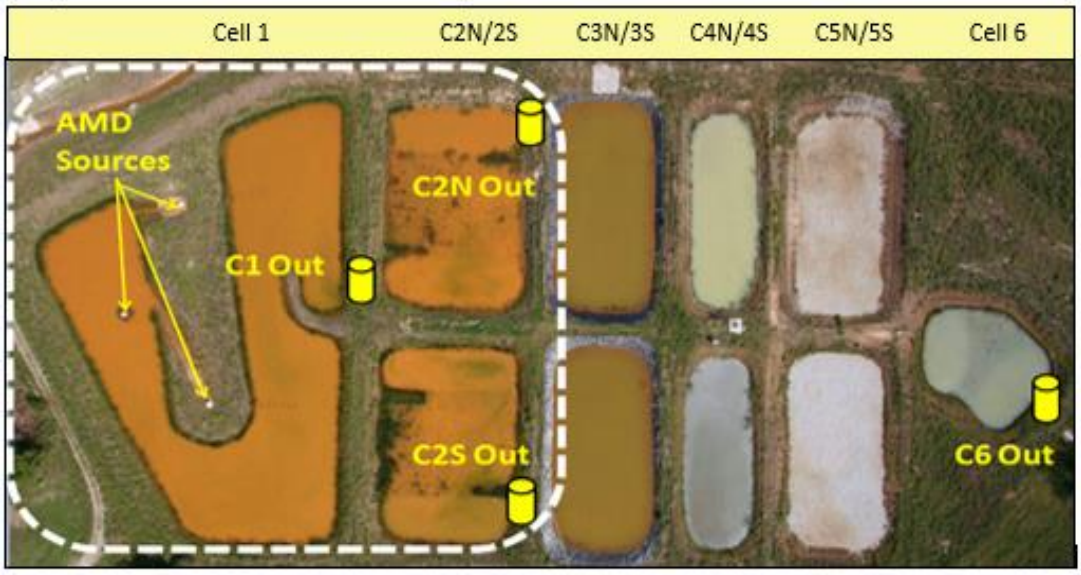

Figure 3.1: Autosampler installation locations at the Mayer Ranch Passive Treatment System (Commerce, OK) including the preliminary oxidative units (dashed box-white) and the system effluent (C6out).

Instrumentation

Sample collection was facilitated by four Sigma Aldrich 900max automatic samplers (autosamplers) installed to sample the effluent of selected ells (Figure 3.1). Precipitation was measured at each autosampler with a tipping bucket rain gauge accessory installed approximately ten feet from the autosampler on a level cinderblock platform with no overhanging structures or vegetation. A continuous, rechargeable power supply was maintained at each remote location via the installation of a 10W-solar panel mounted on a steel pole and oriented due south (180^{o} / 30^{o} fixed angle) that recharges a 12-volt battery (dc). The autosampler and the power supply were housed in a wooden box to minimize damage from environmental conditions and potential vandalism. The rain gage accessory initiated sample collection when the rainfall intensity exceeded an empirically-derived threshold value (cm/hr) and triggered the autosampler to collect samples at pre-programed, non-uniformly spaced, user-defined time increments to capture the first flush, post-storm transport, and return to baseline conditions with enough resolution to describe the transport event. A total

of 24 samples were collected when rainfall intensity exceeded 0.250 cm/hr at initial (first flush), 15 min, 30 min, 45 min, 1 hr, 1.5 hr, 2 hr, 2.5 hr, 3 hr, 3.5 hr, 4 hr, 5 hr, 6 hr, 7 hr, 9 hr,11 hr, 13 hr, 15 hr, 18 hr, 21 hr, 24 hr, 27 hr, 31 hr, 35 hr, and 39 hr after each triggered event in 2011. This program was refined to trigger at 1.00 cm/hr and collect at first flush, 20 min, 40 min, 1hr, 1.5 hr, 2 hr, 2.5 hr, 3.8 hr, 4.5 hr, 5.5 hr, 6.5 hr, 7.5 hr, 8.5 hr, 9.5 hr, 10.5 hr, 11.5 hr, 12.5 hr, 14.5 hr, 16.5hr, 18.5 hr, 22.5 hr, 26.5 hr, and 30.5 hr for 2012-2013 storm events. Sample was pumped through Teflon-lined polyethylene tubing (0.95 cm id) terminating in a Teflon/stainless steel strainer suspended in the water column of the Agri Drain® in-line water control structure, with three rinses before dispensing sample into a radial array of 24 HDPE 1.0-L sample bottles via peristaltic pump.

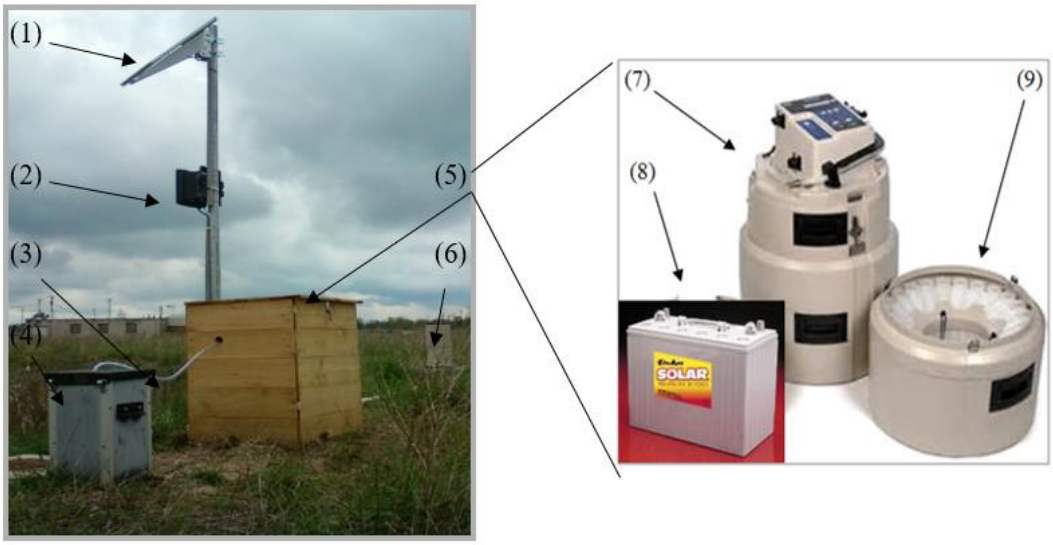

Figure 3.2: Example of Autosampler installation featuring accessories: (1) Solar panel, (2) Solar regulator, (3) Sampling tubing, (4) In-line flow control structure (Agri Drain®), (5) Autosampler housing, (6) Rain gauge, (7) 900max portable sampler, (8) Solar rechargeable 12V-battery, and (9) 24-bottle collection array. (photos from installation location and The Hach Company)

Flowrate and Mass Loading

The influent flow to the MRPTS is the sum of three mine seeps that were monitored monthly from 2009-2011, and then quarterly from 2012-2013 to measure the flow dynamics and water

quality for loading calculations. Grab samples for total and dissolved metals analysis and *in-situ* water quality parameter measurements were collected at the effluent of Cell 1, Cell2North, Cell 2South, and Cell 6 over the same time. The average flow rate for each season was used to calculate mass loading for individual storm events for Cell1, C2N, and C2S: Spring (March, April, May = 27,639 L/hr), Summer (June, July, Aug = 23,467 L/hr), Fall (Sept, Oct, Nov = 20,786 L/hr) and Winter (Dec, Jan, Feb = 23,586 L/hr). The average system effluent flow rate for each season was used to calculate mass loading for individual storm events for C6out: Spring (March, April, May = 24,903 L/hr), Summer (June, July, Aug = 24,415 L/hr), Fall (Sept, Oct, Nov = 22,001 L/hr) and Winter (Dec, Jan, Feb = 27,497 L/hr).

Sample Collection and Processing

Within one week of the completion of the 30+hr sample collection event, HDPE autosampler bottles were exchanged with a spare set of acid-washed bottles to minimize instrument downtime between site visits. All 24 samples were acidified with concentrated nitric acid, capped, and placed in a cooler for transport back to the laboratory. Precipitation data were logged in 15-minute increments over the duration of each storm transport event, and were downloaded while samples were prepared for transport. At the laboratory, each autosampler bottle was repeatedly inverted to ensure uniform mixing before the contents were transferred to 250-mL HDPE bottles. A transfer duplicate was included with each set of samples to evaluate the reproducibility of the transfer process. The autosampler bottles and caps were acid washed, dried, and packaged for field deployment while the transferred samples were digested via EPA Method 3015A with a CEM MARSXpress V unit and analyzed with a Varian Vista-PRO Simultaneous Axial Inductively Coupled Plasma-Optical Emission Spectrophotometer (ICP-OES; EPA Method 6010A) for total metals concentrations (Al, As, Ca,

Cd, Co, Cr, Cu, Fe, K, Mg, Mn, Na, Ni, Pb, Zn). QAQC standard operating procedures dictated the inclusion of laboratory blanks, duplicates, and standard spikes for the aqueous digestion and total metals analysis. Instrument calibration and verification via check standards (1 ppm and 10 ppm) was also included.

Storm Classification and Transport

Precipitation data obtained from the Oklahoma Mesonet (Station 65, Miami, OK) from 1998-2008 (pre-system construction) were used to develop storm classification criteria based on rainfall intensity: Low (0.25-0.99 cm/hr), Moderate (1.00-1.99 cm/hr), High (2.00-2.99 cm/hr), and Extreme (≥3.00 cm/hr).

Mass loading of iron into and out of each cell was calculated by multiplying the concentration of iron in each sample by the average seasonal flow rate corresponding to the rainfall event, and the distribution of mass loadings over the 30+hr sampling period were plotted. The area under each curve represents gross iron transport, which is a composite of the baseline transport that would have happened regardless of storm disturbance and the storm-induced transport (net transport) which can be found by subtracting the baseline transport from the measured gross transport. Baseline transport was determined using the minimum value of each mass transport profile to define baseline transport conditions that had been restored after the disturbance event. The baseline mass transport was applied uniformly over the 30+hr time interval (simulating conditions in which no storm event had occurred). Mass transport of iron (kg/storm intensity classification) was calculated for individual storm events covering the full range of storm intensity categories. Comparisons were made between the total amount of iron transported for each classification of storm event with respect to storm intensity, duration, and yield. Statistical significance of net iron transport with respect to baseline

transport was evaluated over all rainfall intensity classifications with the t-test of two unpaired data series of unequal variance ($\alpha = 0.05$) in Microsoft Excel 2016.

Results and Discussion

Performance of the Mayer Ranch Passive Treatment System oxidative unit is summarized in Table 3.1 as a series of discrete measurements averaged over a five-year period. Cell 1 performs within design expectations for iron removal via oxidation and hydrolysis, achieving the target surface area adjusted removal rate of 19 $g/m^2/day$. However, 21.3% of the iron loaded into Cell 1 is transported into Cell 2N and 2S. The secondary oxidation cells (2N/S) perform consistently with each other with an average total (gross) iron transport approaching 18%. Cell 6 is transporting 33.8% of its loaded iron, however this is 107 kg/year out of the 36,036 kg/year loaded into Cell 1 for treatment (0.30% system transport with respect to loading).

Table 3.1: Comparison of MRPTS iron removal and transport (2011-2013)

MRPTS Cell	Fe Loading (kg/year)	Total Fe Exported (kg/year)	Total Fe Retention (kg/year)	Surface Area Adjusted Removal Rate ($g/m^2/day$)	% of Influent Fe Exported in Effluent
Cell 1	36,036	7682	28,354	19.02	21.3%
C2N	7682	1381	6301	11.51	18.0%
C2S	7682	1358	6324	11.55	17.7%
Cell 6	317	107	210	0.53*	32.1%

*value is load limited.

Storm Classification

There was an average of 109 storms per year ($\sigma = 25.5$) between 2011-2013 with each month including storms of measurable precipitation (>0.25 cm/hr) (Figure 3.3). Applying the storm classification system of Low (0.25-0.99 cm/hr), Moderate (1.00-1.99 cm/hr), High (2.00-2.99 cm/hr), and Extreme (≥3.00 cm/hr) storm intensity events in Figure 3.4 indicates that the

majority (60%) of storms observed are considered low intensity. Extreme intensity storms compose approximately 20% of the frequency distribution with moderate (10%) and high (10%) intensity events occurring less frequently. A total of 40 storms were sampled for iron transport profiles with an intensity distribution as follows: 4 Extreme, 10 High, 13 Moderate, and 13 Low intensity storms. Storm intensity classifications of Low, Moderate, High, and Extreme were sampled at all four locations except C2Sout, which does not have low intensity storms represented in the dataset due to an extended autosampler malfunction. The average storm intensity distribution observed each month is depicted in Figure 3.4 with a monthly average of five low intensity storms (0.25-0.99 cm/hr), one moderate intensity (1.00-1.99 cm/hr), one high intensity (2.00-2.99 cm/hr), and two extreme intensity storms (>3.00 cm/hr).

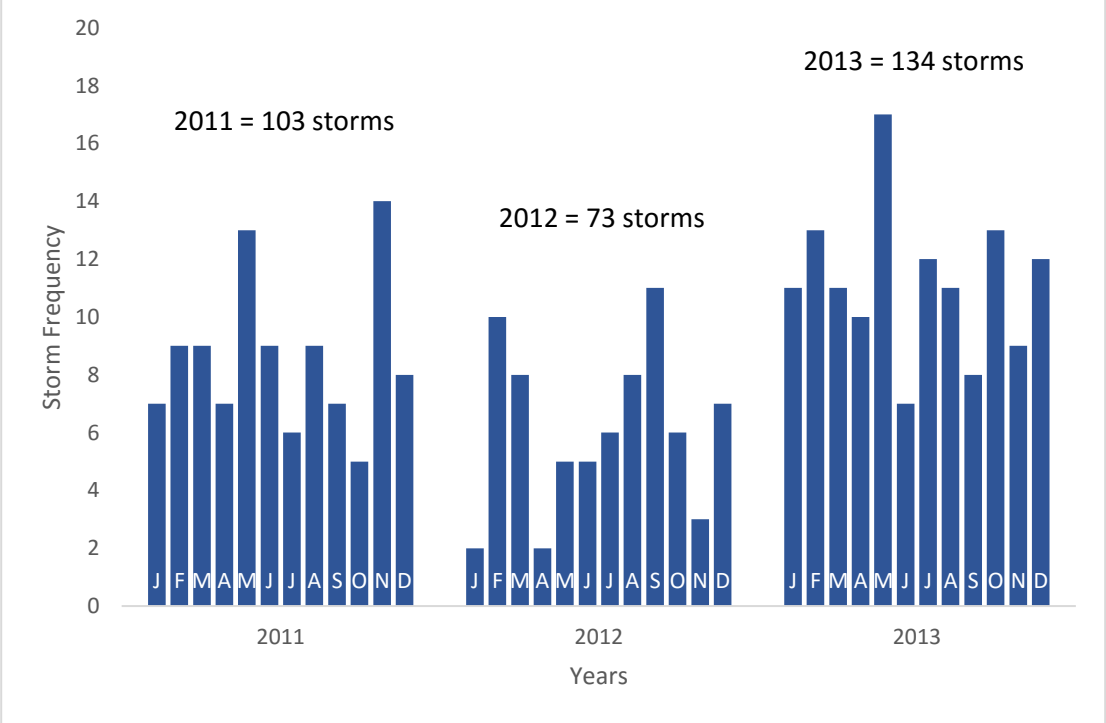

Figure 3.3: Monthly storm frequency distributions for Miami, OK from 2011-2013 indicate that there is an inconsistent distribution of storms from month to month, yet each month has at least two storm events.

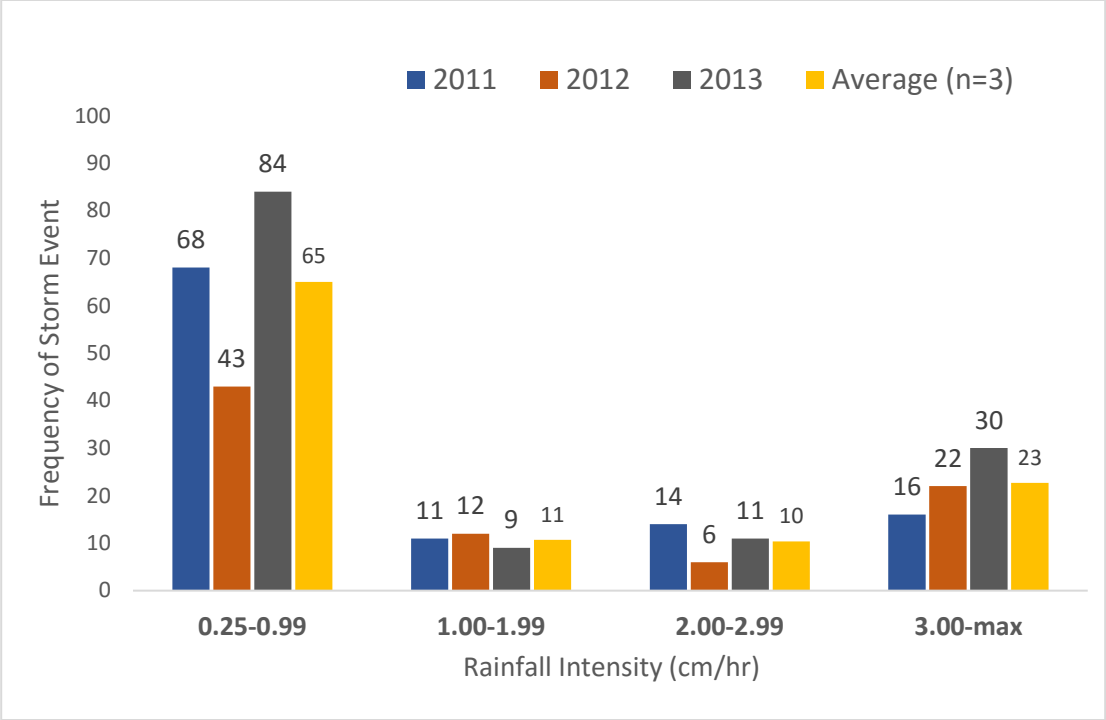

Figure 3.4: Frequency of storm events classified based on maximum rainfall intensity for Miami, OK (2011-2013). Note that low intensity storms are more frequent than all other storm categories combined.

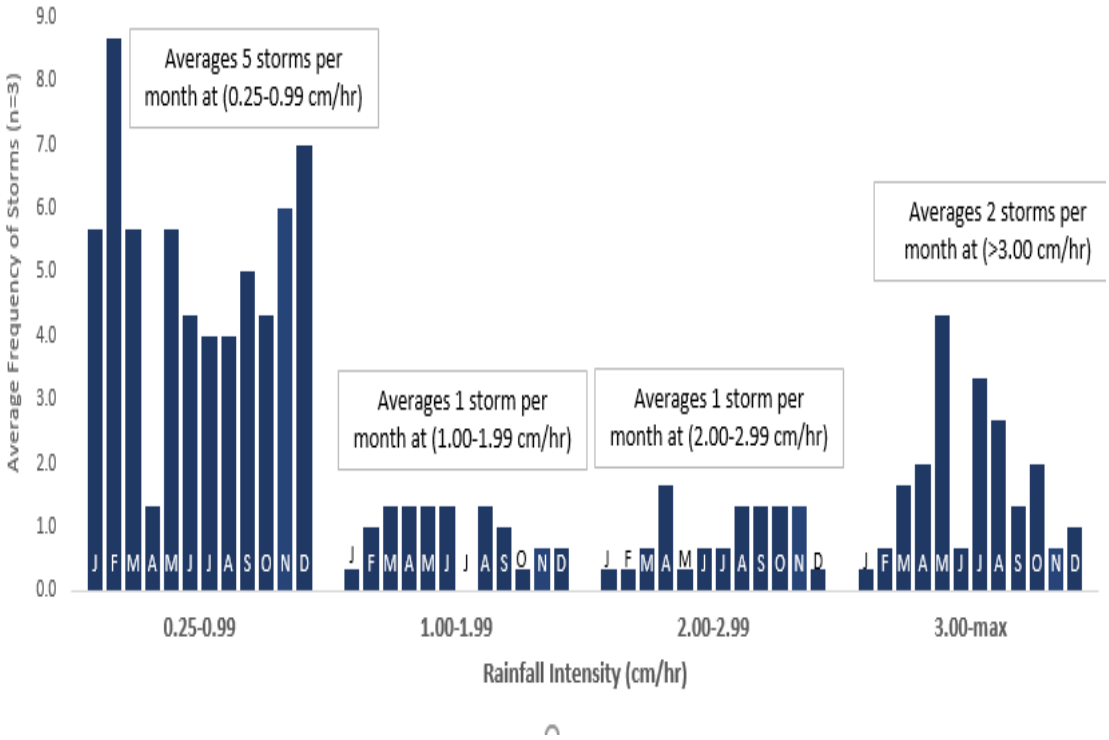

Figure 3.5: Average monthly storm frequency distribution for 2011-2013 based on storm intensity classification

The average annual precipitation from 2011-2013 was 107 cm (σ = 16.5 cm) with a disproportionate amount of the total rainfall accumulation originating from extreme intensity storms (65.5 cm/yr; 61% of average yield). Storms of all four intensity categories are observed seasonally, however, extreme intensity storms in the spring deliver the greatest yield of rainfall.

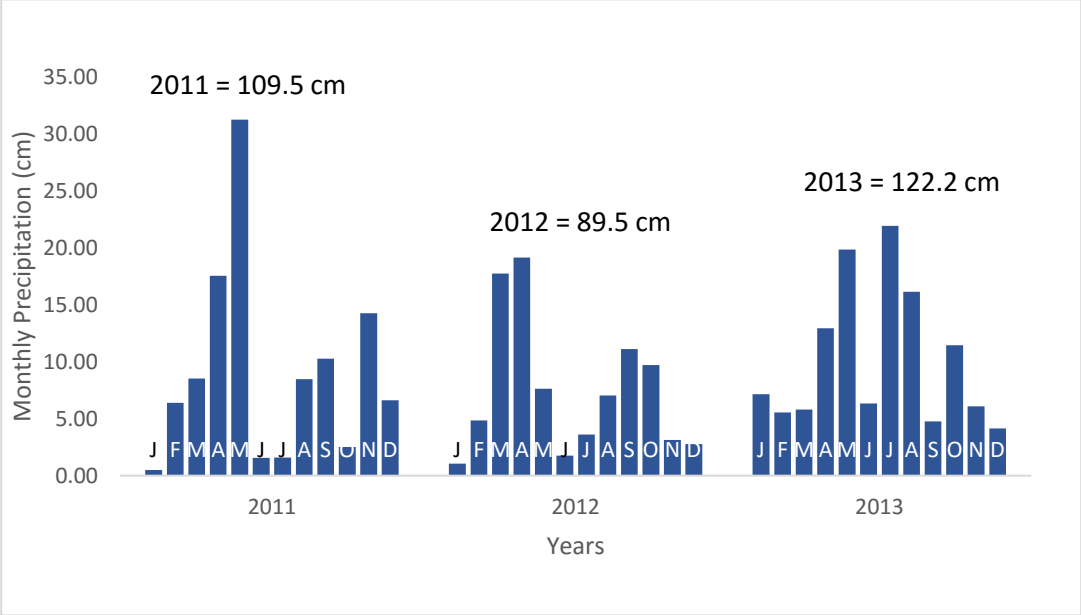

Figure 3.6: Monthly distribution of precipitation yield for Miami, OK from 2011-2013

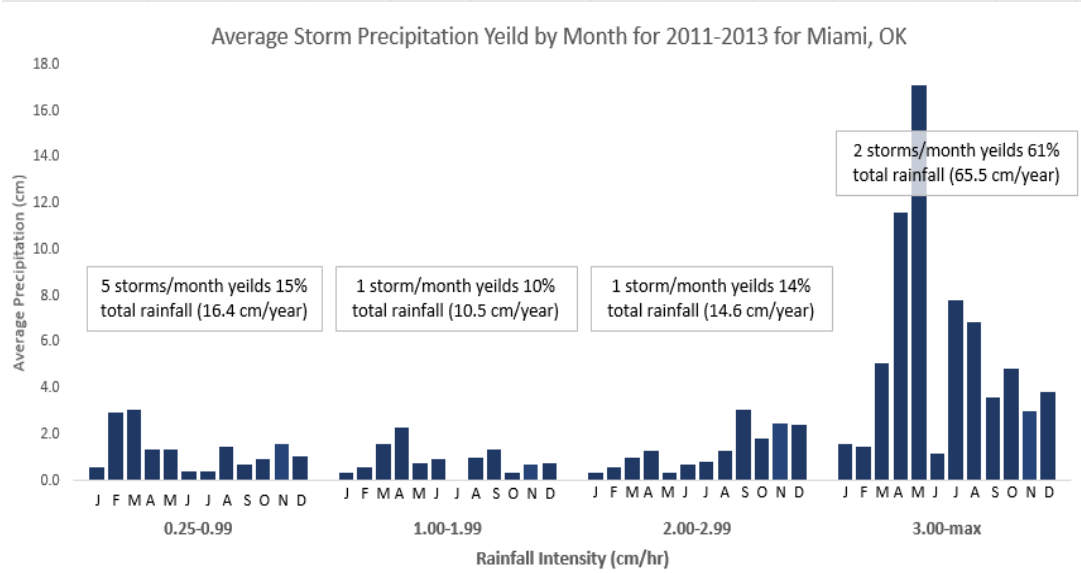

Figure 3.7: Average precipitation yield distribution by month from 2011-2013 for Miami, OK

Seasonal Flow Rates

There was no statistical difference between the average and median flow rates for the Oxidative Unit (Average = 22,560 L/hr; Median = 22,988 L/h; t-stat = -0.182; t-Critical = 2.31; α=0.05) indicating that flow rates into the MRPTS are normally distributed about the mean. Average flowrates were evaluated for statistical significance (Table 3.2) with respect to the five-year average (2009-2013) based on seasonal, annual, and the three-year duration of the storm event driven transport dynamic study (2011-2013).

Table 3.2: Statistical Analysis of the Influent System Flow Rate for the Oxidative Unit of the MRPTS

	Mean Flow Rate (L/hr)	STDEV (L/hr)	%RSD	n	t value	P(T<=t) two-tail	t Critical two-tail	Based on 5 Year Mean
5 Year (2009-2013)	23970	4095	17.1	28	--	--	--	--
3 Year (2011-2013)	20131	3786	18.8	9	2.593	0.020	2.13	Significant
Spring (2009-2013)	27639	2018	7.3	7	3.377	0.003	2.086	Significant
Summer (2009-2013)	23467	2716	11.6	7	0.391	0.702	2.145	Not Significant
Fall (2009-2013)	20786	3985	19.2	6	1.767	0.121	2.365	Not Significant
Winter (2009-2013)	23586	4578	19.4	8	0.214	0.835	2.228	Not Significant
2009	24621	2700	11.0	12	0.593	0.558	2.040	Significant
2010	27789	1740	6.3	7	3.761	0.001	2.064	Significant
2011	20613	1740	8.4	3	2.646	0.046	2.571	Significant
2012	22196	5311	23.9	3	0.561	0.631	4.303	Not Significant
2013	17583	3099	17.6	3	3.276	0.047	3.182	Significant

The difference between the flow rates for the 3-year average (2011-2013; 20,131 L/hr), 2010 (27,789 L/hr), 2011 (20,613 L/hr), 2013 (17,583 L/hr), were statistically significant in comparison to the 5-year average (23,970 L/hr). The statistical significance was present at all three levels of consideration (multiyear average, individual years, and seasonal) with differences for the three-year average, 2011, and 2013 having flows less than the 5-year average. The spring seasonal flow and 2010 both had average flows exceeding the 5-year average by nearly 4,000 L/hour. The average spring flow rate exceeding the 5-year average flow rate is consistent with the average number of extreme intensity storms observed in the spring yielding the largest contribution to precipitation (average of 8 extreme storms; extreme storms contributing to 61% of the total precipitation). Due to the variability in flow rates, the seasonal flow rate was applied to storm transport profiles collected within the applied seasonal range for the calculation of mass transport between cells and out of the passive treatment system rather than using the 5-year average.). This mitigates error associated with over/under estimation of total iron mass transport for both the measured profiles of iron transport already collected and the predictions of total iron transport based on rainfall intensities for storms that were not sampled.

The system effluent flowrate was used to approximate the influent and effluent flows for Cell 6 during storm-event driven iron transport studies. Statistical analysis of the system effluent flow rates (Table 4.2) indicates that the 5-year average system influent flow (Table 3.7 23,970 L/hr) and 5-year average system effluent flow (Table 3.3; 24,280 L/hr) are consistent with each other. The 310 L/hr difference (1.3%) is within the standard deviation of range of both data sets (σ = 4095 L/hr influent; σ = 5835 L/hr effluent).

Table 3.3: Statistical Analysis of the MRPTS Effluent Flow Rate Applied to Cell 6 Mass Transport

	Mean Flow Rate (L/hr)	STDEV (L/hr)	%RSD	n	t value	P(T<=t) two-tail	t Critical two-tail	Based on 5 Year Mean
5 Year (2009-2013)	24280	5835	24.0	27	--	--	--	--
3 Year (2011-2013)	19444	5540	28.5	9	2.237	0.0421	2.145	Significant
Spring (2009-2013)	25903	7525	29.1	7	-0.531	0.610	2.306	Not Significant
Summer (2009-2013)	23814	2337	9.8	7	0.326	0.747	2.056	Not Significant
Fall (2009-2013)	21396	5891	27.5	6	1.086	0.313	2.365	Not Significant
Winter (2009-2013)	25593	6549	25.6	7	-0.483	0.641	2.262	Not Significant
2009	27091	3911	14.4	11	1.727	0.095	2.048	Not Significant
2010	26078	5271	20.2	7	0.786	0.450	2.228	Not Significant
2011	23836	6551	27.5	3	0.112	0.921	4.303	Not Significant
2012	16914	5151	30.5	3	2.317	0.103	3.182	Significant
2013	17583	3099	17.6	3	3.170	0.034	2.776	Significant

Of all the flow rate increments investigated, only the 3-year average (2011-2013) and 2013 were determined to be statistically significant with respect to the 5-year average effluent flow rate (24,280 L/hr). Both the 3-year average and the single year average (2013) were lower than the 5-year average (2009-2013) due to 2012 and 2013 having average flow rates much lower than the average of the remaining dataset (16,914 L/hr and 17,583 L/hr respectively). Greater variance (σ^2) between the values of each dataset influenced the significance testing interpretation yielding more datasets that were not statistically significant with respect to the 5-year average as previously seen in Table 3.2 for the system influent flows. Despite the lack of significant difference between the seasonal flow rates and the 5-year average, the seasonal flow rates were used to determine the mass transport for Cell 6 for consistency with the oxidative unit calculations.

Iron Transport Profiles

Cell 1 Storm-Induced Iron Transport Profiles

Eleven storm-induced iron transport profiles were collected at the effluent of the preliminary oxidation cell (C1Out) and their characteristics are summarized in Table 3.4. The average total iron storm transport profile for each storm intensity classification are compared in Figure 3.8.

The average iron loading for 2011-2013 into Cell 1 was 34,767 kg/year (σ = 1485) with an average retention of 31,305 kg/year (σ = 6445) and an average removal rate of 19.0 g/m^2/day (σ = 4). Cell 1 exported an average of 7862 kg Fe/year with 1066 kg/year (σ = 343; XX%) due to storm-induced transport. Iron exported out of Cell 1 is an average of 3.1% relative to the mass loading from the three AMD seeps (A, B, D) annually, with 13.6% of the total transported iron being due to storm disturbance. Storms were observed to transport iron above the Table 3.4: Summary of Individual Storm Induced Iron Transport Events for C1Out. The reported % of Total Export indicates what percentage of iron exported is due to storm transport for the event.

Intensity Class	Intensity (cm/hr)	Duration (hr)	Yield (cm)	Gross Fe Export (kg)	Net Fe Export(kg)	% of Total Export
Low	0.25	1.3	0.31	12.53	10.76	85.9%
Low	0.31	1.3	0.38	23.5	17.44	74.2%
Low	0.43	3.3	1.1	8.04	6.51	81.0%
Low	0.79	2.5	0.63	3.56	2.22	62.3%
Moderate	1.01	6.5	3.3	10.55	8.8	83.3%
Moderate	1.45	6.8	2.1	1.97	1.16	58.9%
Moderate	1.47	4.0	3.4	13.35	10.36	77.6%
Moderate	1.52	3.0	1.8	18.72	15.04	80.3%
High	2.59	4.5	6.7	21.02	15.98	76.0%
High	2.64	10	4.3	4.46	3.17	71.1%
Extreme	3.01	7.5	9.4	5.28	4.18	79.2%

baseline value for all four storm intensities. The average mass of iron transported out of Cell 1 is 11.2 kg/storm (σ=7.4) for all storms sampled, of which 75.4% of the exported iron during the storm event is due to storm disturbance (8.69 kg/storm; σ = 5.76).

Figure 3.8 is a comparison of the average iron transport profiles at each rainfall intensity category. Both the rainfall intensity and the iron concentration were averaged and plotted over time based on the number of storms sampled within each category. As only one extreme storm classification (intensity exceeding 3.00 cm/hr) was recorded for each location, this plot does not represent an average value but rather a single event. The distinguishing features of the average low and moderate intensity profiles are that two iron transport events are observed (at 6-8hrs, and 18-21 hrs respectively). The high and extreme intensity storm profiles have iron transport peaks during the storm event, and show signs of dilution effects over time, as iron concentrations trend towards a minimum at 19 hours before rebounding back to a stable baseline. Due to the extreme storm occurring in the middle of the 30-hour sampling window triggered by a low intensity storm (0.66 cm/hr), sampling terminates before an additional 19 hours of samples could be collected as is required to fully describe dilution and transport events visually.

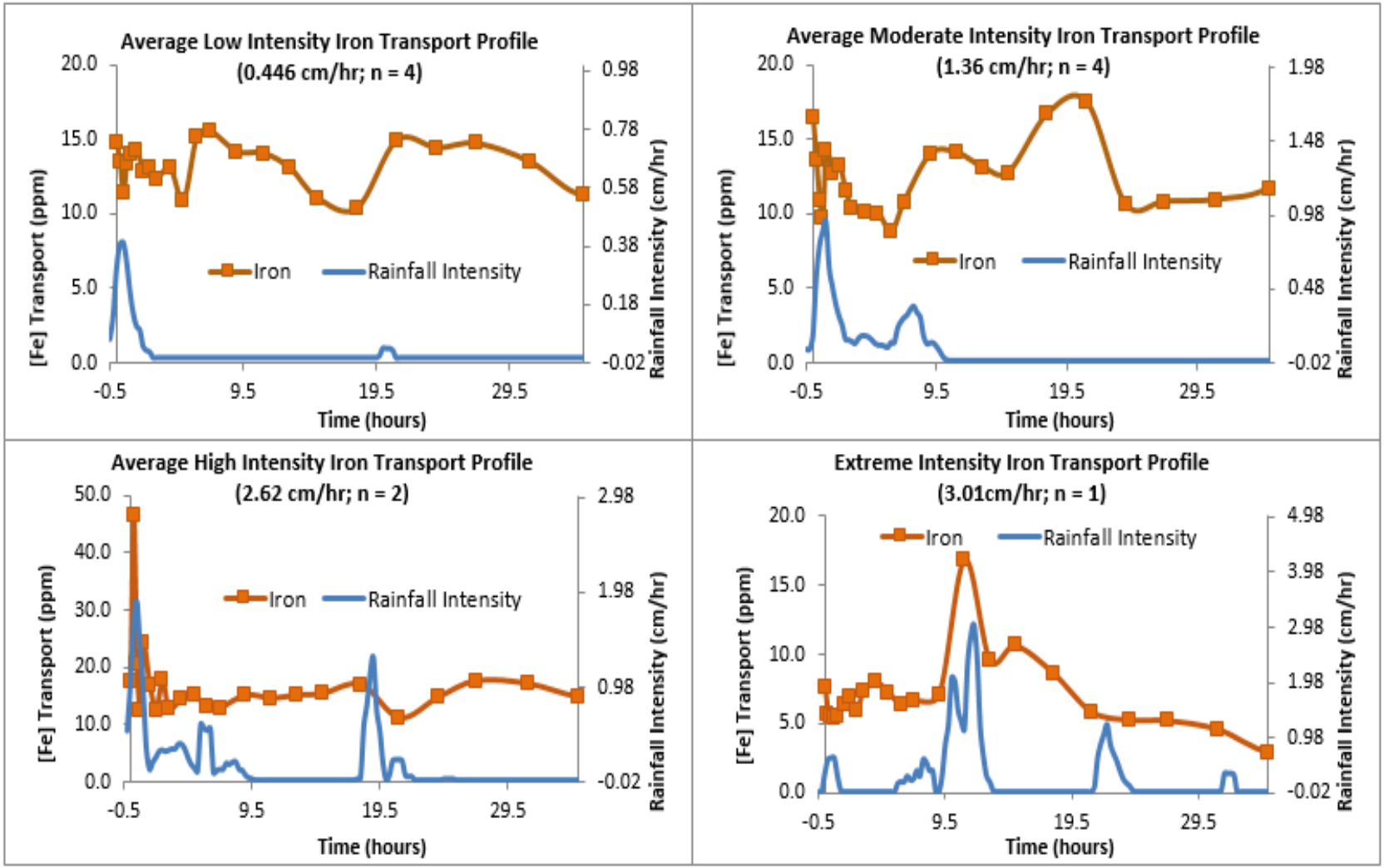

Figure 3.8: Average storm induced iron transport profiles for Cell 1 of the MRPTS based on increasing rainfall intensity ratings: low (0.25-0.99 cm/hr), moderate (1.0-1.99 cm/hr), high (2.0-2.99 cm/hr), and extreme (>3.00 cm/hr). Preliminary Oxidation Cell

Cell 1: Average Storm-Induced Iron Transport Over Time

Eleven storm-induced iron transport profiles were collected at the effluent of the preliminary oxidation cell (C1Out) and were classified based on their rainfall intensity. An average iron mass transport was determined for each classification (Table 3.4).

Table 3.4: Average Iron Mass Transport Based on Storm Intensity Classifications for Cell 1

Intensity	Average Intensity ±σ (cm/hr)	Average Duration ±σ (hrs)	Average Yield ±σ (cm)	Gross Fe Transport ±σ (kg)	Net Fe Transport (kg)	% of Total Export
Low (n = 4)	0.446 ± 0.240	2.06 ± 0.99	0.604 ±0.354	11.9 ±8.6	9.23 ±6.5	77.5%
Moderate (n = 5)	1.32 ± 0.23	4.35 ± 2.26	2.99 ±1.03	13.1 ±7.5	10.3 ±5.9	78.2%
High (n = 1)	2.64	10.0	6.67	4.46	3.17	71.1%
Extreme (n = 1)	3.01	7.50	9.37	5.28	4.18	79.2%

Storms were observed to transport iron above the baseline value for all four storm intensities. The average amount of iron transported out of Cell 1 is 8.69±5.76 kg/storm for all storms sampled, of which 76.5±3.2%; (n = 11) of the transported iron is due to storm disturbance. There is no apparent quantitative relationship between storm intensity and the amount of mass transport of iron. A storm event of any intensity exceeding 0.25 cm/h is a disturbance forcing function driving acute iron export out of Cell 1 (approximately 4-10 kg of Fe per storm; see Table 3.9). Individual storm transport of iron is statistically significant with respect to baseline transport based on a one-tailed Student's-t test (α=0.05; -2.59 t ; 2.35 t Critical). The annual distribution of storm-induced transport of iron shows inconsistencies in iron transport based on the time of year. The positive linear correlation between monthly storm-induced mass transport of iron out of Cell 1 and the average frequency of storms each month for 2011-2013 ($y=8.4405x-6.187$; $r^2 = 0.7895$) supports the statement that the quantity of material being exported above baseline is dependent on storm frequency rather than storm intensity.

Low intensity storms transported the largest quantity of iron consistently each season over the higher intensity events (Figure 3.9). As there are nearly six times as many low intensity storms as moderate and high, and three times as many as the extreme events; the small quantity of iron transported for individual events is additive.

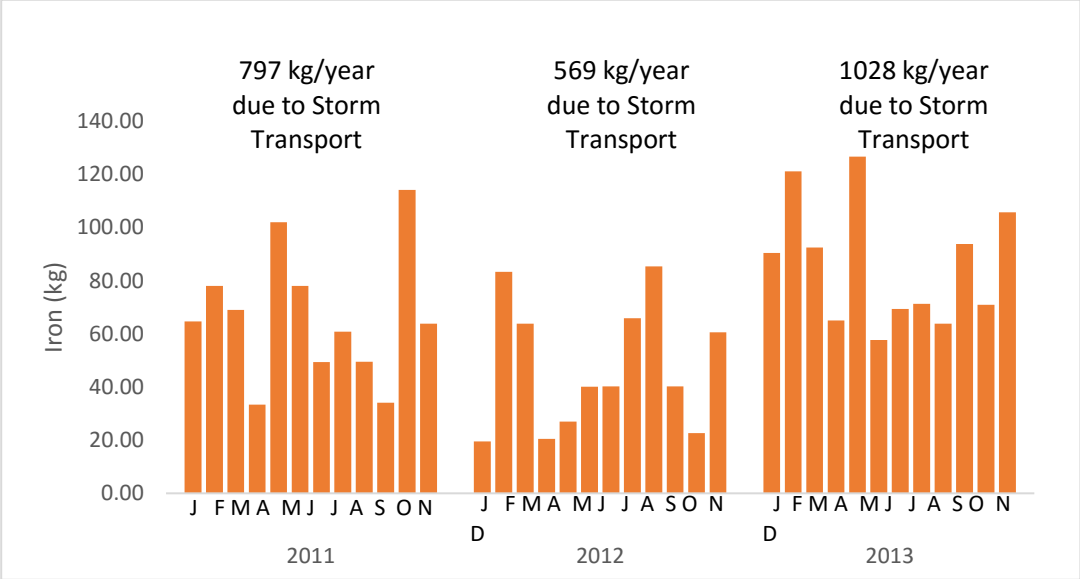

Figure 3.9: Monthly storm induced iron transport distribution over the three-year period of the storm transport profile data collection.

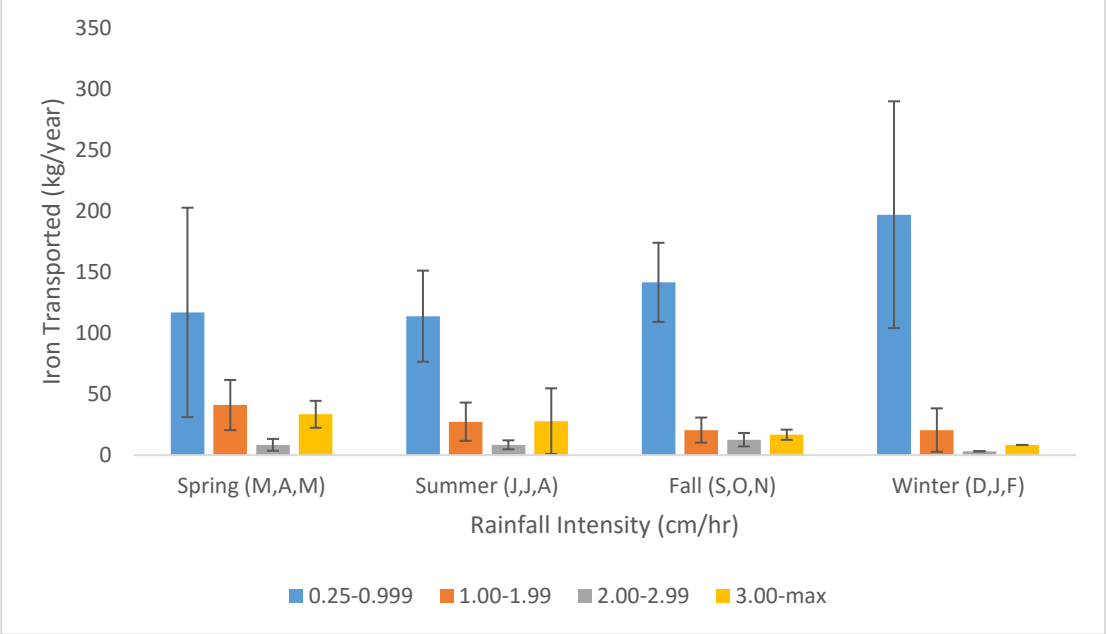

Figure 3.10: Average seasonal iron export from Cell 1 of the MRPTS based on rainfall intensity (2011-2013) with error bars indicating standard deviation (n = 3).

Table 3.5: Summary of Annual Iron Mass Loading and Transport for Cell 1 from 2011-2013

Year	Loading Fe (kg/year)	Gross Fe Transport (kg/year)	Cell Fe Retention (kg/year)	Removal Rate ($g/m^2/day$)	Net Fe Transport (kg/year)	% Transport relative to Fe Loading	% Storm Induced Export
2011 (n = 4)	35509	4203	31305	21.0	852	2.4%	20.3%
2012 (n = 3)	35736	5833	29903	20.1	886	2.5%	15.2%
2013 (n=3)	33058	13551	19507	13.1	1463	4.4%	10.8%
Average (n = 10)	34767	7862	26905	18.0	1067	3.1%	13.6%
STDEV	1485	4994	6445	4.3	343	1.1%	4.7%
%RSD	4.3%	63.5%	24.0%	24.0%	32.2%	37.4%	34.9%

The average iron loading for 2011-2013 into Cell 1 was 34,767 kg/year (σ = 1485) with an average retention of 31,305 kg/year (σ = 6445) and an average removal rate of 18.0 $g/m^2/day$ (σ = 4). Cell 1 exported an average of 7862 kg Fe/year with 1066 kg/year (σ = 343) due to storm-induced transport. Iron exported out of Cell 1 averages of 3.1% of the mass loading from the three AMD seeps (A, B, D), with 13.6% of the transported iron being due to storm disturbance.

Cell 2N and 2S Storm Induced Iron Transport Profiles

The comparison of the three-year average performance of Cell 2N and 2S show consistency in removal efficiency and storm induced iron transport. The average iron loading for 2011-2013 into Cell2N and 2S was 7862 kg Fe/year (σ=5608) with an average retention of 7002 kg/year (σ = 4903) and an average removal rate of 12.8 $g/m^2/day$ (σ = 9) for Cell 2N. Cell 2S had an average retention of 6844 kg/year (σ = 4268) and an average removal rate of 12.5 $g/m^2/day$ (σ = 8). Cell2N transported 118 kg Fe/yr (σ = 37) which represents 15.4% of the mass loading into the cell. Of the material being transported out of Cell 2N, 9.3% of the transported material is storm induced. Cell2S transported 115 kg/yr (σ = 34) which represents 13% of the mass loading into the cell. Of the material being transported out of Cell2S, 13% of it is storm induced

transport. Tables 3.6 and 3.7 summarize individual storm events for both surface flow wetland cells (C2N and C2S).

Table 3.6: Cell 2N Storm Induced Iron Transport Summary (2011-2013)

Intensity Class	Intensity (cm/hr)	Duration (hr)	Yield (cm)	Gross Fe Transport(kg)	Net Fe Transport (kg)	% of Total Export
Low	0.26	1.50	0.37	1.20	0.87	72.7%
Low	0.34	7.00	0.26	1.45	1.07	74.2%
Moderate	1.02	7.25	3.3	1.64	1.50	91.7%
Moderate	1.02	2.50	2.8	0.86	0.68	78.9%
Moderate	1.40	3.00	1.2	1.42	1.11	78.3%
Moderate	1.42	3.50	2.1	1.28	0.98	76.8%
Moderate	1.60	6.75	3.7	0.89	0.59	67.2%
High	2.18	4.75	2.5	0.99	0.60	60.1%
High	2.21	3.75	6.0	2.64	1.47	55.7%
High	2.87	9.75	3.5	0.59	0.43	74.1%
Extreme	8.51	9.75	18.4	2.77	0.73	26.2%

Cell2N had an average export of 0.98 kg Fe/storm (σ = 0.50 kg Fe/storm, n = 11) with total cell export consisting of 68% storm-induced transport (σ = 16%, n = 11) on average for individual storms. Cell2S had an average export of 3.21 kg Fe/storm (σ = 3.66 kg Fe/storm, n = 7) with the total cell export consisting of 80% storm-induced transport (σ = 10%, n = 11) on average for individual storms.

Table 3.7: Cell 2S Storm Induced Iron Transport Summary (2011-2013)

Intensity Class	Intensity (cm/hr)	Duration (hr)	Yield (cm)	Gross Fe Transport (kg)	Net Fe Transport (kg)	% of Total Export
Moderate	1.02	7.00	3.0	2.59	2.24	86.2%
Moderate	1.40	3.50	2.31	10.14	9.25	91.2%
Moderate	2.82	2.75	1.19	11.79	8.67	73.5%
Moderate	1.02	2.50	2.21	0.86	0.68	79.0%
High	3.38	3.75	2.72	1.81	1.17	64.7%
High	4.67	4.00	3.35	0.77	0.67	87.5%
Extreme	3.23	7.25	9.49	0.66	0.49	75.4%

The comparison of average storm induced transport out of the preliminary oxidation cell and the secondary oxidation cells indicates that the secondary surface flow wetlands serve as an iron removal buffer during times of storm disturbance. The average amount of iron being transported to the vertical flow bioreactors due to storm activity was mitigated by 47% due to the cooperative function of the secondary oxidation cells. Cells 3N and 3S would receive an average iron loading of 7862 kg Fe/year (σ=5608) from Cell 1 if the secondary oxidation cells had not been included in the system design.

There is no apparent relationship between storm intensity, duration, or yield with respect to the amount of iron transported from Cell2N and Cell2S. The Cell2N and Cell2S iron transport profiles indicate that iron transport peaks during the storm events with a steady decline in transported iron as the cell returns to baseline While the Cell 1 transport mechanism was dominated by post-storm disturbance transport, Cells 2N and 2S exhibit a mechanism of transport maximized during each storm event. Low and moderate intensity storms show the largest relative amount of transported material over time;67-86% of Fe transport is storm induced in comparison to high and extreme storms (26%-74%) for Cell 2N.

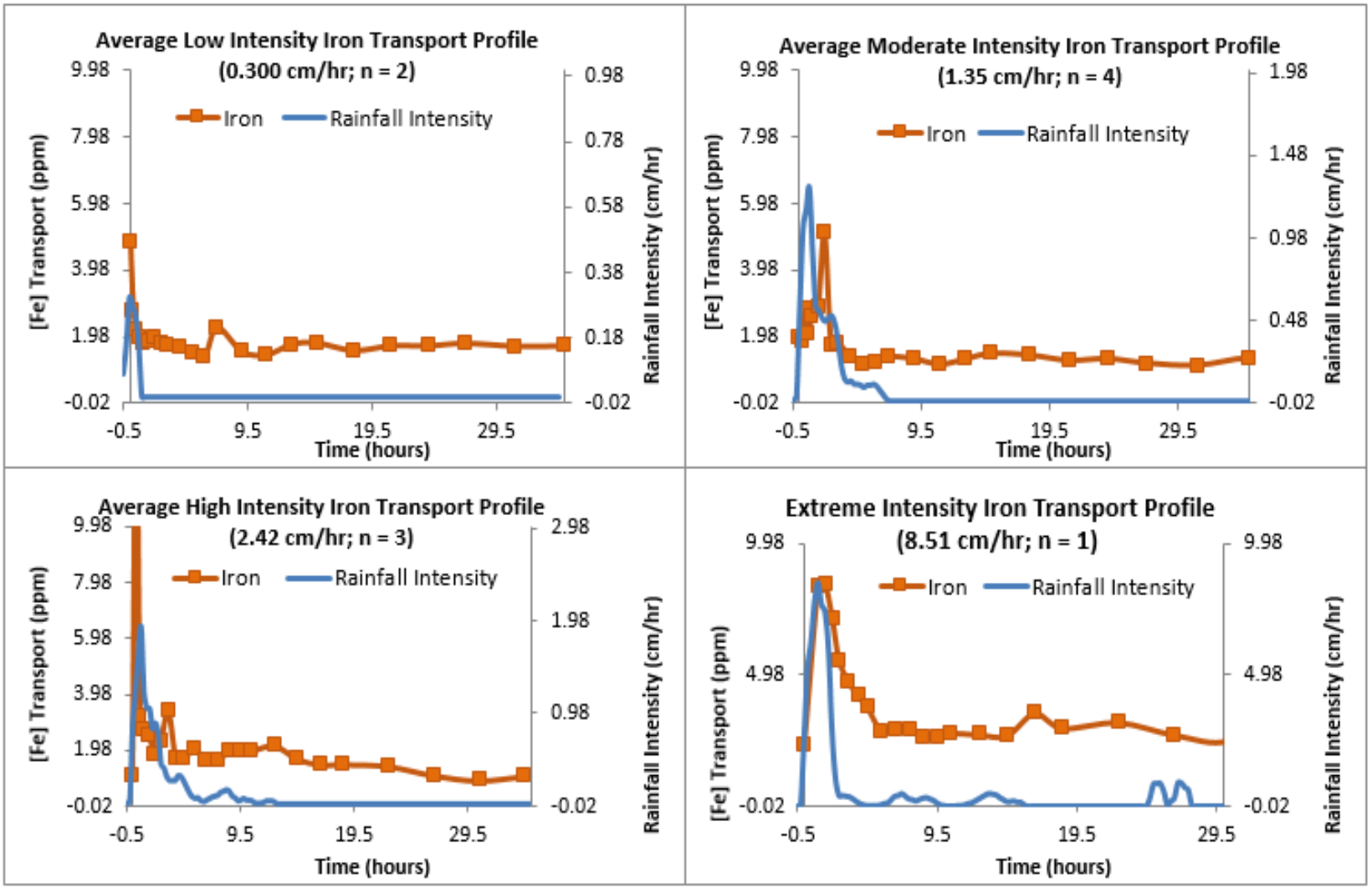

Figure 3.9: Storm induced iron transport profiles for C2NOut based on increasing rainfall intensity ratings: low (0.25-0.99 cm/hr), moderate (1.0-1.99 cm/hr), high (2.0-2.99 cm/hr) and extreme (>3.00 cm/hr)

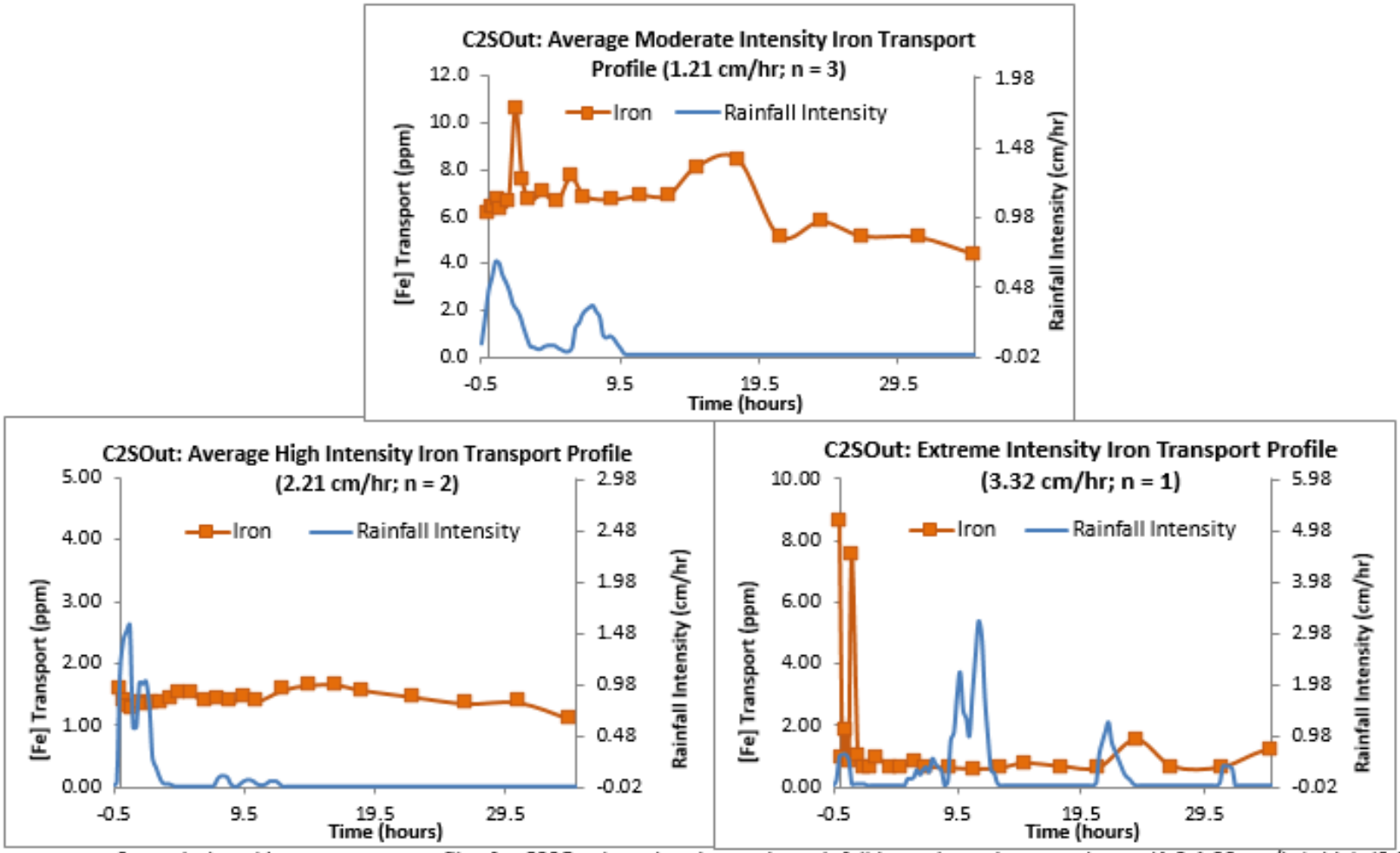

Figure 3.10: Storm induced iron transport profiles for C2SOut based on increasing rainfall intensity ratings: moderate (1.0-1.99 cm/hr), high (2.0-2.99 cm/hr) and extreme (>3.00 cm/hr). No low intensity storms (0.25-0.99 cm/hr) were collected at this location.

High and extreme intensity storms show less % mass transport relative to low and moderate intensity storms. As with the Cell 1 results, it appears that the total amount of mass transported by storms is most sensitive to the number of storm events (storm frequency) observed for a region rather than intensity, duration, or yield. Moderate intensity storms have the largest net transport as dilution is minimized, while the rainfall intensity is suitable for disturbing each cell.

Cell 2N: Average Storm-Induced Iron Transport Over Time

Eleven storm-induced iron transport profiles were collected at the effluent of the northern surface flow wetland (C2Nout) and were classified based on their rainfall intensity. An average iron mass transport was determined for each classification (Table 3.11).

Table 3.8: Average Iron Mass Transport Based on Storm Intensity Classifications for Cell2N

Intensity	Average Intensity ±σ (cm/hr)	Average Duration ±σ (hrs)	Average Yield ±σ (cm)	Gross Fe Transport ±σ (kg)	Net Fe Transport (kg)	% of Total Export
Low (n = 3)	0.527 ± 0.395	5.17 ± 3.18	1.75 ±0.74	1.39 ±0.74	0.777 ±0.074	55.7%
Moderate (n = 4)	1.36 ± 0.25	3.94 ± 1.92	1.11 ±0.28	0.841 ±0.247	0.753 ±0.055	89.5%
High (n = 3)	2.42 ± 0.39	6.08 ± 3.21	1.41 ± 1.09	0.836 ± 0.558	0.633 ± 0.096	75.7%
Extreme (n = 1)	1.99	5.08	1.51	0.887	0.610	68.8%

Storms were observed to transport iron above the baseline value for all four storm intensities. The average amount of iron transported out of Cell2N was 0.980±0.510 kg/storm for all storms sampled, of which 68.2±16.4%; (n = 11) of the transported iron was due to storm disturbance. There is no apparent quantitative relationship between storm intensity and the amount of mass transport of iron. A storm event of any intensity exceeding 0.25 cm/h exports iron out of Cell 2N (less than 1.00 kg of Fe per storm; see Table 3.8). Average individual storm transport

of iron is statistically significant with respect to baseline transport based on the one-tailed Student's t test (α=0.05; -1.93 t stat; 1.72 t Critical).

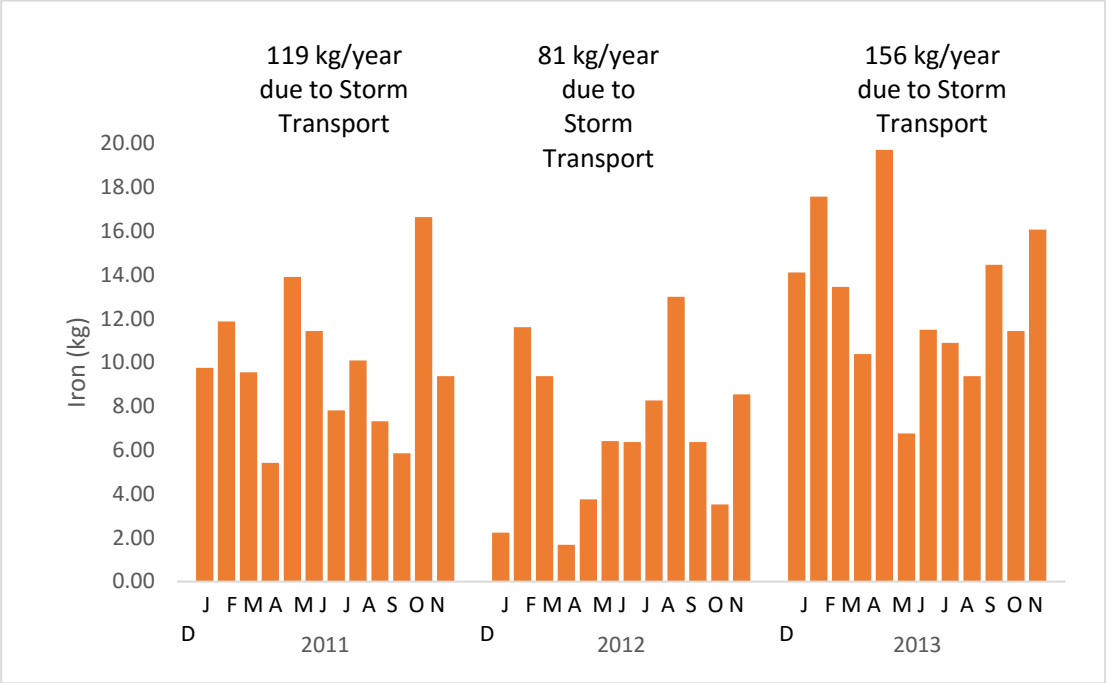

Figure 3.13: Monthly storm induced iron transport distribution over the three-year period of the storm transport profile data collection for Cell2N

The positive linear correlation between monthly storm induced mass transport of iron out of Cell 1 and the average frequency of storms each month for 2011-2013 ($y=0.6795x+1.895$; $r^2 = 0.8150$) supports the statement that the quantity of material being exported above baseline is dependent on storm frequency rather than storm intensity. Low intensity storms transported the largest quantity of iron consistently each season over the higher intensity events (Figure 3.13). As there are nearly six times as many low intensity storms than moderate and high, and three times as many as the extreme events; the small quantity of iron transported for individual events is additive resulting in the largest contribution with increasing time.

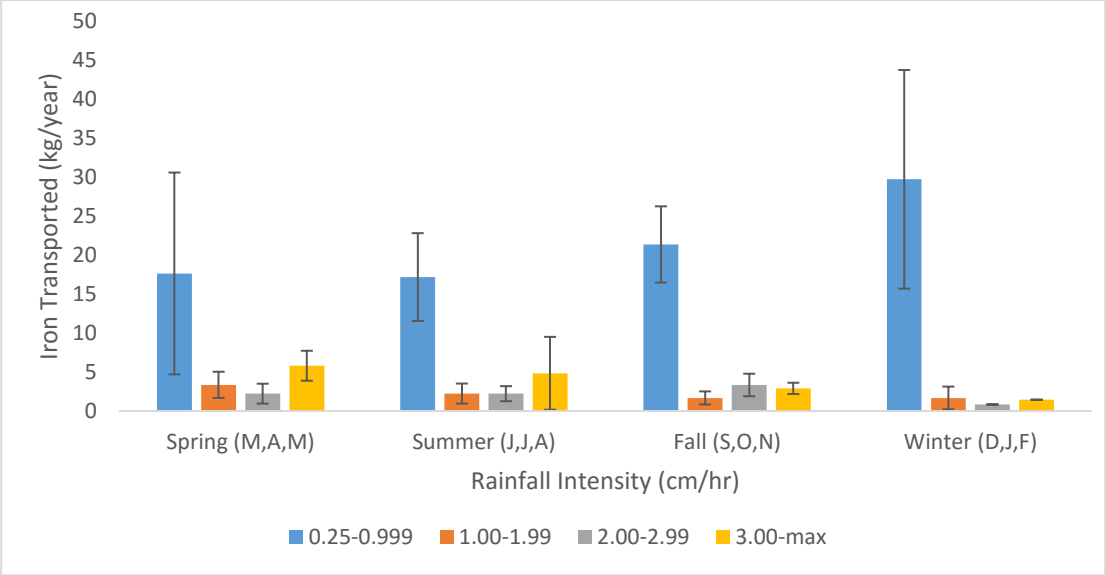

Figure 3.14: Average seasonal iron export from Cell 2N of the MRPTS based on rainfall intensity (2011-2013) with error bars representing the standard deviation of the iron transport between individual events at each intensity.

Table 3.9: Summary of Annual Iron Mass Loading and Transport for Cell 2N from 2011-2013

Year	Loading Fe (kg/year)	Gross Fe Transport (kg/year)	Cell Fe Retention (kg/year)	Removal Rate ($g/m^2/day$)	Net Fe Transport (kg/year)	% Transport relative to Fe Loading	%Storm Induced Export
2011 (n = 4)	4203	881	3322	6.1	127	21.0%	14.5%
2012 (n = 3)	5833	833	5000	9.1	135	14.3%	16.3%
2013 (n=3)	13551	1946	11605	21.2	231	14.4%	11.9%
Average (n = 10)	7862	1220	6642	12.1	165	15.5%	13.5%
Standard Deviation	4994	629	4379	8.0	58	3.8%	2.2%
%RSD	63.5%	51.6%	65.9%	65.9%	35.1%	24.7%	16.3%

The average iron loading for 2011-2013 into Cell 2N was 7,862±4994 kg/year with an average retention of 6642±4379 kg/year and an average removal rate of 12.1±8.0 $g/m^2/day$. Cell 2N exported an average of 1220±629 kg Fe/year with 165±58 kg/year due to storm induced transport. Iron exported out of Cell 2N averages of 15.5% of the mass loading from Cell 1 with

storm-induced transport of iron consisting of 16.3% of the transported iron. The storm induced iron export from Cell2N is 0.50% of the mass loading from the three AMD seeps supplying the system with AMD for treatment (165 kg/year Cell 2N export in comparison to 34,767 kg/year system loading). This is consistent with the metals transport mitigation function of the pond-marsh-pond design of the aerobic surface flow wetland cells to remove and retain any iron transported in the dissolved or particulate state from the preliminary iron oxidation and retention cell (Cell 1).

Cell 2S: Average Storm-Induced Iron Transport Over Time

Seven storm induced iron transport profiles were collected at the effluent of the southern surface flow wetland (C2Sout) and were classified based on their rainfall intensity. An average iron mass transport was determined for each classification (Table 4.7).

Table 3.10: Average Iron Mass Transport Based on Storm Intensity Classifications for Cell 2S

Intensity	Average Intensity ±σ (cm/hr)	Average Duration ±σ (hrs)	Average Yield ±σ (cm)	Gross Fe Transport ±σ (kg)	Net Fe Transport (kg)	% of Total Export
Moderate (n = 4)	1.24 ± 0.25	4.00 ± 2.21	2.25 ±0.86	6.11 ±5.66	5.02 ±4.56	82.3%
High (n = 2)	2.21 ± 0.29	3.88 ± 0.18	3.03 ± 0.45	1.29 ±0.74	0.922 ± 0.355	71.5%
Extreme (n = 1)	3.23	7.25	9.49	0.655	0.494	75.4%

Storms were observed to transport iron above the baseline value for all four storm intensities. The average amount of iron transported out of Cell2S is 3.21±3.95 kg/storm for all storms sampled, of which 76.0±0.5%; (n = 7) of the transported iron is due to storm disturbance. There is no apparent quantitative relationship between storm intensity and the amount of mass transport of iron. A storm event of any intensity exceeding 0.25 cm/h exports iron out of Cell 2S (Table 3.10). Average individual storm transport of iron is not statistically significant

with respect to baseline transport based on the one-tailed Student's t test (α=0.05; -1.58 t stat; 1.89 t Critical). This is most likely due to the small sample size (n = 7) and the high variability of storm induced iron transport on a storm by storm basis. The combination of the C2N and C2S datasets yields an average gross iron transport of 2.46±3.18 kg Fe of which 1.85±2.63 kg Fe is storm-induced transport (73.0±15.2% of total transport per storm). Average individual storm transport of iron is statistically significant with respect to baseline transport for the combined C2N/C2S dataset based on the one- tailed Student's t test (α=0.05; 1.90 t stat; 1.72 t Critical).

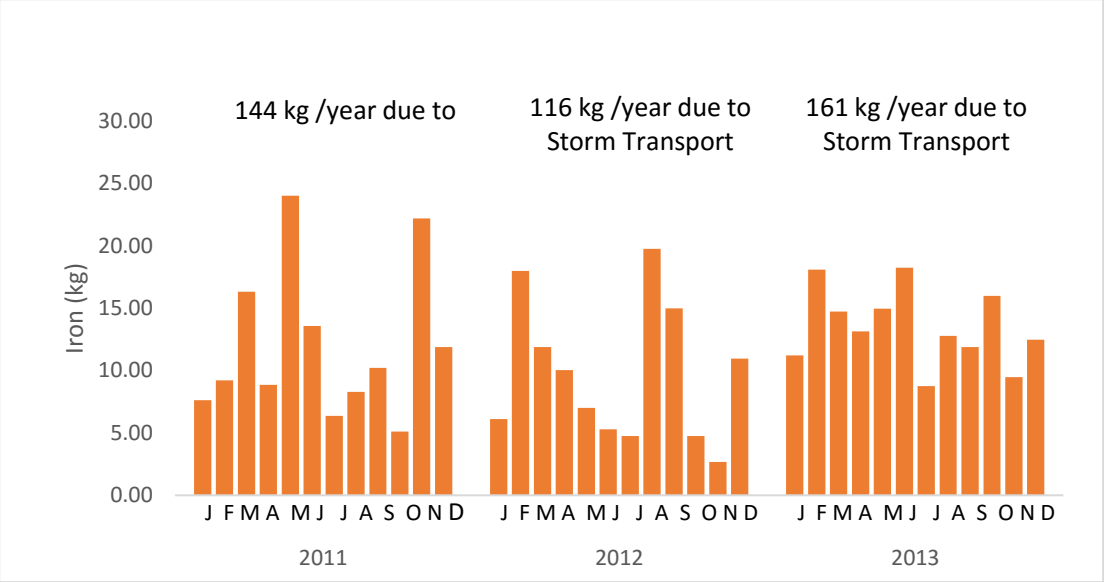

Figure 3.15: Monthly storm induced iron transport distribution over the three-year period of the storm transport profile data collection for C2SOut.

Low and moderate intensity storms transported the greatest quantity of iron consistently each season over the higher intensity events (Figure 3.16). The high frequency of low intensity events leads to a cumulative effect for iron transport with low intensity storms transporting the largest fraction of the iron mass loading. The contribution of moderate storms to the export of iron from Cell 2S, that was not observed for Cell 2N, is due to a vegetation loss in the

surface flow wetlands section of the cell. Muskrat activity and water levels exceeding design severely impacted the success of emergent hydrophyte species between growing seasons. Vegetative cover is the primary difference between the Cell 2N and Cell 2S units, as they receive the same iron mass loading (7862±3783 kg/year) exported from Cell 1, and have the same design profile (surface area, aspect ratios, design hydraulic treatment volume, etc.).

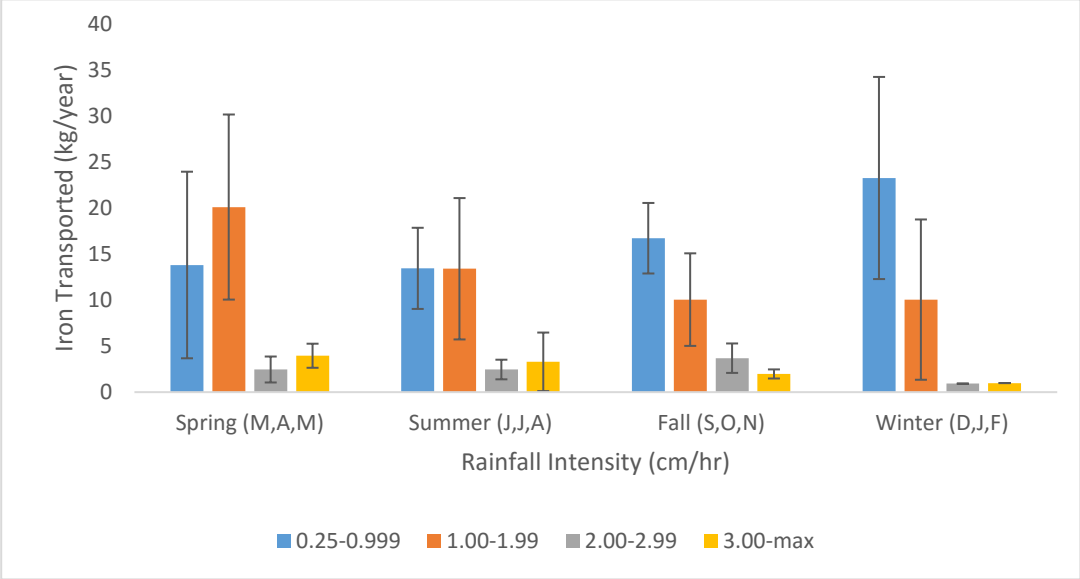

Figure 3.16: Average seasonal iron export from Cell 2S of the MRPTS based on rainfall intensity (2011-2013) with standard deviation of average iron transport values for each intensity.

Table 3.11 Summary of Annual Iron Mass Loading and Transport for Cell 2S from 2011-2013

Year	Loading Fe (kg/year)	Gross Fe Transport (kg/year)	Cell Fe Retention (kg/year)	Removal Rate ($g/m^2/day$)	Net Fe Transport (kg/year)	% Transport relative to Fe Loading	%Storm Induced Export
2011 (n = 4)	4203	625	3578	6.54	76.1	14.9%	12.2%
2012 (n = 3)	5833	552	5281	9.65	142	9.46%	25.8%
2013 (n=3)	13551	1879	11673	21.3	121	13.9%	6.47%
Average (n = 10)	7862	1019	6844	13.0	113	12.7%	14.8%
Standard Deviation	4994	746	4268	7.79	33.9	0.77%	9.90%
%RSD	63.5%	73.2%	62.4%	62.4%	29.9%	6.0%	66.8%

The average iron loading for 2011-2013 into Cell 2S was 7,862±4994 kg/year which is identical to Cell 2N as the effluent from Cell 1 is split into parallel flows. Cell 2S has an average retention of 6844±4268 kg/year and an average removal rate of 13.0±7.8 g/m^2/day. Cell 2S exported an average of 1019±746 kg Fe/year with 113±34 kg/year due to storm induced transport. Iron exported out of Cell 2S averages of 12.7% of the mass loading from Cell 1 with storm-induced transport of iron consists of 14.8% of the transported iron being due to storm disturbance. The storm induced iron export from Cell2N is 0.33% of the mass loading from the three AMD seeps supplying the system with AMD for treatment (113 kg/year Cell 2N export in comparison to 34,767kg/year system loading). This is consistent with the metals transport mitigation function of the pond-marsh-pond design of the aerobic surface flow wetland cells to remove and retain any iron transported in the dissolved or particulate state from the preliminary iron oxidation and retention cell (Cell 1).

The comparison of the three-year average performance of Cell 2N and 2S show consistency in removal efficiency and storm induced iron mass transport. The average iron loading for 2011-2013 into Cell2N and 2S was 7862 kg Fe/year (σ=5608) with an average retention of 7002 kg/year (σ = 4903). Cell 2N has an average removal rate of 12.8 g/m^2/day (σ = 9). Cell 2S has an average retention of 6844 kg/year (σ = 4268) and an average removal rate of 12.5 g/m^2/day (σ = 8). Cell2N transported 118 kg Fe/yr (σ = 37) which represents 0.34% of the mass loading into the cell. Of the material being transported out of Cell 2N, 13.5% of the transported material is storm induced. Cell2S transported 113 kg/yr (σ = 34) which represents 12.7% transport of the mass loading into the cell from the preliminary oxidation cell. Of the material being transported out of Cell2S, 14.8% of it is storm induced transport.

Cell 6Out Storm-Induced Iron Transport Profiles

Storm- induced transport of iron at Cell 6 (Table 3.12) is only observed during the active rainfall period of each storm event (301 kg/year; σ = 82) and averages 0.33 kg Fe/storm (σ = 0.27 kg Fe/storm, n = 11). The total iron transported during the sampling period (152 kg/year; σ=58) represents 16.2% of the loading into Cell 6, with an average of 32% of the transported iron due to storm disturbance. The surface area-adjusted removal rate for Cell 6 averaged 0.50 $g/m^2/day$ and is limited by low iron loading at this stage of the treatment process.

Table 3.12: Storm Induced Iron Transport for Cell6 (System Effluent) Based on Storm Intensity Classification

Intensity Class	Intensity (cm/hr)	Duration (hr)	Yield (cm)	Gross Fe Transport (kg)	Net Fe Transport (kg)	% of Total Export
Low	0.26	1.50	0.26	0.18	0.15	79.6%
Low	0.56	3.25	2.05	0.12	0.09	72.4%
Low	0.74	1.25	0.76	0.81	0.60	74.0%
Moderate	1.02	7.00	3.30	0.73	0.55	75.3%
Moderate	1.29	9.25	1.96	0.41	0.12	28.3%
Moderate	1.42	4.00	2.16	0.86	0.74	85.9%
Moderate	1.73	3.00	0.26	0.87	0.75	85.4%
High	2.13	2.75	2.51	0.28	0.12	41.9%
High	2.26	4.25	6.86	0.16	0.09	58.6%
High	2.67	10.50	3.48	0.21	0.15	74.6%
Extreme	7.88	4.25	15.3	0.43	0.25	57.8%

Storm induced iron transport out of Cell 6 was observed for low, moderate, high, and extreme storm classifications, yet the average mass transported per storm event averaged only (0.33kg/storm event). Transport was at its maximum during the precipitation period for the low, high, and extreme storm events, while moderate storm events transported material during the storm event as well as after the event (Figure 3.11).

Cell6: Average Storm-Induced Iron Transport Over Time

Eleven storm induced iron transport profiles were collected at the effluent of the passive treatment system polishing surface flow wetland (C6out). The same rainfall intensity criteria that were applied to Cell 1, Cell 2N, and Cell 2S were also applied to C6Out (low, moderate, high, extreme). The seasonal flow rates used to calculate mass loadings for Cell 6 were determined from five years of flow measurements collected at the MRPTS weir (2009-2013). The short- term impact of rainfall events on the influent and effluent flow rates of the cell over a 30+hr period is negligible due to retention time of the passive treatment system (cells 1-5) exceeding the sample collection time increment. Seasonal flow rates measured at the MRPTS weir were used to adjust the influent and effluent mass loadings for Cell 6 based on assuming a steady state condition with respect to flow for acute storm events. The use of seasonal flow rates averaging three months of measurements is intended to correct for seasonality in mass loading as a chronic event. Table 3.13 is a summary of the average intensity, duration, and yield of storms sampled at C6Out as it relates to the average amount of iron export from MRPTS.

Table 3.13: Average Iron Mass Transport Based on Storm Intensity Classifications for Cell6

Intensity	Average Intensity ±σ (cm/hr)	Average Duration ±σ (hrs)	Average Yield ±σ (cm)	Gross Fe Transport ±σ (kg)	Net Fe Transport (kg)	% of Total Export
Low (n = 4)	0.63 ± 0.30	3.25 ± 2.65	0.91 ±0.68	0.46 ±0.36	0.35 ±0.27	75.3%
Moderate (n = 3)	1.11 ± 0.31	5.38 ± 3.49	2.02 ±1.04	0.70 ±0.20	0.50 ±0.27	65.9%
High (n = 3)	1.64 ± 0.37	4.75 ± 3.50	1.89 ± 1.30	0.61 ± 0.30	0.43 ± 0.36	60.4%
Extreme (n = 1)	2.20	3.05	2.87	0.378	0.277	65.1%

Storms were observed to transport iron above the baseline value for all four storm intensities. The average amount of iron transported out of Cell6 is 0.54±0.15 kg/storm for all storms

sampled, of which 66.7±6.3% of the material transported during the mean storm event (n = 11) of the transported iron is due to storm disturbance for individual storms. There is no apparent quantitative relationship between storm intensity and the amount of mass transport of iron. A storm event of any intensity exceeding 0.25 cm/h exports iron out of Cell6 (less than 0.50 kg of Fe per storm; see Table 3.13). Average individual storm transport of iron is statistically significant with respect to baseline transport based on the one-tailed Student's t test (α=0.05; 2.26 t stat; 1.78 t Critical).

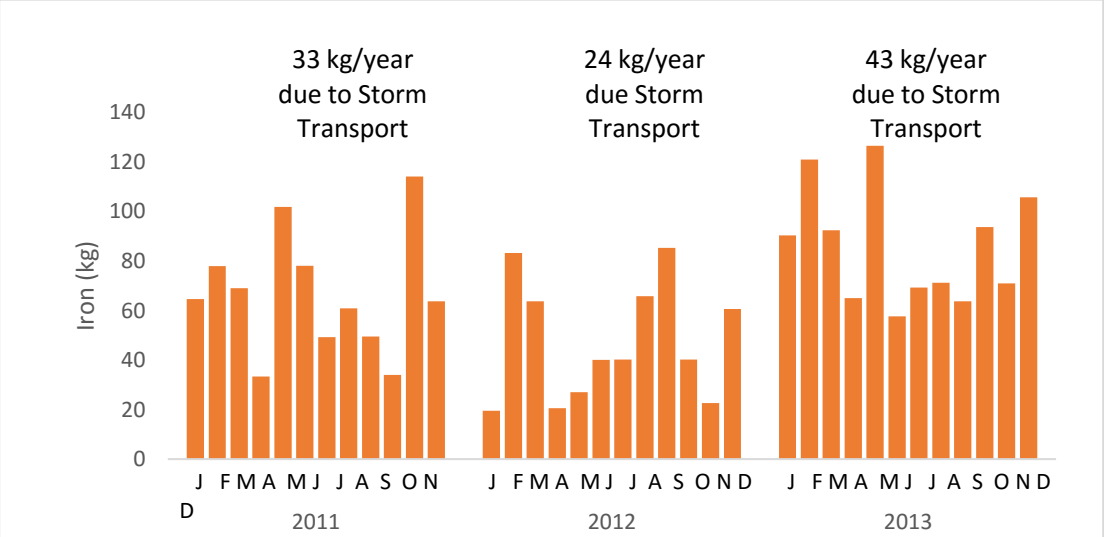

Figure 3.17: Monthly storm induced iron transport distribution over the three-year period of the storm transport profile data collection for Cell6

The positive linear correlation between monthly storm induced mass transport of iron out of Cell 6 and the average frequency of storms each month for 2011-2013 ($y=2.54x+1.54$; r^2 = 0.9111) supports the statement that the quantity of material being exported above baseline is dependent on storm frequency rather than storm intensity. Low intensity storms transported the largest quantity of iron consistently each season over the higher intensity events (Figure 3.17). As there are nearly six times as many low intensity storms than moderate and high, and three times as many as the extreme events; the small quantity of iron

transported for individual events is additive resulting in the largest contribution with increasing time.

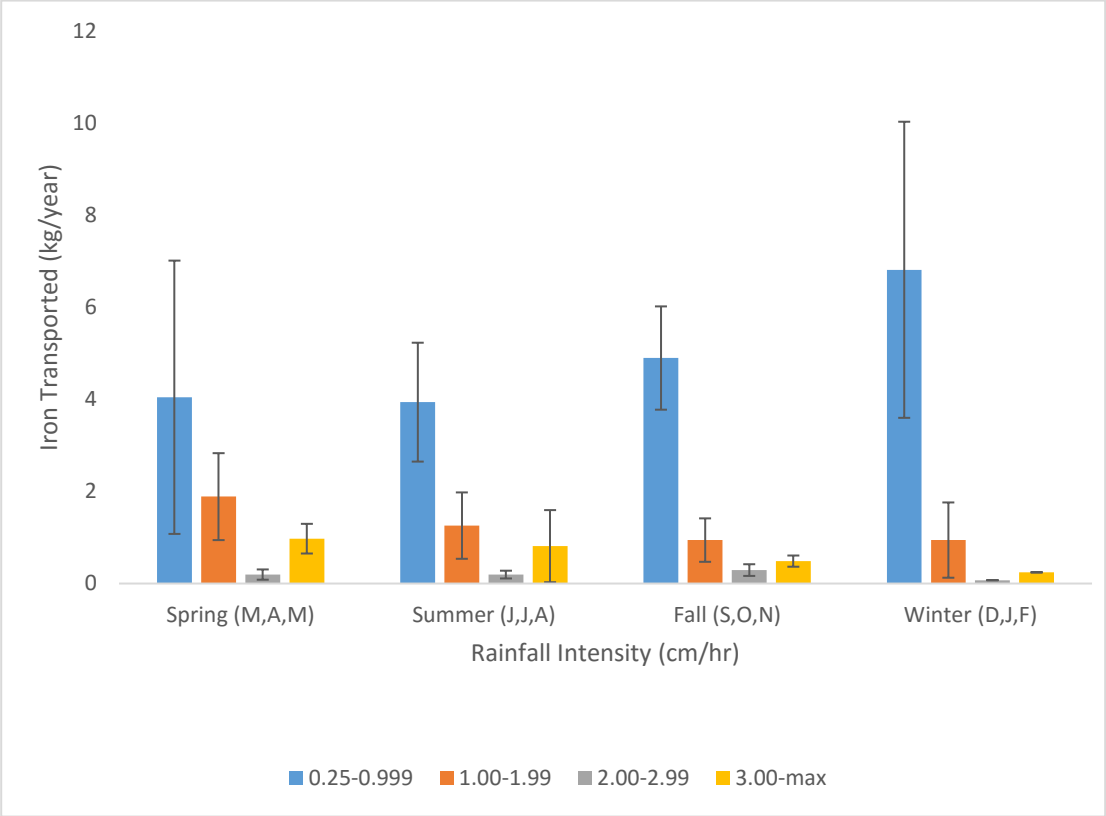

Figure 3.18: Average seasonal iron export from Cell6 of the MRPTS based on rainfall intensity (2011-2013) with error bars representing the standard deviation of the iron transport between individual events at each intensity.

Table 3.14: Summary of Annual Iron Mass Loading and Transport for Cell6 from 2011-2013

Year	Loading Fe (kg/year)	Gross Fe Transport (kg/year)	Cell Fe Retention (kg/year)	Removal Rate ($g/m^2/day$)	Net Fe Transport (kg/year)	% Transport relative to Fe Loading	%Storm Induced Export
2011 (n = 4)	230	106	124	0.31	35.1	15.3%	33.1%
2012 (n = 3)	281	217	64.5	0.54	42.7	15.2%	19.7%
2013 (n=3)	391	133	258	0.64	68.6	17.6%	51.5%
Average (n = 10)	301	152	149	0.50	48.8	16.0%	34.8%
Standard Deviation	82	58	99	0.17	17.6	1.3%	16.0%
%RSD	27.4%	37.9%	66.6%	34.5%	36.0%	8.3%	46.0%

The average iron loading for 2011-2013 into Cell6 was 301±82 kg/year with an average retention of 149±99 kg/year and an average removal rate of 0.45±0.17 g/m^2/day. Cell6 exported an average of 152±58 kg Fe/year with 49 ±18 kg/year due to storm induced transport. Iron exported out of Cell6 averages of 16.0% of the mass loading into Cell6 with storm-induced transport of iron consists of 34.8% of the transported iron being due to storm disturbance on a yearly basis. The storm induced iron export from Cell6 is 0.87% of the mass loading from the three AMD seeps supplying the system with AMD for treatment (301 kg/year Cell6 export in comparison to 34,767kg/year system loading). This is consistent with the metals transport mitigation function of the pond-marsh-pond design of the aerobic surface flow wetland cells to remove and retain any iron transported in the dissolved or particulate state.

Mass transport out of Cell6 was only observed during storm events, with no secondary transport observed over the 30+hr period. This indicates that the iron transport only occurred during the rainfall event which coincides with the first flush of sampling from a dormant autosampler. It is suspected that the flush of iron observed may be partially due to accumulated solids and biomass on the autosampler weighted sieve. Even with the three consecutive flush protocol preceding sample collection, there may not have been enough time between the rinsing phase and the sample collection phase for these first flush samples for this materials to clean out and not cause a false positive for iron in the transport profile samples (less than five minutes between first rinse, and sample #1 collection; 20 minutes to the second sample collection). Inclusion of these values into the mass transport was suspected to lead to a false positive overestimation of total iron exported from the MRPTS that was significantly different from the average mass export of 49 ±18 kg/year due to storm induced

transport of iron. The storm induced mass transport of iron determined from the dataset with the first flush outliers removed is 36.0±10.6 kg/year which is not significantly different from the uncorrected value (t stat = 1.08; t Critical = 2.35; one tailed Student's t test with unequal variances).

The calculation of iron mass loading is based on the area under the 24 measurement transport profiles rather than the concentration of a single data point like the first flush or the average of data points that may be skewed by artificially elevated concentrations within the first flush period. This procedure mitigates the impact of any single data point which may be acting as an outlier, and instead focuses on trends in transport over time. As most of the mass transport for all cells occurs due to the disturbance of the precipitated iron oxyhydroxides in the water column, the transport profile is observed after the storm event. Only extreme storm events have peaks of iron transport that coincide with storm events of sufficient rainfall intensity to have triggered sampling.

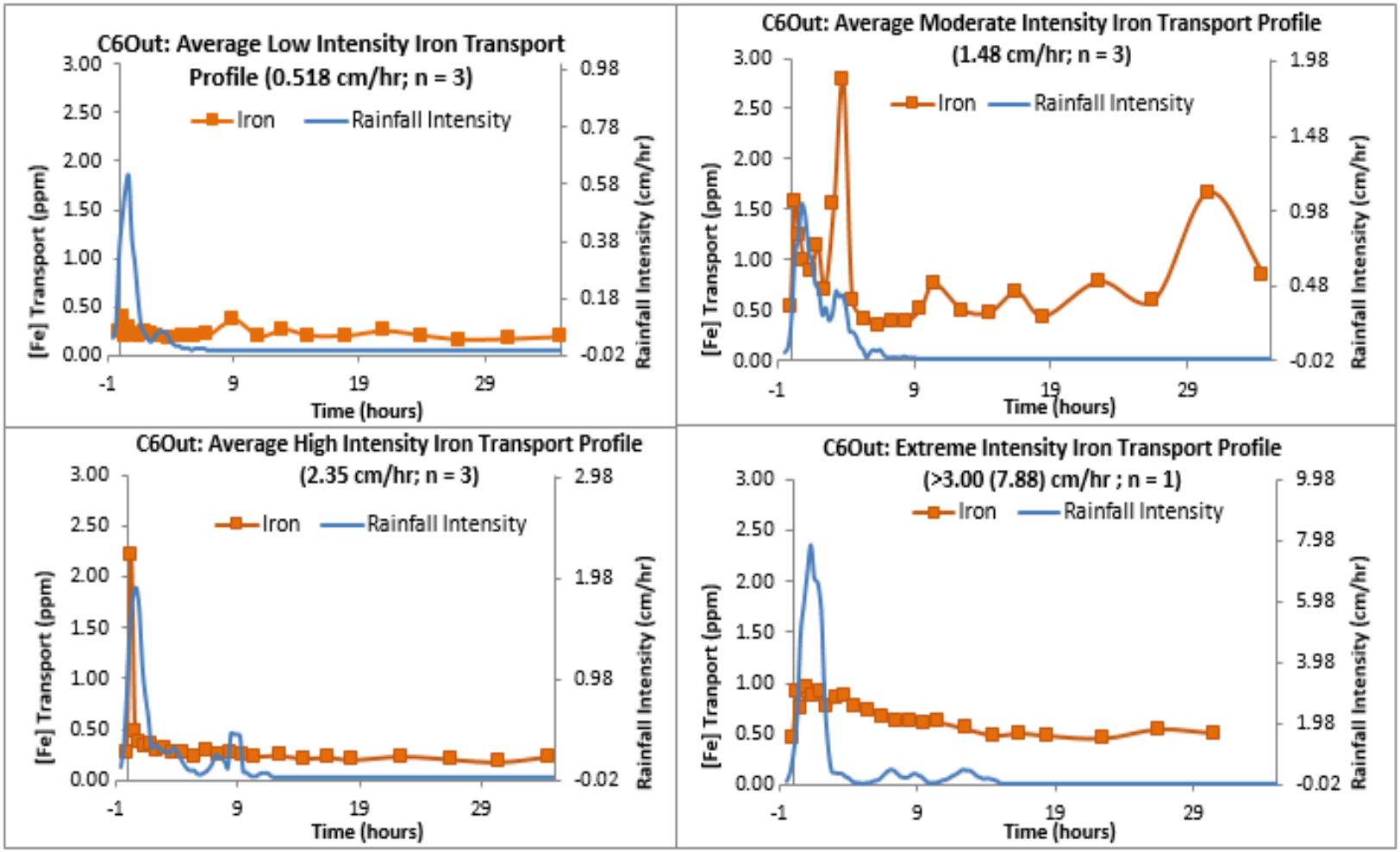

Figure 3.11: Storm induced iron transport profiles for C6Out based on increasing rainfall intensity ratings: low (0.25-0.99 cm/hr), moderate (1.0-1.99 cm/hr), high (2.0-2.99 cm/hr) and extreme (>3.00 cm/hr)

Significance of Transport

The statistical significance of storm induced mass transport with respect to baseline transport was evaluated using a single tailed t-test ($\alpha = 0.05$) for unpaired data with unequal variance. Although the amount of iron transported by individual storm events does not scale with increasing storm activity, the amount of iron being transported due to individual storm disturbances was statistically significant with respect to the baseline transport at all four locations (Table 3.6). This confirms that storms of any intensity will increase the concentration of transported iron significantly over the baseline concentration that would have persisted without storm disturbance. Sampling during acute transport events (during precipitation or for 30+ hrs following precipitation) will lead to falsely positive total iron concentrations.

Table 3.15: t test results ($\alpha = 0.05$, 1 tailed, unpaired) for storm transport by location

	Average Transport (kg/storm) ± σ					
Location	Storm Induced	Baseline	df	t Stat	T Critical	Interpretation
Cell 1	8.69±5.76	2.49±1.74	12	3.42	1.78	Significant
Cell 2N+S	0.96±0.47	0.44±0.50	20	1.9	1.72	Significant
Cell 6	0.33±0.27	0.13±0.08	12	2.56	1.78	Significant

Mechanism of Transport

There are two main lines of thought regarding the mechanism of storm-induced total iron transport. Both perspectives focus on the transport of precipitated iron oxyhydroxides

between cells with their principle difference centered on the source of the transported solids. Shallow treatment wetlands and oxidative channels are both susceptible to re-suspension of sequestered iron oxides from accumulated solids due to their shallow water columns (wetlands) and infrequent scouring flows (channels).

Alternatively, a second mechanism for the transport of iron oxyhydroxides due to storm events focuses on the disruption of floc formation and settling rates within the water column rather than the resuspension of sequestered materials. Transport via resuspension in Cell 1 is unlikely due to the design depth of the treatment cell (> 1.5m) being too deep for even the most intense rain event to penetrate through the water column to re-suspend the solids held in storage. The lack of a correlation between storm intensity and mass transport at all four locations including Cell 1 supports this idea, suggesting that the source of the mobilized iron is finite within the time constraints of the storm. Transport of solids suspended from the accumulated storage layers would mean that a nearly infinite supply of source material was available for resuspension. However, iron transport profiles observed for Cell 1 suggest that intense storm activity agitates the water column near the surface of the treatment cell resulting in (1) mixing of the settling profile over a smaller and more localized depth, and (2) fragmentation of floc structure diminishing the size and drag of particles yielding slower settling rates. Average particle sizes were measured using a LISST laser diffractometer for each section of Cell 1 from the stabilized catwalk structures. Average particle sizes at the surface of the water were 7.34 µm (Section 1), 12.53 µm (Section 2), 8.66 µm (Section 3), and 11.72 µm for C1Out (cell export) under standard operating conditions (no storm disturbance; May 2016). Particles from Section 1 coagulate to form larger flocs that favor sedimentation. Larger average particles are observed at C1Out due to a vertical perforated pipe collecting a composite sample from the water column in Cell 1 rather than surface overflow. Stokes' law settling velocities are second order with respect to floc diameter, so a decrease in floc diameter due to disturbance would decrease settling velocity ($v \alpha d^2$). Iron oxides that are slow to settle out before leaving the preliminary iron oxidation pond will be transported into the C2N and C2S surface flow wetlands.

Systemic Storm Impact

The rain event on 09/22/2011 (moderate storm of 1.02 cm/hr maximum intensity; 7.25 hr duration; with 2.31 cm of precipitation yield) was sampled at all four passive treatment system locations simultaneously. The frequency of storms preceding the 9/22/2011 storm event was evaluated to determine if there was a relationship between the number and timing between serial storms preceding the sampled storm event and the total amount of material being mass transferred between units. A series of rainfall events on the 16th, 17th, and 18th of September preceded this moderate intensity storm event, with accumulation of more than 7.6 cm of precipitation. Multiple storms facilitating iron transport three days in advance of the 9/22 storm would have disrupted the settling of iron oxides over a much longer period of time than a single storm event within the oxidative unit. Figure 3.12 depicts the iron transport profiles at all four locations (C1Out, C2Nout, C2Sout, and C6out).

Transport events with storm activity occurring greater than two days before the sampled profile do not show transport to be elevated above the average storm transport at each location. This is consistent with the observation that storm transport profiles return to baseline transport concentrations within 30 hours after the storm event, unless there were serial storm events immediately preceding the profile or that occurred during the profile collection. Extreme storm profiles collected at all four locations consisted of serial storm events, but did not show increasing larger amounts of transported iron. This is likely due to the 30 hr-window of observation not being long enough to catch storm-induced secondary transport of the disturbed flocs before the conclusion of sample collection in the autosampler program.

In Cell 1, some transport is observed during the rain event (1.5 kg or 14.8% of the total iron transported during this event), with most of the iron is being transported after the conclusion of the seven hour 9/22/2011 storm event. These observations support rainfall disruption of iron floc sedimentation, as the hydraulic retention time of Cell 1 exceeds 14 and 28 hrs. Re-suspended materials from the accumulation of iron oxides in the AMD mixing zone of Cell 1 would not have had time to reach the cell effluent for sample collection if they were mobilized by the 9/22/2011 storm. Also, they would have likely settled out again within the oxidation pond without further disturbance as the design retention time for Cell 1 is nearly 6 days. Settling disruption from sequential storms would impact the cell as a whole, and settling disruption in the U-bend or effluent bay sections of Cell 1 would not have allowed time for the disturbed flocs to form and re-settle out of solution.

Two peaks in iron concentration are observed at 14 hrs and 28 hrs for not just the C1Out data, but for the C2N and C2S datasets as well. As these samples were collected simultaneously, the peaks observed for each location are not due to mass transfer between the cells in series. Rather, the consistency in the timing of the peaks suggests that this transport was caused by an event that impacted more than one treatment unit at the same time. Cell 2N and Cell 2S transported 2.24 kg and 1.50 kg respectively, and had a noted difference in peak morphology. Neither of the surface flow wetlands showed significant amounts of iron being transported during the storm event, yet Cell2N showed two transport peaks at approximately 14 hrs and 28 hrs as were observed for Cell 1. Cell 2S also showed a transport peak profile for the same time, but the amplitude of the peaks is notably lower (approximately 4 ppm rather than 10 ppm). These differences in peak shape and intensity are due to cell-specific variables like water level and vegetative cover as these are planted cells. Figure 3.20 is an aerial photograph of the

oxidative unit collected by Google Earth on 9/29/2011, which is approximately one week after the 9/22/2011 storm event.

Figure 3.20: MRPTS Oxidative Unit 9/29/2011. Note the low vegetative coverage due to high water levels in Cell 2S in comparison to vegetated marsh section of Cell 2N. Iron floc mats are visible in all cells.

Cell 2S lacks mature vegetative cover in the marsh section of its design due partially to muskrat pressure and water level fluctuations not supporting emergent hydrophytes. Storm-induced transport into Cell 2N attenuates the mass transport peak and mass loading into Cell 3N, which is noted qualitatively in Figure 3.20 through distinct color changes from orange in the treatment cell fore bay, and green in the effluent bay. The wetland section is vegetated with a heterogeneous community of emergent and submerged hydrophytes.

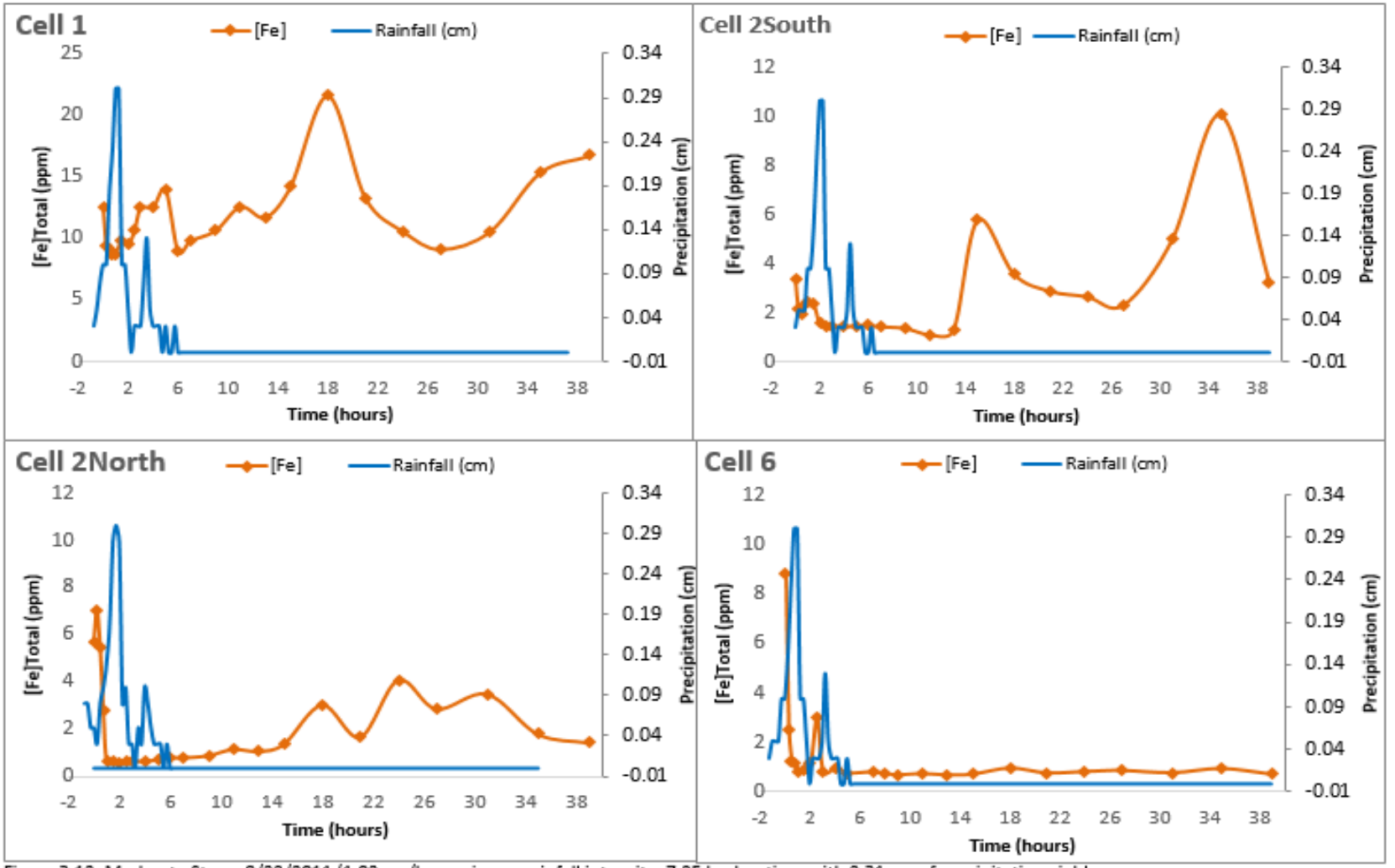

Figure 3.12: Moderate Storm 9/22/2011 (1.02 cm/hr maximum rainfall intensity; 7.25 hr duration; with 2.31 cm of precipitation yield

Oxidative treatment cells remove iron from AMD through oxidation and hydrolysis reactions, and are designed to facilitate the sedimentation and storage of the accumulated solids over time. Pairing an oxidation pond with surface flow wetland treatment cells is one approach to mitigating iron transport into vertical flow bioreactors within the serial design motif of most passive treatment systems. Baseline transport of iron occurs between the treatment cells of the system, and in the system effluent; yet the amount of mass transported is dependent on cell loading and removal efficiency. Intense storm events are typically not included in design decisions for passive treatment systems beyond construction of a by-pass channel to divert surface runoff from entering the treatment system and allowance of ample excess storage for the design storm. The role of rainfall intensity in iron transport has not been previously investigated with a quantitative approach. This three-year study was undertaken to determine if the amount of iron transported due to storm events was significant with respect to the baseline transport observed during times of typical system operation (no precipitation).

Storms were classified based on their rainfall intensity in an effort to determine if the intensity of the storm (low, moderate, high, and extreme) correlates to the amount of mass transported between cells. Storm activity in NE Oklahoma is frequent with an average of one storm of each intensity occurring within a month, and most storms having low rainfall intensity. Storm-induced iron transport is observed for intensities greater than 0.25 cm/hr for the preliminary oxidation cells, surface flow wetlands, and in the polishing wetland at the system outflow. Mass transport of iron for each location was significant over the baseline transport, yet did not correlate to rainfall intensity. The mechanism for storm induced transport is likely disruption of settling of iron flocs within the water column of the treatment cell rather than a re-suspension of sequestered material. Vegetative cover in surface flow wetlands also

mitigated the amount of iron transported to the vertical flow bioreactors, thus delaying maintenance issues with iron oxide accumulation.

Conclusions

The role of rainfall intensity on iron transport between the cells of the oxidative unit of a full scale passive treatment system had not been previously investigated with a quantitative approach for the determination of iron mass transport. A three-year study of storm events classified by rainfall intensity (Low = 0.25-0.99 cm/hr; Moderate = 1.00-1.99 cm/hr; High = 2.00-2.99 cm/hr; Extreme = >3.00 cm/hr) determined the average mass of iron transported at C1Out, C2N, C2S and C6Out per storm event, season, year, and three-year study period. There was no correlation between rainfall intensity and the mass of iron transported at all four locations sampled, as had been expected. Iron is transported for any storm with an intensity greater than 0.25 cm/hr, yet the consistency in the amount transported with increasing rainfall intensity suggests a transport mechanism other than resuspension of sequestered materials (which should scale with increasing intensity due to large volumes of material with the potential for resuspension). However, as this was not observed, the mechanism for storm induced transport is most likely due to disruption of the settling of precipitated FeOOH flocs within the water column for the oxidative unit, and solids accumulation on the sampling apparatus for Cell 6.

There is a positive linear correlation between average total iron transport per month and the average frequency of storms per month at all locations. This indicates that the mobilization of iron is strongly influenced by the total number of storms in a region rather than the intensity of the storms. Low intensity storms had the largest influence on the total mass of iron transported as there were over six times as many 0.25-0.99 cm/hr storms in a year than the

other storm intensity classifications. Storm-induced net iron mass transport for individual storms over the transport baseline was statistically significant for individual storm events at all four locations. Averages of storm-induced iron transport for seasonal and annual events were statistically significant over the baseline transport for all locations due to the high frequency of low intensity storms, and the distribution of low intensity storms throughout seasonal and annual periods.

Literature Cited

Chen S, Luo H, Li T, Chen W. 2009. A Soft Computing Approach to Rainfall Intensity Classification Using TRMM / TMI Data. JAC III. 12:6. p 516-522.

Cohen MJ, Brown MT. 2007. A model examining hierarchical wetland networks for watershed stormwater management. Ecol. Modell. 201:179–193.

Eger, P. and Wagner, J., 2002. The Use of Wetlands to Remove Nickel from Mine Drainage - Is Perpetual Treatment Really Possible? Proceedings of American Society of Mining and Reclamation Meeting, Lexington, Kentucky, June 9-13, 2002.

Gaál L, Molnar P, Szolgay J. 2014. Selection of intense rainfall events based on intensity thresholds and lightning data in Switzerland. Hydrol. Earth Syst. Sci. 18:1561–1573.

Hall GH, Puhlmann T. 2005. Spatial distribution of iron oxidation in the aerobic cells of the Wheal Jane Pilot Passive Treatment Plant. Sci. Total Environ. 338:73–80.

Hedin RS, Nairn RW. 1992. Designing and Sizing Passive Mine Drainage Treatment Systems. U.S. Bureau of Mines, Pittsburgh Research Center

Jennings SR, Blicker S, Neuman P, Dennis R. 2008. Acid mine drainage and effects on fish health and ecology: a review. , 2008. Reclam. Res. Gr. 1:1–26.

Kruse NAS, Gozzard E, Jarvis a. P. 2009. Determination of hydraulic residence times in several UK Mine water treatment systems and their relationship to iron removal. Mine Water Environ. 28:115–123.

Van der Lee WTB. 2000. Temporal variation of floc size and settling velocity in the Dollard estuary. Cont. Shelf Res. 20:1495–1511.

Nordstrom DK. 2009. Acid rock drainage and climate change. J. Geochemical Explor. 100:97–104.

Petrus J M Visser. 2001. The Storm-Structure-Severity method for the identification of convective storm characteristics with conventional weather radar. Meteorol. Appl. 8:1–10.

Pratt DR, Pilditch CA, Lohrer AM, Thrush SF. 2014. The effects of short-term increases in turbidity on sandflat microphytobenthic productivity and nutrient fluxes. J. Sea Res. 92:170–177.

Sandén P, Karlsson S, Düker A, Ledin A, Lundman L. 1997. Variations in hydrochemistry, trace metal concentration and transport during a rain storm event in a small catchment. J. Geochemical Explor. 58:145–155.

Skousen, J. G., A. Sexstone PFZ. 2000. Acid Mine Drainage Control and Treatment. In: R. I. Barnhisel, R. G. Darmody WLD, editor. Reclaimation of Drastically Disturbed Lands. 1st ed. Madison, WI: Agron. Monogr. p. 131–168.

Vymazal J. 2011. Constructed wetlands for wastewater treatment: Five decades of experience. Environ. Sci. Technol. 45:61–69.

Walling, D. E., and I. D. L. Foster. 1975. Variations in natural chemical concentration of river water during flood flows, and the lag effect: Some further comments. J. Hydrol 26:237–244.

Watzlaf GR, Schroeder KT, Kleinmann RLP, Kairies CL, Nairn RW, Street WB. 2004. The Passive Treatment of Coal Mine Drainage. :1–72. DOE/NETL-2004/1202

Wiseman, IM; Edwards P. 2004. Constructed Wetlands for Minewater Treatment: Performance and Sustainability. Journal 18:127–132.

Younger P. Banwart, S. Hedin R. 2002. Mine Water: Hydrology, Pollution, Remediation. Volume 5. Springer Science+Business Media Dordrecht. p 127-148

Chapter 4 – Characterization of the Spatial Iron Accumulation in the Preliminary Oxidative Cells of a Passive Treatment System

Contents of this chapter have been formatted for submission to *Environmental Science and Technology.*

Abstract

Iron oxidation, hydrolysis, and settling are key processes promoted in passive treatment systems to remove iron from influent acid mine drainage (AMD). A solids accumulation profile is a spatially-derived sample collection with the goal of mapping the localized accumulation of materials within a passive treatment cell, rather than just assuming a uniform distribution. Development of a solids accumulation profile for the oxidative unit of a passive treatment system provides insight into system performance and recovery/reuse applications. This study delineates the deposition profile of accumulated iron oxide precipitates over the first full seven years (2009-2015) of operation for the Mayer Ranch Passive Treatment System receiving ferruginous lead-zinc mine drainage at the Tar Creek Superfund Site. Depth-integrated measurements of discrete core samples within the initial oxidation pond and secondary surface flow wetlands were used to map the accumulation of solids. *In-situ* water measurements included pH, temperature, specific conductance, dissolved oxygen, and oxidation-reduction potential; turbidity and total alkalinity were measured on site and water samples were collected for laboratory determination of total and dissolved metals (and sulfate concentrations. Core samples were characterized for color, density, surface area, % crystallinity, % residual moisture content, % organic content, and mineral phases via Raman microscopy and SEM microscopy. A rhodamine tracer study was conducted to determine the hydraulic retention time for Cell 1 and Cells 2N/2S after seven years of operation. Rhodamine-WT (3.8 L) was introduced to the three influent seeps simultaneously (volume proportionate

to individual seep flows, Q_{total} = 7.42 L/sec), and concentrations were measured with YSI-rhodamine sensors (#6130) continuously (15-minute logging interval) and discretely (1 sample every hour via programmable autosampler) over 14 days. Cell 1 has a HRT of 5.5 days which is less than the design of 7.7 days. Cells 2N/2S have a design HRT of 3.5 days yet when tested with rhodamine tracer dye in 2009, they indicated 2.5 days for their average HRT. This suggests that the shorter than expected HRT for Cell 1 may be due to flow short circuiting rather than solely due to solids accumulation. Extended HRTs were observed for Cells 2N/2S (averaging 9.0 days) due to restricted hydraulic conductivity through the down gradient vertical flow bioreactors (VFBRs). High system water levels for both Cell 2N and 2S were due the frequency of rainfall events.

Introduction

Passive treatment oxidation cells are designed to retain precipitated iron oxyhydroxides for the design life of the system with regular intervals of extraction to maintain function (Hedin 2008). Removal rates calculated from empirical sources have a wide range of reported values (20 ±10 g/m^2/day) based on the area-adjusted mass removal concept (Kruse et al. 2009; Sapsford and Watson 2011; Kusin et al. 2012). Relative removal efficiencies of iron oxidation cells have been reported to range from 24% to 99% with no clear trend emerging based on oxidation cell type (pond/wetland; Kusin 2013). Lessons learned from how iron removal rates and accumulation of precipitated solids impact function of mature systems have inspired refinement in second and third generation passive treatment systems design. System performance metrics, design-phase iron removal predictions, and federal iron discharge standards already define project success indicators (Skousen et al 2005). Long- term operation and maintenance decisions are impacted by the spatial distribution of accumulated solids,

change in treatment system hydraulics, and the loss of available treatment volume over time and have not been fully resolved (Coghlan and V Raj, 2000). Therefore, it is essential to understand how the accumulation profile of iron oxides within sedimentation ponds and surface flow wetlands impacts physical and chemical performance for a mature system (> 5 years of operation) (Hedin et al. 2010).

Although cell design incorporates storage of solids into the long- term operation and maintenance plan for a system, physical extraction is the ultimate mechanism for sustainable operation. Extracted materials may be landfilled offsite, stored on site, or marketed as a commodity within the pigmentation and sorbent industries (Hedin 2002; Marcello et al. 2008;). Characterization of the physical and chemical properties of accumulated iron oxyhydroxides is essential to determine their suitability for reuse or disposal options (Schwertmann 2003; Kairies et al. 2005). Physical and chemical characteristics have been documented to vary spatially based on formation and storage conditions over time (Nordstrom 2011), yet reuse characterization practices focus principally on the bulk phase properties of the material after extraction is complete. Dried and sieved solid composites are typically characterized for their particle size, shape, surface area, structure, and sorption/desorption properties (Cornell and Schwertmann 2003; Neely 2010). Variables that define the characteristics of the precipitates and their saturation indices include the following: relative concentration and diversity of analytes within the matrix, pH, dissolved oxygen, oxidation reduction potential (ORP), and flow conditions (channel verses pond) (Cravotta 2008). Core samples of the accumulated iron oxides can be used to not only quantify the volume of solids accumulated for each cell of the oxidative units, but also the distribution of the accumulation. As most water quality evaluation methods focus only on the influent and effluent metals loadings to define treatment success, this is a novel approach centering on the production and accumulation of a resource.

Collecting a spatial profile within each cell of the oxidative units will yield higher resolution intracellular accumulation data to guide efficient iron recovery methodologies.

The overall goal of this research chapter was to demonstrate how the development of empirically derived solids accumulation profiles, in conjunction with the supporting materials characterization data, can be used to delineate mechanisms impacting cell performance. Comparisons between design-based predictions and observed performance will support a growing body of literature on passive treatment system assessment methodologies (Skousen and Ziemkiewicz 2005; Sapsford and Williams 2009; Sapsford and Watson 2011). Additionally, understanding the localized differences in physical and chemical properties of iron oxides based on their spatial distribution will increase our understanding of how formation and storage conditions influence resource properties over time. Applications of this information could lead to the development of a selective resource harvesting approach to target materials of specific composition for specialty markets unlike bulk phase extractions methodologies.

Methods

Iron Accumulation Profiling

An accumulation profile was constructed through the collection and measurement of iron oxide core samples. The accumulated solids within the oxidative unit of the MRPTS (Cell 1, Cell 2N, Cell 2S) were systematically sampled via discrete coring from a stabilized catamaran to minimize disturbance (Figure 4.1). The catamaran consists of two aluminum canoes lashed together with three boards and clamps to endure stability. A tow rope was used to maneuver the catamaran rather than paddles as to mitigate disturbance of the water column. Tension between bow and stern tow lines was used to maintain position within the cell as each of the core samples was collected. Sample collection was conducted for the entire treatment cell on

the same day, and sample collections days were selected based on low wind conditions to further aid in stability of the catamaran and the safety of the crew. Catwalk samples were collected using a series of aluminum scaffolding walk boards on pre-existing structural supports to form a type of stabilized dock for replicate and feldspar QAQC sample collection. Cores depth measurements made from samples featuring a Feldspar marker were used for verification of core depth measurements based on the clay boundary.

Figure 4.1: Sampling catamaran assembled with C-clamps to stabilize two canoes for core sampling of accumulated iron oxyhydroxides while minimizing disturbance of solids.

Site selection was based on spatial distribution to describe accumulation throughout each cell, rather than just focusing on the influent or effluent locations. Fourteen locations within Cell 1 were cored, with additional replicate cores collected from the catwalk sampling structures located in sections 1, 2, and 3 of the treatment cell. Nine core samples were collected from each of the surface flow wetland cells on a grid pattern so that three cores from each pond (3)-marsh(3)-pond(3) section of the cell were represented. Feldspar markers (46x46 cm brilliant white solids) installed during the construction of Cell 1 were used to validate core collection and accumulation measurement methodologies via visual boundary delineation

between the accumulated iron oxides and the clay liner. Positive measurement bias was avoided by delineating the boundary between the clay liner and the iron oxides based on color and texture of material. Negative measurement bias due to poor sampling technique (partial core only) was avoided as only cores collected with a clay plug were measured and characterized. Comparison of core depths at these locations to samples collected just outside of the feldspar marker area (46 X 46 cm) provides confidence that measured core depths accurately reflect the depth of stored iron oxyhydroxides. Core sample locations for Cell 1, Cell 2N, and Cell 2S are illustrated in Figure 4.2.

Core samples were collected by embedding a clear, acrylic pipe (0.98-cm internal diameter, 1.86 meters long) perpendicular to the bottom of the cell until the clay liner securely plugged the pipe ensuring an intact and continuous sample of solids as the core was retrieved. The tube was capped at the top and bottom with rubber stoppers, Parafilm® and Duct tape® when extracted vertically from the water column to preserve the quality (spatial distribution of material) and quantity (total depth of material) for immediate measurement of accumulation. The depth of material in the tube from the solids / liquid interface to the clay liner was measured on site (Figure 4.3) and recorded along with photos of the cores to document appearance (color and texture), as some compaction was expected during transport to laboratory facilities.

Figure 4.2: MRPTS oxidative unit core sample locations. White arrows indicated direction of influent and effluent flows. Core samples lined up to show relative amounts of accumulated iron oxides transported for solids characterization back at the CREW laboratories.

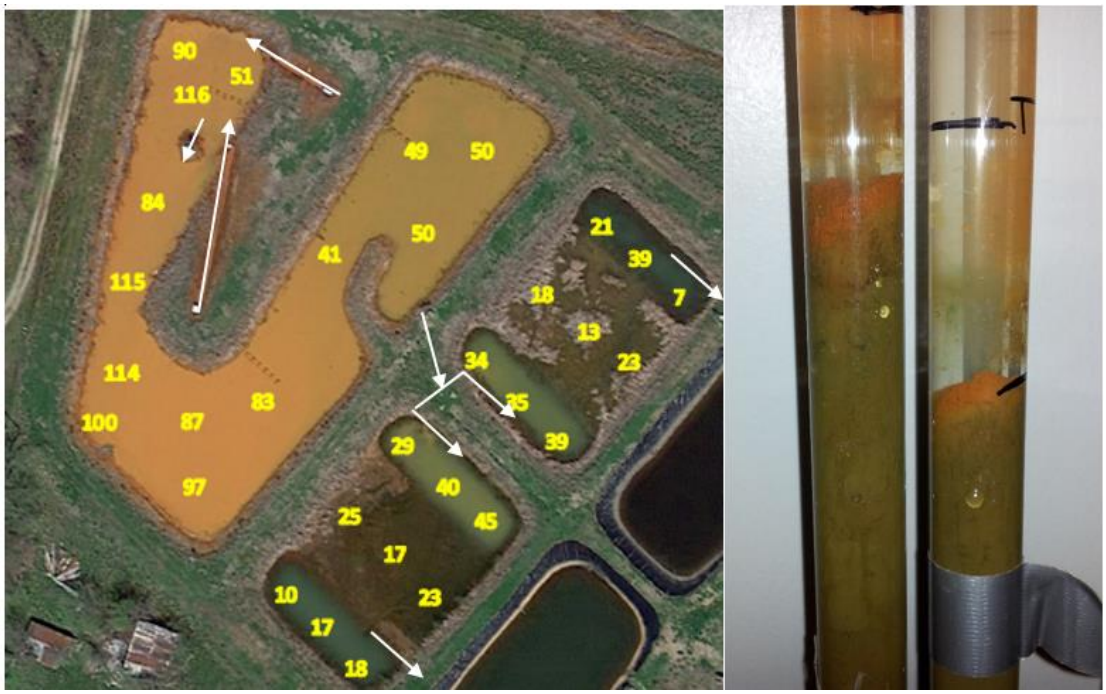

Figure 4.3: MRPTS oxidative unit core depths in centimeters from the bottom of the cell (clay liner). White arrows indicated direction of influent and effluent flows.

Results and Discussion

The accumulation of iron oxyhydroxides precipitates was not uniformly distributed for any of the cells within the oxidative unit. Accumulation depths were at their deepest for all three cells within section 1 (closest to the influent discharge) with a general trend of decreasing accumulation depths along the flow path prior to reaching the cell outlet. A preliminary core sampling from only the catwalk structures within Cell 1 suggested an average linear trend ($y = -2.75x+298.5$; $r^2 = 0.9938$) when decreasing accumulated solids were plotted versus increasing distance from the cell influent AMD discharge. Figure 4.4 is a summary of average accumulated depth for each section of Cell 1. Cell 1 had the deepest accumulation of material out of the three oxidative cells (≤ 116 cm), yet that accumulation was not uniformly distributed throughout the cell nor within section 1 of Cell 1. Figure 5.5 reflects the relationship between accumulated solids depths versus their distance from the influent AMD discharges.

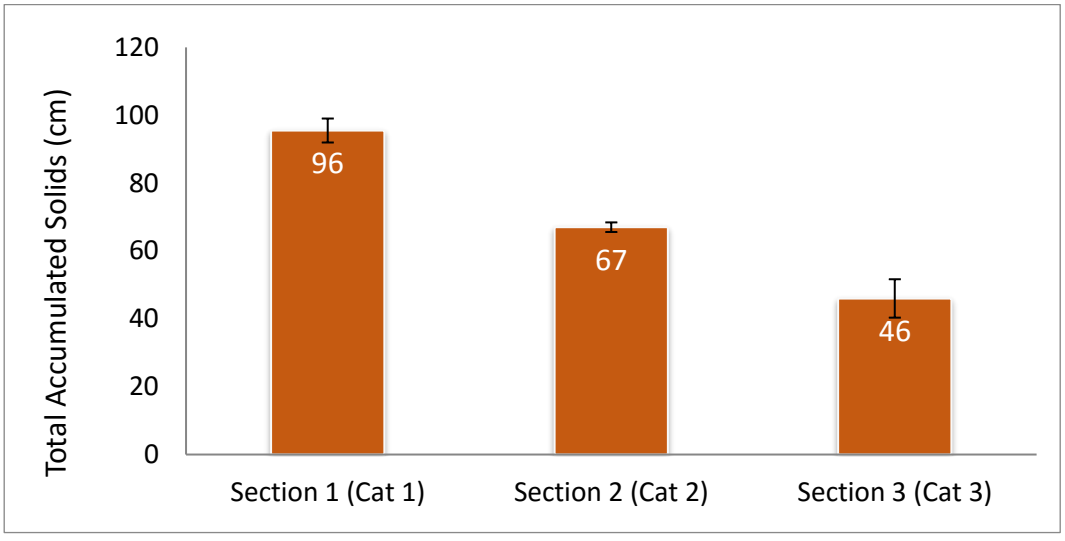

Figure 4.4: Preliminary iron oxide accumulation in Cell 1 of the MRPTS in 2014 measured by replicate core samples collected from the stabilized catwalk sampling platforms (n=6). Error bars indicate standard deviation.

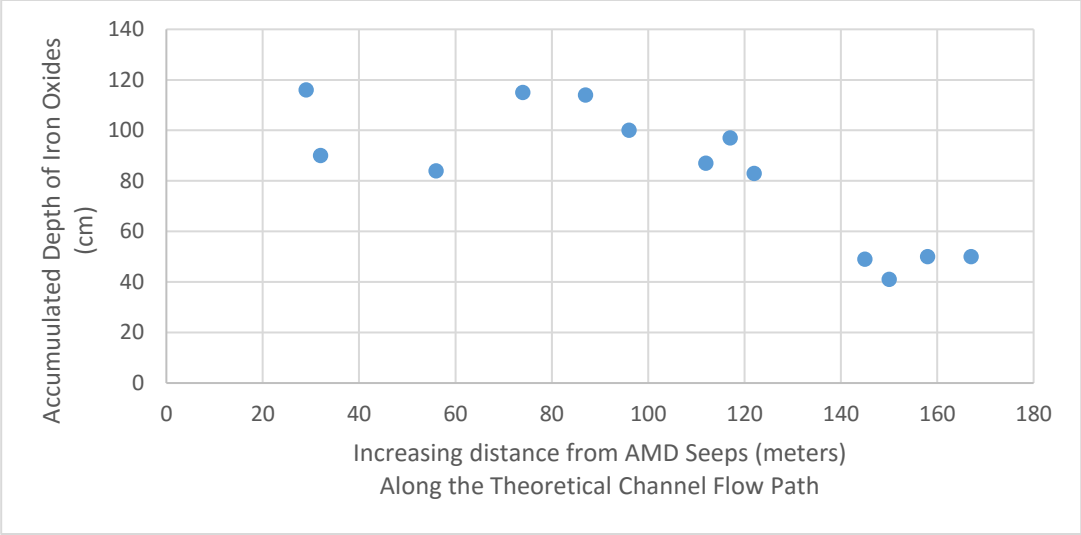

Figure 4.5: Accumulated depth of iron oxides within Cell 1 with increasing distance from the average AMD seeps input. Accumulation in sections 1 and 2 of Cell 1 while short circuiting in section 3 leads to iron export.

Iron accumulation from settled suspended solids is observed in sections 1 and 2 of Cell 1 but not Section 3 as flow short circuiting exports iron. This trend in accumulation is qualitatively consistent with field observations when the emergency flow bypass was used to draw down water levels for maintenance, and it is consistent with the trend observed in Figure 4.4 for the exploratory core samples collected at each catwalk. However, the ratio of accumulation with increasing distance decreased from -2.75 cm Fe/m to 0.454 cm Fe/m when more data points were included in the analysis. The poor linear fit of Figure 4.5 indicates that within each section of the cell, and for the cell overall, there is a heterogeneity in the deposition of iron oxides. The inclusion of additional core samples (n = 14) beyond those collected at the catwalks (n = 6) in refining this relationship increases the area of the treatment cell with high iron oxide accumulated storage. Accumulated iron oxides extend from section 1 into section 2 following along the linear flow path towards the bottom of the U-bend of the cell (sample locations 1-7). The measurements of accumulated iron oxides in the latter half of section 2 and all of section 3 of Cell 1 are likely due to most iron being transported in the dissolved state

(~70%) in these locations and thus not undergoing precipitation and sedimentation before effluent transport into Cells 2N and 2S.

A summary of average iron accumulation depth for Cell 2N and 2S is plotted in Figure 4.6 based on spatial location within the cells. An average of 37 cm of iron accumulation was measured in the first ponded section of C2N/C2S, and 19-20 cm of accumulation for the planted marsh (section 2) and the second ponded area (section 3). There is not a distinct linear trend when plotting the individual accumulated iron oxides versus distance from influent AMD flow ($y = -0.50x+37.7$; $r^2 = 0.2224$) as these cells are not designed to operate on a linear flow path. The accumulation of iron in section 1 of the surface flow wetlands is consistent with the expected performance of the cell as the initial ponded area allows for additional storage of accumulated volumes. The planted zones function to remove suspended solids by slowing down the flow and thus promoting conditions favoring the sedimentation of solids.

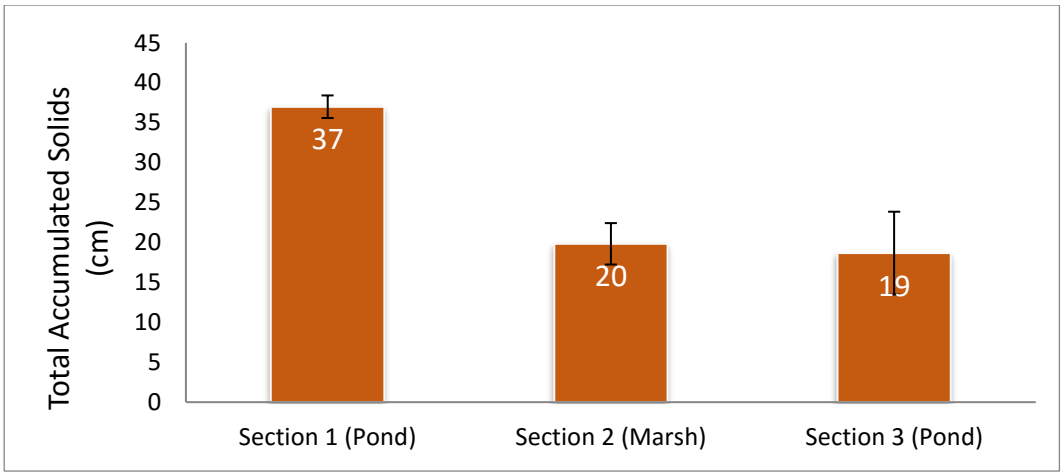

Figure 4.6: Average iron accumulation via discrete core sampling of C2N and C2S based on the spatial distribution of material throughout the pond: marsh: pond design.

Core Sample Characterization

All core samples were returned to the CREW laboratories for sectioning and subsequent properties characterization. Each core sample was sectioned into the oldest material (bottom 10% of the iron oxide column) and the newest material (top 10% of the column) and were air

dried at room temperature. Dry samples were milled into fine powders, but were not size selected via sieving due to limited sample yield of dried material. Composite samples were prepared by mixing equal masses of dried solids from each section of the treatment cells and were characterized for % residual moisture content (gravimetric analysis), % organic material content (Loss on Ignition: LOI) , mineral phase via Raman microscopy, % crystallinity via acid-oxalate extraction, color (Munsell), and particle morphology (Scanning Electron Microscopy: SEM) as detailed in Table 4.1. Each composite was analyzed using a LISST laser diffractometer to determine mean particle size (µm), particle size distribution (D60/D10), and mean surface area (cm^2). Characterization protocols were based on (Mukhopadhyay 2003; Schwertmann 2003; Perkins et al. 2007; and Tessier et al. 1979)

Table 4.1: Summary of iron oxide characterization methodologies for characterization of core samples

Test	Method	Purpose	Citation
Laser Diffraction	LISST: Laser Diffraction via small-angle forward laser light scattering (laser diffraction)	Surface Area Particle Size Particle Density	(Perkins et al. 2007) (Cornell and Schwertmann 2003)
Raman Microscopy	inVia confocal Raman Microscope (Renishaw)	Mineral phase identification of amorphous iron oxides	(Mukhopadhyay 2003; Das and Hendry 2011a)
Particle size and morphology	SEM microscopy via AuPd sputter coating	Size and particle shapes to support mineral phase data	(Neely 2010)
Color Classification	Powders, Munsell Color Scale	Dry bulk powder value, hue, chroma	(Cornell and Schwertmann 2003)
%Organic Matter Content	Gravimetric analysis (relative weight loss on ignition at 375°C (LOI)	% Composition of organic material	(Tessier et al. 1979; Howard and Howard 1990; Salehi et al. 2011)
% Crystallinity	Acid Oxalate Extractions (AOE)	% Crystallinity of iron oxides	(Cornell and Schwertmann 2003; Kim and Kim 2003; Peretyazhko et al. 2009)

A portable LISST laser diffractometer (LISST-XR) from Sequoia Scientific Inc. was used to determine the particle size distribution of hydrated samples of iron oxides from the top (newest material deposited) and the bottom (oldest material deposited) for each composite sample (Davies et al. 2012; Felix et al. 2013; Markussen and Andersen 2013). Table 4.2 is a summary of results for the oxidative unit. The LISST utilizes small-angle forward laser light scattering (laser diffraction), compliant with the ISO-13320-1 standard (Sequoia 2016). The average effective density of the iron oxyhydroxides was reported as 2.65 g/cm^3

Table 4.2: Average particle size, distribution, and surface area for the solids recovered from the oxidative unit based on depth of accumulated iron oxyhydroxides (±standard deviation)

	Top (Newest) $FeOOH_{(s)}$			Bottom (Oldest) $FeOOH_{(s)}$		
	Mean Size (µm)	D60/D10	SA (cm^2)	Mean Size (µm)	D60/D10	SA (cm^2)
Cell 1	12.51±3.35	15.98±1.78	0.61±0.07	10.80±0.06	12.62±1.09	0.58±0.02
Cell 2N	18.84±5.26	12.60±1.55	0.44±0.10	18.18±3.57	10.23±0.50	0.40±0.08
Cell 2S	21.02±2.93	11.96±2.94	0.36±0.04	18.22±0.82	12.17±3.22	0.42±0.02

Mean particle size increased between Cells 1 and 2 for both the newest and the oldest material sequestered in the treatment cells. Surface area decreased between Cell 1 and Cells 2N/2S. Both observations are consistent with the flocculation of increasingly larger particle size settling out over time. The uniformity coefficient (D60/D10) decreases for the newest material as one moves through the treatment cells, while the oldest material remains consistent. The high value for the uniformity coefficient indicates that larger diameter particles (D60) are more abundant than smaller particles (D10) and thus is less uniform in particle size distribution.

All samples contained less than 2% residual moisture after air drying in the laboratory (Table 4.3). All the samples had low organic matter content, with Cell 1 having more than Cells 2N/2S.

The percent mass of organic matter decreases with increasing material age. Crystallinity of the iron oxides increased between Cell 1 and Cell 2N/2S and increased with increasing age of the material. Raman microscopy suggested poor crystallinity and the presence of ferrihydrite in the newest samples transitioning to goethite in the oldest samples by matching composite spectra to values reported in the literature for acid mine drainage (Das and Hendry 2011b). Raman bands at 244, 299, 385, 480, 548, and 681 are indicative of goethite, with 385 being most prominent. In contrast, ferrihydrite Raman bands include 370, 510, and 710 with the 710 band being the most prominent (Hanesch 2009).

Table 4.3: Average residual moisture (%), organic matter (%), and crystallinity (%) for the oxidative unit based on the depth of the accumulated iron oxyhydroxides (±standard deviation)

	Top (Newest) $FeOOH_{(s)}$			Bottom (Oldest) $FeOOH_{(s)}$		
	Residual Moisture (%)	LOI Organic Matter (%)	Crystallinity (%)	Residual Moisture (%)	LOI Organic Matter (%)	Crystallinity (%)
Cell 1	1.6±0.2	3.4±1.6	18.7±0.2	0.9±0.1	5.2±3.1	16.0±0.01
Cell 2N	0.8±0.2	2.4±1.8	60.0±0.5	0.6±0.2	1.8±1.0	73.3±0.3
Cell 2S	1.1±0.2	2.4±1.7	41.3±0.6	0.7±0.1	1.7±0.8	84.0±0.3

Scanning electron micrographs were collected for each composite sample to support the characterization of the iron oxides via particle morphology and crystalline structures identification. The Zeiss NEON FEG-SEM duel-beam high resolution microscope was used to visualize samples prepared via vapor deposition of Au/Pd on glass microscope slides with non-conductive iron oxides. Samples were observed to shift from amorphous to crystalline between Cell 1 and Cells 2N/2S and with increasing depth of material. Figures 4.7-4.9 are examples of SEM images collected to document this change in morphology.

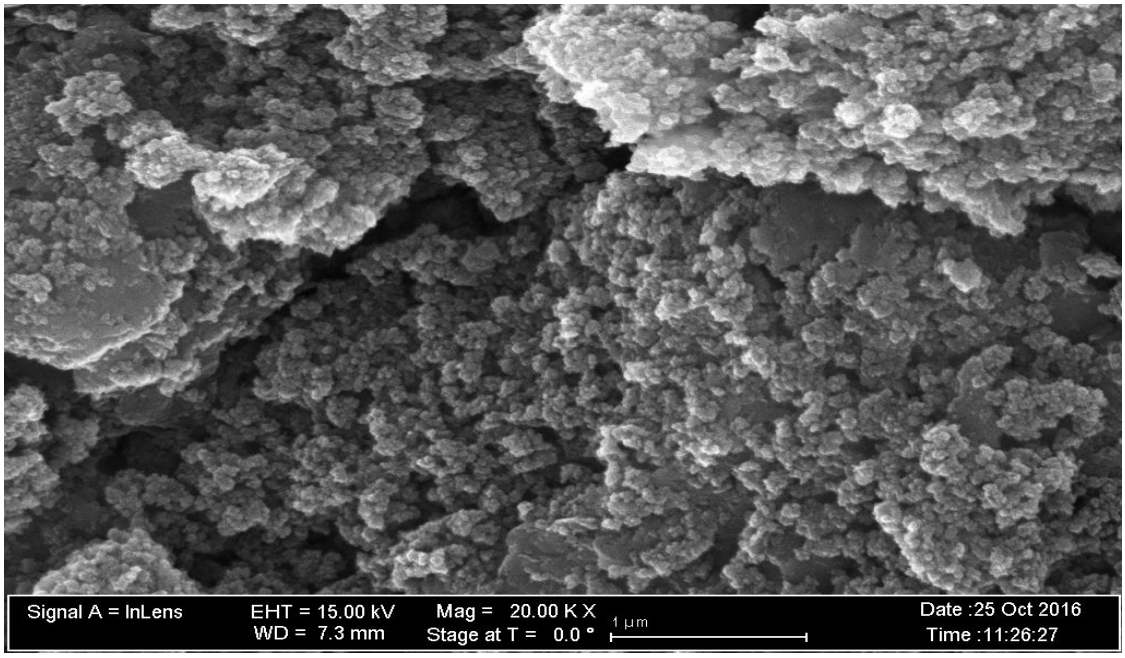

Figure 4.7: Amorphous Ferrihydrite typical of Cell 1 and Cell 2N/2S top (newest) samples.

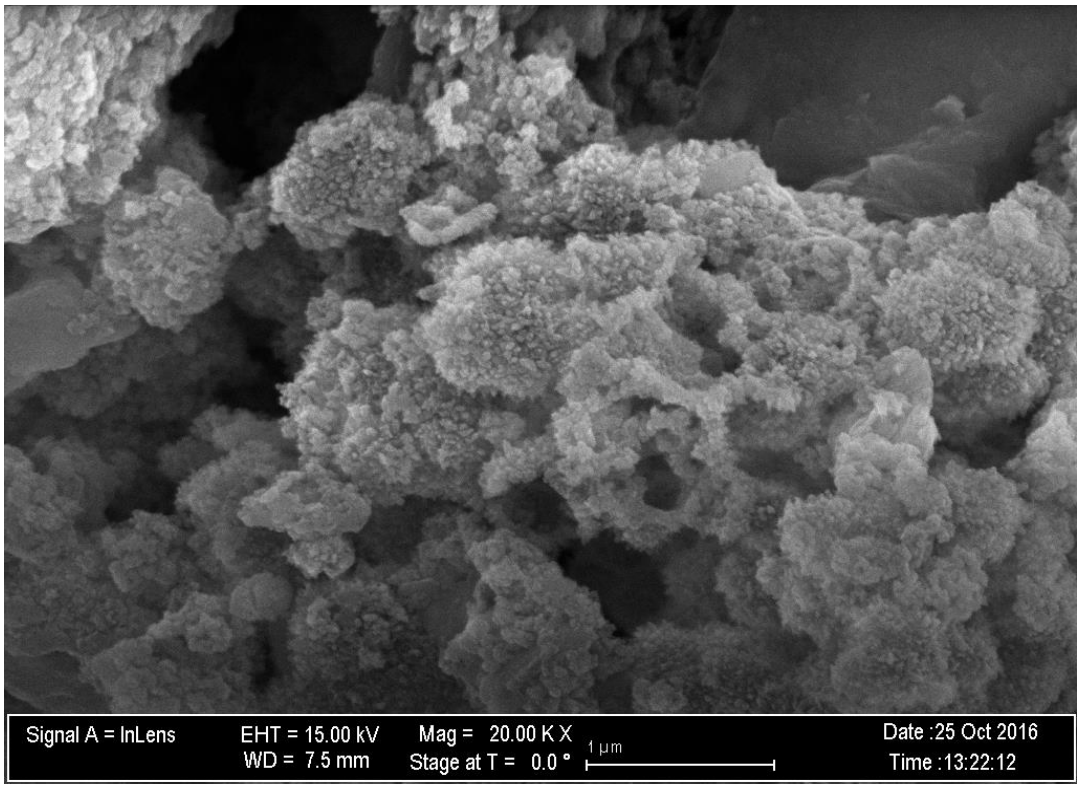

Figure 4.8: Crystallization forming in older iron oxide materials collected from the bottom of the cores.

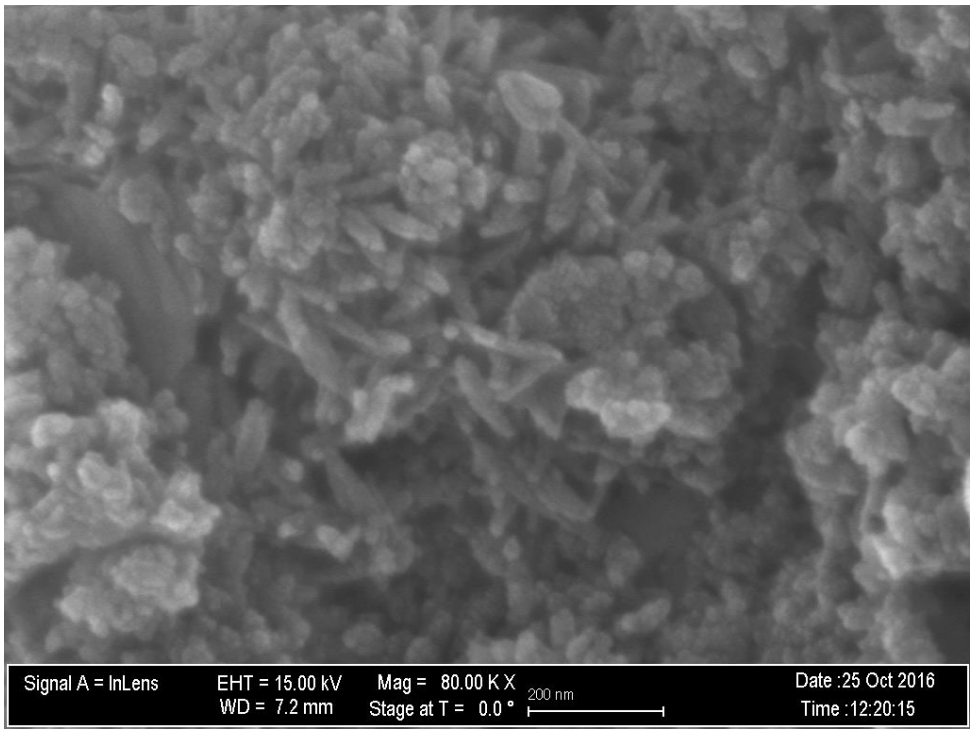

Figure 4.9: Goethite crystallization observed in bottom (oldest samples) 7 years of accumulation.

Characterization Comparison

Iron oxides from the Mayer Ranch Passive Treatment system were previously characterized (Neely 2010) for physical and chemical properties as they relate to the reuse of solids in the sorbent industry. A single sample of iron oxides collected from the concrete raceways that convey AMD into the preliminary oxidation cell was found to be promising with respect to phosphorous sorption (Neely 2010). Table 4.4 summarizes the results of the initial characterization with results obtained from the spatially coordinated sampling effort for all three oxidative treatment cells. The main difference between the samples is the location from which the sample was collected m, and how long it had been there before collection. The 2010 sample was collected at Cell 1 influent prior to entering the treatment cell, while the 2015 samples were accumulated solids from the bottom of the cell collected over an area and then composited for analysis.

Table 4.4: Comparison of physical properties of iron oxide samples collected from MRPTS

Physical Properties	Neely 2010 (Cell 1)	Oxenford 2015 (Cell 1)	Oxenford 2015 (C2N/C2S)
Crystallinity (%)	74.7	17.4	64.5
Mean particle size (μm)	94	11.7	19.0
D60/D10	1.65	14.3	11.74
Surface Area (m^2/g)	270 (BET)	244 (LISST)	162 (LISST)
Color	Yellowish Red	Yellowish Red	Yellowish Red
Organic Content (%)	1.0	4.3	2.1
Mineral phase	Goethite	Goethite	Goethite

The crystallinity of the 2010 samples is consistent with the crystallinity observed in the surface flow wetlands rather than within Cell 1. Differences in mean particle size and uniformity are likely due to differences in preparation and measurement techniques. Higher values for surface area were expected for the 2010 dataset due to the use of a nitrogen gas sorption technique (BET) to include pore volumes versus the using the algorithms to calculate surface areas from laser diffractometry measurements accounting for external surface only. A higher percentage of organic matter in the iron oxide samples collected from within the treatment cells is consistent with the presence of vegetative matter on the edge and in the planted zones of the cells. The 2010 sample was collected from a location that would have little to no organic matter present outside of detritus falling into the channel, or algae growth within the channel (minimal). All the samples were identified to have goethite as their principle mineral phase. It is expected that the bulk material accumulating in Cells 1 and 2N/2S would be similar in their sorption properties with those detailed by Neely (2010), yet additional testing is required for confirmation.

Tracer Study

Rhodamine WT tracer studies were used to evaluate the hydraulic retention time of the oxidative unit with respect to system design. Cells 2N/2S were evaluated just after the treatment system came online in 2009, and they were re-evaluated in 2015 after the system matured through seven years of operation. The hydraulic retention time (HRT) of Cell 1 was determined in the 2015 tracer study by measuring the concentration of rhodamine dye in the cell effluent over time. If the HRT is significantly shorter or longer than prescribed by design, it can result in operational inefficiencies translating into compromised performance or excessive system footprint. Tracer studies are based on the principle of tracking a target analyte as it moves through the system of study and documenting its time of travel and conservative mass recovery (Dierberg and DeBusk 2005).

Table 4.5: Summary of Rhodamine Tracer Dye Characteristics (Environmental 2001; Dierberg and DeBusk 2005)

Characteristic	Rhodamine
Tracer Type	Dye with optical detection, visual confirmation of deployment and progress.
Detection	In field – continuous monitoring. Excitation at 555 nm, emission 580 nm
Conservation	Non-conservative – loss principally due to irreversible sorption (zero order kinetics)
Interferences	Orange iron oxides
Deployment	Solution, mixing required to accommodate specific gravity
Downstream	Attenuation via sorption and photolysis

The tracer dye rhodamine WT was selected due to its unique spectral characteristics to minimize interferences from turbidity and phytoplankton (chlorophyll a) and the availability of *in situ* continuous monitoring in real time with a YSI 6130 rhodamine probe (Range: 0-200 ug/L; Resolution: 0.1 ug/L; Accuracy: +/-5% reading or 1 ug/L, whichever is greater)(Fondriest 2001). Rhodamine sensors were calibrated using a 100 mg/L standard and were deployed at the effluent AgriDrains of Cell 1, Cell2N, and Cell 2S.

The principle limitation to using Rhodamine WT as a tracer dye is its loss via sorption to organic matter (Dierberg and DeBusk 2005) and to iron oxides limiting its mass recovery. Rhodamine was introduced to the system at each of the seeps in a synchronized, volume-weighted addition based on loading contribution of each seep to the system (Seep A (30%), Seep B (60%), and Seep D (10%)). A total of 3800 mL of Rhodamine WT was added to the system where the seeps emerge and discharge and run down channels before spilling into Cell 1 for the most realistic representation of loading. There were no additional amounts of rhodamine added to the system beyond the initial dosing. Thus, the tracer that was transported out of Cell 1 became the mass loading for the Cell 2N/2S tracer study. Photographs and spot checks with a portable rhodamine sensor were used to document progress while the continuous monitoring sensors logged concentration undisturbed for the duration of the study. Rhodamine concentration (µg/mL) was logged over time and plotted via Excel to determine the area under the curve. The hydraulic retention time was determined as the point in which 70% of the area under the curve had been accounted for (Kruse et al 2009).

Tracer Study Results

For the tracer study, the influent flow to the MRPTS was determined to be 151 L/min (Seep A), 265 L/min (Seep B), and 28 L/min (Seep D) for a combined total flow of 444 L/min into Cell 1. The density of rhodamine WT concentrate is 1.16 g/mL so with 3800 mL loaded, an equivalent mass of 4,048 g of rhodamine dye was added. A 20-L bucket was used to dilute the concentration to a density that is more consistent with the influent water quality to prevent mixing issues. Dye was observed to short circuit past the mixing zone of section 1 of Cell 1 through contact with the landmass at the edge of the cell and pass into section 2 of the cell within minutes of its introduction. Figures 4.10 and 4.11 include photos taken just after the

introduction of the rhodamine dye. Figure 4.11 is a series of photographs indicating qualitative observation of tracer dye short-circuiting as dye introduced at the seeps headed to the Section 2 U-bend of Cell 1 rather than mixing in Section 1 as anticipated.

Figure 4.10: Introduction of rhodamine tracer dye at Seep A of the MRPTS. Note higher than design water levels as influent concrete channel is flooded, with water ponding around the seep box. Rust lines on the box indicate historic water levels over the course of seven years of system operation.

Figure 4.11: Tracer dye short circuiting into section 2 after introduction to the MRPTS.

Low concentrations of rhodamine were detectable at the effluent of Cell 1 within 30 minutes of tracer introduction. Tracer clean out of seep raceways was confirmed visually 12 hours later (Figure 4.12)

Figure 4.12: MRPTS Influent Seep with no signs of rhodamine dye loss.

Peak rhodamine was measured at Cell 1 Out AgriDrain in 1.5 days while the hydraulic retention time determined to be 5.75 days. (Figure 4.13; Table 4.7). Rhodamine was detected in Cells 2N/2S within two days of its introduction into the passive treatment system. Rhodamine sensors placed in the AgriDrain for C2Nout and C2Sout were used to monitor the export of tracer dye into the vertical flow bioreactors. Storm activity began on Day 6 of the tracer study and yielded over six centimeters of rainfall overnight, and approximately 9.5 cm over a continuous six-day period (11/26-12/01). This rainfall further increased already high water levels within the treatment system, and led to poor system drainage for all cells above C3N/C3S which are flow restricted due to the hydraulic conductivity of vertical flow through the organic layer. Water stacked into C2N and C2S due to the rate-limited outlet extending

the duration of tracer retention within each cell. The design hydraulic retention time for C2N / C2S is 3.5 days, and the University of Oklahoma Capstone students measured the HRT via a tracer study in 2009 to be 2.7 days. This indicates that the surface flow wetlands were not fully vegetated, which is consistent with what one would expect for February 2009 within the first year of operation. The 2015 tracer study returned a 9-day HRT for C2N/C2S due to storm activity, and artificially-increased hydraulic retention during the study. The peak HRT for both surface flow wetlands is equivalent with the design retention time (3.5 days) with C2N (4.3 days) and C2S (3.7 days) prior to storm activity.

Figure 5.13 features photographs of tracer dye entering C2S with pre-existing high water conditions as well as a qualitative comparison of water elevations between C2N and C3N post storm. The storm-influenced tracer study comparison for the oxidative unit is summarized in Table 4.7. Figure 4.14 is a comparison of the rhodamine transport profiles for C2N and C2S. The rhodamine transport profiles for C2N and C2S are equivalent, but the hydraulic retention time of the cell is much longer than design.

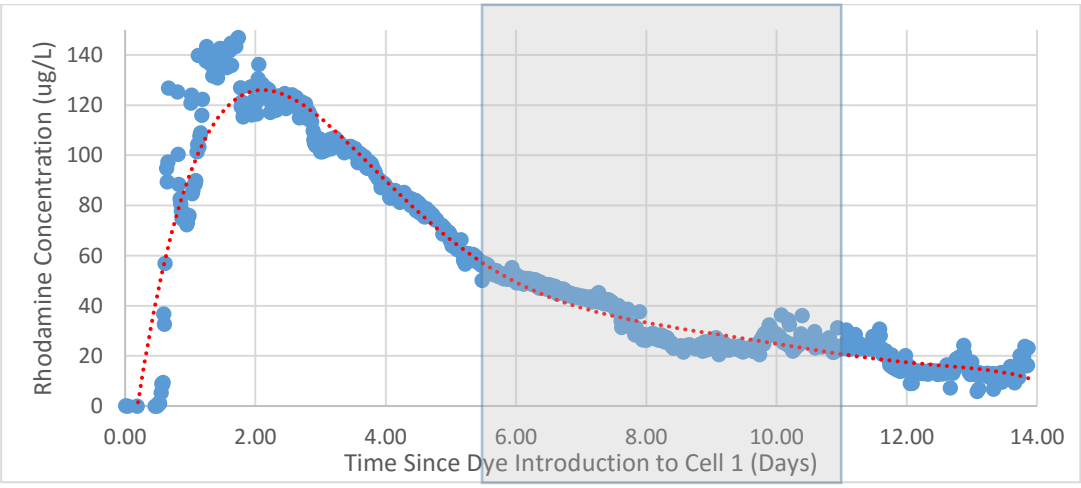

Figure 4.13: Rhodamine transport profile at C1Out (Cell 1 Effluent November 2015). Grey shading indicates a series of high intensity, long duration storms summarized in Table 4.6.

Figure 4.14: Transport of Rhodamine across C2S with high water conditions. Side by side comparison of water levels and rhodamine color of C2N and C3N before 11/26 rain event.

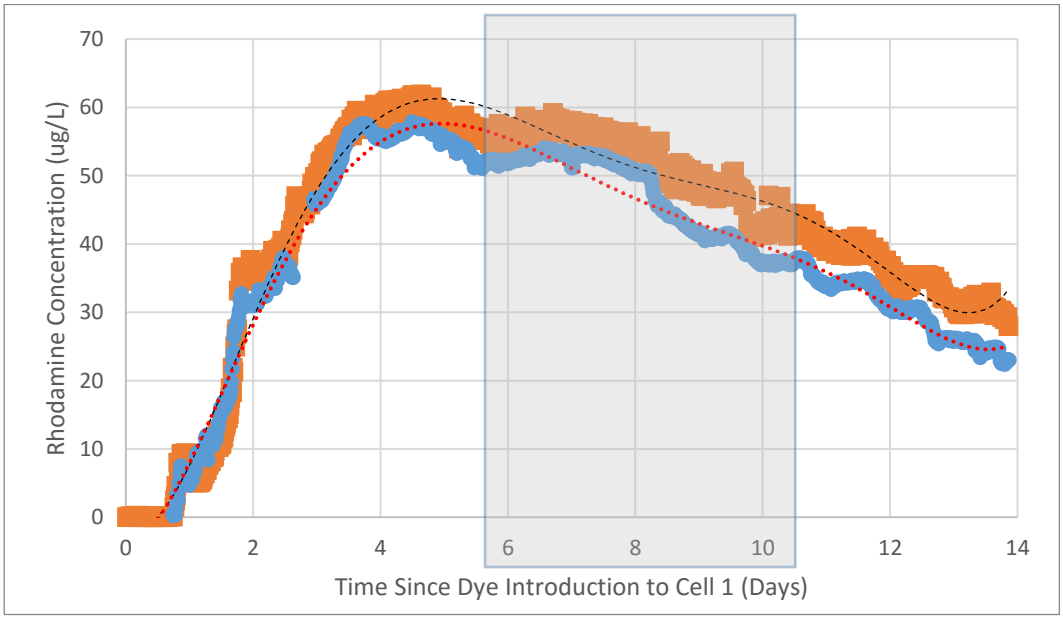

Figure 4.15: Comparison of C2N (Blue) and C2S (Orange) rhodamine transport profiles. Grey shading indicates the time in which a high intensity, long duration series of rain events occurred (Table 4.6)

Table 4.6: Comparison of performance summary for the tracer study of the oxidative unit of the passive treatment system.

	Cell 1	Cell 2N	Cell 2S
Area Adjusted Iron Loading ($g/m^2/day$)	24.4	11.5	11.6
Mean Iron Removal Efficiency (%)	78	82	82
Mass of Iron Removed (kg/day)	87	17.3	17.3
Area Adjusted Removal Rate ($g/m^2/day$)	19.0	11.5	11.6
Peak Residence Time (days)	1.5	4.3	3.7
70% Residence Time (days)	5.75	9.2	9.0
Design HRT (days)	7.7	3.5	3.5
Change in HRT from Design (days)	-2.0	+5.7*	+5.5*

*due to poor hydraulic conductivity and high storm activity impairing transport through the system

Table 4.7 Daily Summary of Storm Activity for the Miami, OK Mesonet Station leading up to the Oxidative Unit Tracer Study. Grey section indicates dates of the tracer study for Cell 1 and Cells 2N/2S

	Daily Storm Yield (cm)	Daily Duration of rain Periods (hrs)	Max Rainfall Intensity (cm/hr)	Classification
15-Nov	1.04	2.5	0.91	Low Intensity
16-Nov	2.39	4.7	3.35	Extreme Intensity
17-Nov	9.42	10.3	7.32	Extreme Intensity
18-Nov	0.00	0.0	0.00	
19-Nov	0.00	0.0	0.00	
20-Nov	0.00	0.0	0.00	
21-Nov	0.74	2.3	0.61	Low Intensity*
22-Nov	0.00	0.0	0.00	
23-Nov	0.00	0.0	0.00	
24-Nov	0.00	0.0	0.00	
25-Nov	0.00	0.0	0.00	
26-Nov	2.31	5.1	0.91	Low Intensity
27-Nov	6.35	11.3	2.13	High Intensity
28-Nov	0.18	0.6	0.30	Low Intensity
29-Nov	0.43	1.3	0.61	Low Intensity
30-Nov	0.25	0.8	0.30	Low Intensity
1-Dec	0.03	0.1	0.30	Low Intensity
2-Dec	0.00	0.0	0.00	
3-Dec	0.00	0.0	0.00	
4-Dec	0.00	0.0	0.00	
5-Dec	0.00	0.0	0.00	
6-Dec	0.00	0.0	0.00	

*no precipitation observed at MRPTS, only documented at the Miami, OK Mesonet Station

Conclusions

Iron oxyhydroxide precipitates formed from the oxidation and hydrolysis of Fe^{2+} accumulate within the preliminary oxidation cell (Cell 1) and the surface flow wetlands (Cells 2N/2S) of MRPTS. The accumulation of iron oxyhydroxides is not uniformly distributed within each cell, with the first section of the cell favoring deeper deposits of material. The characterization of core samples for their physical properties revealed consistency within the cell and between the cells regarding mineral phase. The iron oxide accumulation increases in its relative crystallinity, average particle size, and uniformity with respect to position within the treatment series (Cell 1 to Cell 2N/2S) and with increasing depth. Organic matter is a minor component of the bulk material regardless of treatment cell type, and it decreases with respect to position in the oxidative unit. Accumulation of iron oxides influences a reduction in HRT over time, but other factors like hydraulic conductivity losses within certain cells of a treatment system and storm disturbances can extend retention times. Iron accumulation profiling is a useful tool for the determination of the stage of the treatment process and what section of a cell is most efficient for solids recovery.

Literature Cited

Neely, C. 2010. Characterization and possible sustainable sorbent use of iron oxides produced by acid mine drainage discharges. Masters of Science: Environmental Engineering: University of Oklahoma.

Cornell RM, Schwertmann U. 2003. Ch 4 Crystal Morphology and Size. The Iron Oxides. WIley and Sons. 2nd Edition. p

Cravotta CA. 2008. Dissolved metals and associated constituents in abandoned coal-mine discharges, Pennsylvania, USA. Part 2: Geochemical controls on constituent concentrations. Appl. Geochemistry 23:203–226.

Das S, Hendry MJ. 2011a. Changes of crystal morphology of aged goethite over a range of pH (2-13) at 100 Deg C. Appl. Clay Sci. 51:192–197.

Das S, Hendry MJ. 2011b. Application of Raman spectroscopy to identify iron minerals

commonly found in mine wastes. Chem. Geol. 290:101–108.

Davies EJ, Nimmo-Smith WAM, Agrawal YC, Souza AJ. 2012. LISST-100 response to large particles. Mar. Geol. 307–310:117–122.

Dierberg FE, DeBusk TA. 2005. An evaluation of two tracers in surface-flow wetlands: Rhodamine-WT and lithium. Wetlands 25:8–25.

Fondriest Inc. 2001. Water tracing , in situ dye fluorometry and the YSI 6130 Rhodamine WT Sensor. < http://fondriest.com/>

Felix D, Albayrak I, Boes RM. 2013. Laboratory investigation on measuring suspended sediment by portable laser diffractometer (LISST) focusing on particle shape. Geo-Marine Lett. 33:485–498.

Hanesch M. 2009. Raman spectroscopy of iron oxides and (oxy)hydroxides at low laser power and possible applications in environmental magnetic studies. Geophys. J. Int. 177:941–948.

Hedin R, Weaver T, Wolfe N, Weaver K. 2010. Passive Treatment of Acidic Coal Mine Drainage: The Anna S Mine Passive Treatment Complex. Mine Water Environ. 29:165–175.

Hedin RS (2008) Iron removal by a passive system treating alkaline coal mine drainage. Mine Water Environ 27:200-209.

Hedin RS. 2002. Recovery of Marketable Iron Oxide From Mine Drainage. J. Am. Soc. Min. Reclam. 2002:517–526.

Howard P, Howard D. 1990. Use of organic carbon and loss-on-ignition to estimate soil organic matter in different soil types and horizons. Biol. Fertil. Soils 9:306–310.

Kairies CL, Capo RC, Watzlaf GR. 2005. Chemical and physical properties of iron hydroxide precipitates associated with passively treated coal mine drainage in the Bituminous Region of Pennsylvania and Maryland. Appl. Geochemistry 20:1445–1460.

Kim JJ, Kim SJ. 2003. Environmental, mineralogical, and genetic characterization of ochreous and white precipitates from acid mine drainages in Taebaeg, Korea. Environ. Sci. Technol. 37:2120–2126.

Kruse NAS, Gozzard E, Jarvis a. P. 2009. Determination of hydraulic residence times in several UK Mine water treatment systems and their relationship to iron removal. Mine Water Environ. 28:115–123.

Kusin FM. 2013. A Review of the Importance of Hydraulic Residence Time on Improved Design of Mine Water Treatment Systems. 26:1316–1322.

Kusin FM, Jarvis AP, Gandy CJ. 2012. Hydraulic performance assessment of passive coal mine water treatment systems in the UK. Ecol. Eng. 49:233–243.

Marcello RR, Galato S, Peterson M, Riella HG, Bernardin a. M. 2008. Inorganic pigments made from the recycling of coal mine drainage treatment sludge. J. Environ. Manage. 88:1280–1284.

Markussen TN, Andersen TJ. 2013. A simple method for calculating in situ floc settling velocities based on effective density functions. Mar. Geol. 344:10–18.

Nordstrom DK. 2011. Hydrogeochemical processes governing the origin, transport and fate of major and trace elements from mine wastes and mineralized rock to surface waters. Appl. Geochemistry 26:1777–1791.

Peretyazhko T, Zachara JM, Boily JF, Xia Y, Gassman PL, Arey BW, Burgos WD. 2009. Mineralogical transformations controlling acid mine drainage chemistry. Chem. Geol. 262:169–178.

Perkins M, Effler SW, Peng F, Pierson D, Smith DG, Agrawal YC. 2007. Particle Characterization and Settling Velocities for a Water Supply Reservoir during a Turbidity Event. J. Environ. Eng. 133:800–808.

Salehi MH, Beni OH, Harchegani HB, Borujeni IE, Motaghian HR. 2011. Refining Soil Organic Matter Determination by Loss-on-Ignition. Pedosphere 21:473–482.

Sapsford DJ, Watson I. 2011. A process-orientated design and performance assessment methodology for passive mine water treatment systems. Ecol. Eng. 37:970–975.

Sapsford DJ, Williams KP. 2009. Sizing criteria for a low footprint passive mine water treatment system. Water Res. 43:423–432.

Skousen J, Ziemkiewicz P. 2005. Performance of 116 passive treatment systems for acid mine drainage. Proceedings, Am. Soc. Min. Reclamation, Breckenridge, CO:1100–1133.

Ziemkiewicz P., J.G S, Simmons J. 2003. Long-term Performance of Passive Acid Mine Drainage Treatment Systems. J. Mine Water Environ. 22:118.129.